

**Design of High-Quality Low-Order Nonrecursive
Digital Filters Using the Window Functions**

**Ph.D. Thesis
in
Electrical and Electronics Engineering
University of Gaziantep**

**Supervisor
Prof.Dr. Arif NACAROĞLU**

**by
Kemal AVCİ
September 2008**

Dedicated to the memories of my brothers

HAYDAR and TACİM

**In this life, you both are not with me anymore
but will live in my heart forever...**

ABSTRACT

DESIGN OF HIGH-QUALITY LOW-ORDER NONRECURSIVE DIGITAL FILTERS USING THE WINDOW FUNCTIONS

AVCI, Kemal

Ph.D. in Electrical and Electronics Engineering

Supervisor: Prof.Dr. Arif NACAROĞLU

September 2008, 143 pages

The aim of the thesis study is to present a new window function (or simply window) to provide better nonrecursive filter characteristics than the filters designed by the windows in the literature. To achieve this aim, four windows - namely Exponential, Cosh, modified Cosh and modified Kaiser - are proposed.

The Exponential and Cosh windows are derived by replacing the modified Bessel function of first kind of order zero in the Kaiser window with the exponential and cosine hyperbolic functions, respectively. Unlike the Kaiser window, they have an advantage that they have no power series expansion in their time domain representations. The spectrum design equations are established for these windows. The simulation results show that compared to the Kaiser window for the same window length and mainlobe width, they provide very good sidelobe roll-off ratio characteristic - which may be useful for some applications. But, in terms of the ripple ratio, the Kaiser window performs better results. As for the comparison with the three-parameter Ultraspherical window, the Exponential window performs better in ripple ratio characteristic for narrower mainlobe width and larger sidelobe roll-off ratio with fixing the window length, mainlobe width and sidelobe roll-off ratio. For wider mainlobe width and smaller sidelobe roll-off ratio, it performs worse ripple ratio. The Cosh window performs better ripple ratio characteristic for wider mainlobe width and larger sidelobe roll-off ratio. But, for narrower mainlobe width and smaller sidelobe roll-off ratio, the Ultraspherical window provides better results.

Third and fourth proposed window functions are the modified Cosh and modified Kaiser windows which are derived by proposing a third adjustable

parameter to the two-parameter Cosh and Kaiser windows, respectively. The simulation results show that they provide superior ripple ratio characteristics compared to the Kaiser and Cosh windows.

As for the applications of the proposed windows in the design of nonrecursive digital filters, the filter design equations for the Exponential and Cosh windows are obtained, and then they are compared with the Kaiser window. The simulation results show that the Kaiser window provides better results in terms of the minimum stopband attenuation. But, the Exponential and Cosh windows are better in terms of the maximum stopband attenuation which may be useful for some applications. The optimum solutions for the modified Cosh and modified Kaiser windows are found, and then the simulation results show that these two modified windows performs very good results in terms of the minimum stopband attenuation compared to the Kaiser window.

The comparisons with the well known window functions in literature show that the proposed modified Cosh and modified Kaiser windows can provide the best quality in terms of the minimum stopband attenuation for a fixed filter order, and also provide lowest filter order for a fixed minimum stopband attenuation.

Key words: Nonrecursive Digital Filters, Window Functions, Exponential Window, Cosh Window, Modified Cosh Window, Modified Kaiser Window, Kaiser Window, Ultraspherical Window.

ÖZET

PENCERE FONKSİYONLARI KULLANARAK YÜKSEK KALİTELİ DÜŞÜK DERECELİ YİNELEMESİZ SAYISAL SÜZGEÇLERİN TASARIMI

AVCI, Kemal

Doktora Tezi, Elektrik Elektronik Mühendisliği Bölümü

Tez Yöneticisi: Prof.Dr. Arif NACAROĞLU

Eylül 2008, 143 Sayfa

Tez çalışmasının amacı, yeni bir pencere fonksiyonu (veya basitçe pencere) sunarak literatürde bulunan pencereler tarafından tasarlanmış süzgeçlerden daha iyi yinelemesiz süzgeç karakteristikleri sağlamaktır. Bu amacı gerçekleştirmek için, Üstel, Cosh, geliştirilmiş Cosh ve geliştirilmiş Kaiser adlarında dört pencere önerilmiştir.

Üstel ve Cosh pencereleri, Kaiser penceresindeki sıfır dereceli birinci tür geliştirilmiş Bessel fonksiyonun yerine sırasıyla üstel ve kosinüs hiperbolik fonksiyonlarının konulmasıyla türetilmişlerdir. Kaiser penceresinden farklı olarak, zaman alan gösterimlerinde güç serileri bulunmama avantajına sahiptirler. Bu pencereler için spektrum tasarım denklemleri oluşturulmuştur. Benzeşim sonuçları göstermektedir ki aynı pencere uzunluğu ve analob genişliği için Kaiser penceresine kıyaslan bazı uygulamalar için kullanışlı olabilecek çok iyi yanlob azalma karakteristiği sağlamaktadırlar. Fakat tepecik oranı açısından Kaiser penceresi daha iyi sonuçlar vermektedir. Üç-parametrelili Ultraspherical pencereyle kıyaslamada ise, aynı pencere uzunluğu, analob genişliği ve yanlob azalma oranı için daha dar analob genişliği ve daha büyük yanlob azalma oranında Üstel pencere daha iyi tepecik oranı karakteristiği sağlamaktadır. Daha geniş analob genişliği ve daha küçük yanlob azalma oranında ise daha kötü tepecik oranı sağlar. Cosh pencere, daha geniş analob genişliği ve daha büyük yanlob azalma oranında daha iyi tepecik oranı karakteristiği sağlamaktadır. Fakat, daha dar analob genişliği ve küçük yanlob azalma oranında ise Ultraspherical pencere daha kötü sonuçlar verir.

Üçüncü ve dördüncü önerilen pencere fonksiyonları, sırasıyla iki parametrelili Cosh ve Kaiser pencerelerine üçüncü bir ayarlanabilir parametrenin önerilmesiyle türetilmiş olan geliştirilmiş Cosh ve geliştirilmiş Kaiser pencereleridir. Benzeşim sonuçları göstermektedir ki Kaiser ve Cosh pencerelerine kıyaslan çok daha iyi tepecik oranı karakteristiği sağlamaktadırlar.

Önerilen pencerelerin yinelemesiz sayısal süzgeçlerin tasarlanmasındaki uygulamaları için ise, Üstel ve Cosh pencereleri için süzgeç tasarım denklemleri elde edilmiş ve sonrada Kaiser penceresiyle kıyaslanılmışlardır. Benzeşim sonuçları minimum geçirmeyen bant azaltması açısından Kaiser penceresinin daha iyi sonuçlar verdiğini göstermektedir. Fakat Üstel ve Cosh pencereleri bazı uygulamalar için faydalı olabilecek maksimum geçirmeyen bant azaltması açısından daha iyidirler. Geliştirilmiş Cosh ve geliştirilmiş Kaiser pencereleri için optimum sonuçlar bulundu, ve sonra benzeşim sonuçları gösterdi ki bu iki geliştirilmiş pencere minimum geçirmeyen bant azaltması açısından Kaiser penceresine göre daha iyi sonuçlar sağlamaktadırlar.

Literatürde iyi bilinen pencere fonksiyonlarıyla yapılan karşılaştırmalar, önerilen geliştirilmiş Cosh ve geliştirilmiş Kaiser pencerelerinin sabit bir süzgeç derecesinde minimum geçirmeyen bant azaltması açısından en iyi kaliteyi, ayrıca sabit bir minimum geçirmeyen bant azaltmasında ise en düşük süzgeç derecesini sağlayabileceğini göstermektedir.

Anahtar Kelimeler: Yinelemesiz Sayısal Süzgeçler, Pencere Fonksiyonları, Üstel Pencere, Cosh Pencere, Geliştirilmiş Cosh Pencere, Geliştirilmiş Kaiser Pencere, Kaiser Pencere, Ultraspherical Pencere.

ACKNOWLEDGEMENTS

First of all, the author would like to express his sincere gratitude to his thesis supervisor, *Prof. Dr. Arif Nacaroğlu*, for his guidance, nurturing, encouragement, and support in every stage of this thesis. The author learned from him how to approach a problem, to ask relevant questions, how to make a plan and finally how to present useful results. His knowledge, kindness, patience, open-mindedness, and vision have provided the author with lifetime benefits.

The author would like to express his sincere gratitude and appreciation to the people from his doctoral thesis monitoring committee. *Prof. Dr. Muhammet Köksal* from the Department of Electrical and Electronics Engineering in Fatih University, and *Prof. Dr. Gülay Tohumoğlu* from the author's department guided him throughout his work. Their constructive criticisms, suggestions and comments for evaluating and improving this thesis were extremely valuable for him.

The author would like to express his special thanks to the people, especially *Özhan Koca* and *Fatih Çilek*, from the Department of Electronics Engineering in the University of Erlangen-Nuremberg in Germany for their academic support and friendships.

Special thanks to his colleagues *Amira Tandiroviç Gürsel*, *Berrin Süslüoğlu* and *Hasari Karci*. They shared not only a room but also very good moments.

The author extends his thanks and appreciation to his family, especially his mother *Gafure* and his father *Abuzer*, for their continual encouragement and support. They always kept him away from family responsibilities and encouraged him to concentrate on his study.

The author dedicated this thesis to the memories of his elderly brother, *Haydar Avci*, who died on 31st October 2003, due to a tragic traffic accident, and his younger brother, *Tacim Avci*, who died on 9th July 1995, due to being leukemia.

ABSTRACT	i
ÖZET	iii
ACKNOWLEDGEMENTS	v
CONTENTS	vi
LIST OF FIGURES	ix
LIST OF TABLES	xiv
LIST OF SYMBOLS AND ABBREVIATIONS	xvi
CHAPTER 1: INTRODUCTION	1
1.1. Background	1
1.2. Problem Definition	2
1.3. Thesis Objective	2
1.4. Literature Summary	2
1.5. Structure of Thesis	4
CHAPTER 2: REVIEW OF DIGITAL FILTERS	6
2.1. Introduction	6
2.2. Digital Filters	6
2.3. Types of Digital Filters	8
2.3.1. Recursive digital filters	8
2.3.2. Nonrecursive digital filters	9
2.3.3. Linear-phase nonrecursive digital filters	10
2.4. Digital Filters Design Methods	11
2.4.1. Recursive digital filters design methods	11
2.4.2. Nonrecursive digital filters design methods	13
2.5. Comparison of Recursive and Nonrecursive Digital Filters	15
CHAPTER 3: WINDOWING IN NONRECURSIVE FILTERS DESIGN	16
3.1. Introduction	16
3.2. Filter Design Using the Fourier Series	16
3.3. Gibbs' Phenomena	17
3.4. Nonrecursive Digital Filters Design Using the Windowing Method	18
3.5. Window Functions	19
3.5.1. Definition of window function	19
3.5.2. Spectral characteristic of windows	20
3.6. Well-Known Windows in Literature	22
3.6.1. Fixed windows	22
3.6.1.1. Rectangular window	22
3.6.1.2. Von Hann window	23
3.6.1.3. Hamming window	24
3.6.1.4. Blackman window	24
3.6.1.5. Spectral comparison of fixed windows	25
3.6.2. Adjustable windows	26
3.6.2.1. Dolph-Chebyshev window	27
3.6.2.2. Kaiser window	28
3.6.2.3. Saramaki window	29
3.6.2.4. Ultraspherical window	30
CHAPTER 4: PROPOSED WINDOW FUNCTIONS	33
4.1. Introduction	33
4.2. Exponential Window	33

4.2.1. Definition.....	33
4.2.2. Spectrum design equations	35
4.2.3. Spectrum comparisons.....	41
4.2.3.1. Comparisons with Kaiser window.....	41
4.2.3.2. Comparisons with Ultraspherical window	42
4.3. Cosh Window	44
4.3.1. Definition.....	44
4.3.2. Spectrum design equations	47
4.3.3. Spectrum comparisons.....	52
4.3.3.1. Comparisons with Exponential and Kaiser windows	52
4.3.3.2. Comparisons with Ultraspherical window	54
4.3.3.3. Comparison with the combinational windows including Hamming Window	56
4.4. Modified Cosh Window.....	57
4.4.1. Definition.....	57
4.4.2. Spectrum design equations	58
4.4.3. Spectrum comparisons with Cosh and Kaiser windows.....	62
4.5. Modified Kaiser Window	66
4.5.1. Definition.....	66
4.5.2. Spectrum design equations	67
4.5.3. Spectrum comparisons.....	70
4.5.3.1. Comparisons with modified Cosh and Kaiser windows.....	70
4.5.3.2. Comparisons with Ultraspherical window	72
CHAPTER 5: NONRECURSIVE FILTERS DESIGN USING THE PROPOSED WINDOW FUNCTIONS	73
5.1. Introduction.....	73
5.2. Nonrecursive Filters Design Using the Exponential Window	73
5.2.1. Filter design equations.....	74
5.2.2. Filter spectrum comparisons with Kaiser window	79
5.3. Nonrecursive Filters Design Using the Cosh Window	81
5.3.1. Filter design equations.....	82
5.3.2. Filter spectrum comparisons with Exponential and Kaiser windows.....	87
5.4. Nonrecursive Filters Design Using the Modified Cosh Window	88
5.4.1. Optimal filter design by the modified Cosh window	89
5.4.2. Filter spectrum comparisons with Cosh, Exponential and Kaiser windows	92
5.5. Nonrecursive Filters Design Using the Modified Kaiser Window	92
5.5.1. Optimal filter design by the modified Kaiser window	94
5.5.2. Filter spectrum comparisons with modified Cosh, Cosh, Exponential and Kaiser windows	96
5.5.3. Filter length comparison with modified Cosh, Cosh, Exponential and Kaiser windows	97
5.6. Comparison Examples for the Filters Designed by the Proposed and Well- Known Windows.....	98
5.6.1. Comparison example for minimum stopband attenuation quality	98
5.6.2. Comparison example for filter order	103
CHAPTER 6: CONCLUSIONS AND FUTURE WORKS.....	107

6.1. Conclusions to Spectrum Analysis of the Proposed Windows	107
6.2. Conclusions to Nonrecursive Filters Design Using Proposed Windows.	109
6.3. Recommendations for Future Work	111
REFERENCES	113
APPENDIX: MATLAB PROGRAMS	117
A.1. Matlab Program for the Proposed Windows.....	117
A.2. Matlab Programs for the Ultraspherical Window.....	120
CURRICULUM VITAE	125

LIST OF FIGURES	Page
Figure 2.1 Lowpass filter amplitude specifications	7
Figure 3.1 Amplitude responses of the lowpass filter for $N = 11, 31,$ and 51	18
Figure 3.2 A typical normalized window function plotted for $N = 31$	20
Figure 3.3 A typical window's normalized logarithmic amplitude spectrum.....	21
Figure 3.4 Four common fixed windows in time domain for $N = 51$	23
Figure 3.5 Spectrums of four common fixed windows for $N = 51$	25
Figure 3.6 Dolph-Chebyshev window spectrums for various R with $N = 51$	27
Figure 3.7 Relation between α_k and R for the Kaiser window with $N = 51$ and 101	29
Figure 4.1 Amplitude characteristics of the functions $\exp(x)$ and $I_0(x)$	33
Figure 4.2 Exponential window in time domain for $\alpha_e = 0, 2, 4, 6,$ and 8 with $N =$ 51	34
Figure 4.3 Exponential window spectrums in dB for $\alpha_e = 0, 2,$ and 4 with $N = 51$..	35
Figure 4.4 Relation between α_e and R for the Exponential window with $N = 51$ and 101	36
Figure 4.5 Approximated model for α_e of the Exponential window with $N = 101$..	37
Figure 4.6 Error curve of approximated α_e versus R for $N = 101$	37
Figure 4.7 Relation between D_w and R for the Exponential window with $N = 51$ and 101	38
Figure 4.8 Approximated model for D_w of the Exponential window for $N = 101$...	39
Figure 4.9 Relative error of approximated D_w for the Exponential window in percent versus R with $N = 101$	39
Figure 4.10 Relation between D_w and S for the Exponential window with $N = 51$ and 101	40
Figure 4.11 Ripple ratio comparison between the Exponential and Kaiser windows for $N = 101$	41

Figure 4.12 Sidelobe roll-off ratio comparison between the Exponential and Kaiser windows for $N = 101$	42
Figure 4.13 Comparison of the Exponential and Ultraspherical windows for narrower mainlobe width and larger sidelobe roll-off ratio with $N = 51$..	43
Figure 4.14 Comparison of the Exponential and Ultraspherical windows for wider mainlobe width and smaller sidelobe roll-off ratio with $N = 51$	44
Figure 4.15 Amplitude characteristics of the functions $\cosh(x)$, $\exp(x)$ and $I_0(x)$	45
Figure 4.16 Cosh window in time domain for $\alpha_c = 0, 2, 4, 6,$ and 8 with $N = 51$	45
Figure 4.17 Computation time comparison between the Cosh and Kaiser windows for various window length.....	46
Figure 4.18 Cosh window spectrums in dB for $\alpha_c = 0, 2,$ and 4 with $N = 51$	47
Figure 4.19 Relation between α_c and R for the Cosh window with $N = 51$ and 101 ..	48
Figure 4.20 Approximated model for α_c of the Cosh window with $N = 101$	49
Figure 4.21 Error curve of approximated α_c versus R for $N = 101$	49
Figure 4.22 Relation between D_w and R for the Cosh window with $N = 51$ and 101	50
Figure 4.23 Approximated model for D_w of the Cosh window with $N = 101$	51
Figure 4.24 Relative error of approximated D_w for the Cosh window in percent versus R with $N = 101$	51
Figure 4.25 Relation between D_w and S for the Cosh window with $N = 51$ and 101	52
Figure 4.26 Ripple ratio comparison between the Cosh, Exponential and Kaiser windows for $N = 101$	53
Figure 4.27 Sidelobe roll-off ratio comparison between the Cosh, Exponential and Kaiser windows for $N = 101$	53
Figure 4.28 Comparison of the Cosh and Ultraspherical windows for narrower mainlobe width and smaller sidelobe roll-off ratio with $N = 51$	54
Figure 4.29 Comparison of the Cosh and Ultraspherical windows for wider mainlobe width and larger sidelobe roll-off ratio with $N = 51$	55
Figure 4.30 Comparison of the Cosh, Kaiser and combinational windows with the Hamming window for $N = 51$ and $w_R = 0.272$ rad/sample	56
Figure 4.31 Effect of ρ_{mc} on the modified Cosh window for $N = 51$ and $\alpha_{mc} = 2$	58

Figure 4.32 Effect of the adjustable parameters on the modified Cosh window for N = 51	59
Figure 4.33 Optimum modified Cosh windows for N = 51 and 101.....	60
Figure 4.34 Relation between α_{mc} and ρ_{mc} of the optimum modified Cosh window for N = 51 and 101	61
Figure 4.35 Ripple ratio comparison between the optimum modified Cosh, Kaiser and Cosh windows for N = 51.....	62
Figure 4.36 Ripple ratio comparison between the optimum modified Cosh, Kaiser and Cosh windows for N = 101.....	63
Figure 4.37 Spectrums of the modified Cosh, Kaiser and Cosh windows for R = - 60 dB and $w_R = 0.158$ rad/sample with enlarged figure around the first sidelobe	64
Figure 4.38 Effect of ρ_{mk} on the modified Kaiser window for N = 51 and $\alpha_{mk} = 2$...	67
Figure 4.39 Effect of the adjustable parameters on the modified Kaiser window for N = 51	68
Figure 4.40 Optimum modified Kaiser windows for N = 51 and 101	69
Figure 4.41 Relation between α_{mk} and ρ_{mk} of the optimum modified Kaiser window for N = 51 and 101.....	69
Figure 4.42 Ripple ratio comparison between the optimum modified Kaiser, modified Cosh and Kaiser windows for N = 51	71
Figure 4.43 Ripple ratio comparison between the optimum modified Kaiser, modified Cosh and Kaiser windows for N = 101	71
Figure 4.44 Ripple ratio comparison between the modified Kaiser and Ultraspherical windows for the same mainlobe width and sidelobe roll- off ratio with N = 51	72
Figure 5.1 Lowpass filters designed by the Exponential window for $\alpha_e = 0, 2,$ and 4 with N = 51	74
Figure 5.2 Relation between α_e and A_s for the Exponential window with N = 51 and 127	75
Figure 5.3 Approximated model for α_e of the Exponential window with N = 127...	75
Figure 5.4 Error curve of approximated α_e versus A_s for N = 127.....	76

Figure 5.5 Relation between D_f and A_s for the Exponential window with $N = 51$ and 127	77
Figure 5.6 Approximated model for D_f of the Exponential window with $N = 127$...	77
Figure 5.7 Relative error of approximated D_f for the Exponential window in percent versus A_s with $N = 127$	78
Figure 5.8 Relation between D_f and A_{ms} for the Exponential window for $N = 51$ and 127	79
Figure 5.9 Minimum stopband attenuation comparison of the filters designed by the Exponential and Kaiser windows for $N = 127$	80
Figure 5.10 Maximum stopband attenuation comparison of the filters designed by the Exponential and Kaiser windows for $N = 127$	80
Figure 5.11 Lowpass filters designed by the Cosh window for $\alpha_c = 0, 2,$ and 4 with $N = 51$	81
Figure 5.12 Relation between α_c and A_s for the Cosh window with $N = 51$ and 127	82
Figure 5.13 Approximated model for α_c of the Cosh window with $N = 127$	83
Figure 5.14 Error curve of approximated α_c versus A_s for $N = 127$	84
Figure 5.15 Relation between D_f and A_s for the Cosh window with $N = 51$ and 127	84
Figure 5.16 Approximated model for D_f of the Cosh window with $N = 127$	85
Figure 5.17 Relative error of approximated D_f for the Cosh window in percent versus A_s with $N = 127$	86
Figure 5.18 Relation between D_f and A_{ms} for the Cosh window for $N = 51$ and 127.	86
Figure 5.19 Minimum stopband attenuation comparison of the filters designed by the Cosh, Exponential and Kaiser windows for $N = 127$	87
Figure 5.20 Maximum stopband attenuation comparison of the filters designed by the Cosh, Exponential and Kaiser windows for $N = 127$	88
Figure 5.21 Lowpass filters designed by the modified Cosh window for various ρ_{mc} with $\alpha_{mc} = 2$ and $N = 51$	89
Figure 5.22 Effect of the adjustable parameters on the lowpass filters designed by the modified Cosh window for $N = 127$	90
Figure 5.23 Minimum stopband attenuation characteristic of the optimum filters designed by the modified Cosh window for $N = 51$ and 127	91

Figure 5.24 Relation between α_{mc} and ρ_{mc} of the modified Cosh window for the optimum filters with $N = 51$ and 127	91
Figure 5.25 Minimum stopband attenuation comparison of the filters designed by the optimum modified Cosh, two-parameter Cosh, Exponential and Kaiser windows for $N = 127$	92
Figure 5.26 Lowpass filters designed by the modified Kaiser window for various ρ_{mk} with $\alpha_{mk} = 2$ and $N = 51$	93
Figure 5.27 Effect of the adjustable parameters on the lowpass filters designed by the modified Kaiser window for $N = 127$	94
Figure 5.28 Minimum stopband attenuation characteristic of the optimum filters designed by the modified Kaiser window for $N = 51$ and 127	95
Figure 5.29 Relation between α_{mk} and ρ_{mk} of the modified Kaiser window for the optimum filters for with $N = 51$ and 127	96
Figure 5.30 Minimum stopband attenuation comparison of the filters designed by the four proposed windows and Kaiser window for $N = 127$	96
Figure 5.31 Minimum stopband attenuation comparison of the filters designed by the four proposed windows and Kaiser window with various filter length N and $\Delta w = 0.2$ rad/sample	98
Figure 5.32 Amplitude responses of the filters designed by (a) modified Cosh, modified Kaiser, and Ultraspherical windows, (b) Saramaki, Kaiser and Dolph-Chebyshev windows, (c) Cosh and Exponential windows for $w_{ct} = 0.5\pi$ rad/sample, $\Delta w = 0.248$ rad/sample and $N = 101$	100
Figure 5.33 Comparison of the filters designed by (a) modified Kaiser window, (b) Ultraspherical window, (c) Saramaki window, (d) Kaiser Window, (e) Dolph-Chebyshev window for $w_p = 1$ rad/sample, $w_{st} = 1.2$ rad/sample and $A_s = 80$ dB	105

LIST OF TABLES	Page
Table 2.1 Frequency responses of linear-phase nonrecursive digital filters for various cases.....	10
Table 3.1 Comparison of four common fixed windows for $N = 51$	26
Table 3.2 Comparison of four fixed windows in terms of the ripple ratio and mainlobe width for $N = 51$ and 101	26
Table 4.1 Data for the Exponential window spectrum for various α_e with $N = 51$...	35
Table 4.2 Data for the Exponential and Ultraspherical windows used in the first comparison example.....	42
Table 4.3 Data for the Exponential and Ultraspherical windows used in the second comparison example.....	43
Table 4.4 Data for the Cosh window spectrum for various α_c with $N = 51$	47
Table 4.5 Data for the Cosh and Ultraspherical windows used in the first comparison example.....	54
Table 4.6 Data for the Cosh and Ultraspherical windows used in the second comparison example.....	55
Table 4.7 Data for the comparison of the Cosh, Kaiser and combinational windows with the Hamming window for $N = 51$	57
Table 4.8 Data for the effect of ρ_{mc} on the modified Cosh window with $\alpha_{mc} = 2$ and $N = 51$	58
Table 4.9 Data for the effect of adjustable parameters on the modified Cosh window for $N = 51$	59
Table 4.10 Data for the window length comparison between Kaiser, Cosh and the modified Cosh windows for $R = -60$ dB and $w_R = 0.158$ rad/sample	63
Table 4.11 Data for the comparison of the windows in terms of the ripple ratio and contrast ratio with $N = 101$ and $w_R = 0.121$ rad/sample	65
Table 4.12 Data for the effect of ρ_{mk} on the modified Kaiser window with $\alpha_{mk} = 2$ and $N = 51$	66

Table 4.13 Data for the effect of adjustable parameters on the modified Kaiser window for $N = 51$	67
Table 5.1 Data for the lowpass filters designed by the Exponential window for various α_e with $N = 51$	74
Table 5.2 Data for the lowpass filters designed by the Cosh window for various α_c with $N = 51$	82
Table 5.3 Data for the lowpass filters designed by the modified Cosh window for various ρ_{mc} with $\alpha_{mc} = 2$ and $N = 51$	88
Table 5.4 Data for the effect of adjustable parameters on the lowpass filters designed by the modified Cosh window with $N = 127$	89
Table 5.5 Data for the lowpass filters designed by the modified Kaiser window for various ρ_{mk} with $\alpha_{mk} = 2$ and $N = 51$	93
Table 5.6 Data for the effect of adjustable parameters on the lowpass filters designed by the modified Kaiser window with $N = 127$	94
Table 5.7 Data for the minimum stopband attenuation comparison of the filters designed by the proposed and well-known windows with $w_{ct} = 0.5\pi$ rad/sample and $N = 101$	99
Table 5.8 Data for the spectrums of the windows used in the filter comparison example	102
Table 5.9 Data for the filter order comparison of the filters designed by proposed and well-known windows for $w_p = 1$ rad/sample, $w_{st} = 1.2$ rad/sample, and $A_s = 80$ dB	103

LIST OF SYMBOLS AND ABBREVIATIONS

n	Discrete time index
w	Angular frequency in rad/sample
z	Index for z - frequency domain
T	Sampling period in rad/sample
w_s	Sampling frequency
N	Window or filter length
w_R	Mainlobe half width in radians/sample
w_M	Mainlobe width
S	Sidelobe roll-off ratio in dB
R	Ripple ratio in dB
D_w	Normalized mainlobe width
$D_{w,Appr}$	Approximated normalized mainlobe width
D_f	Normalized transition width
$D_{f,Appr}$	Approximated normalized transition width
$A(w)$	Amplitude spectrum
$\theta(w)$	Phase spectrum
$H(z)$	Filter transfer function
$H(e^{jwT})$	Frequency spectrum of filter
$W(e^{jwT})$	Frequency spectrum of window
w_{ct}	Filter cut-off frequency in rad/sample
w_p	Filter passband frequency in rad/sample
w_{st}	Filter stopband frequency in rad/sample
Δw	Filter transition width in rad/sample
h_{nc}	Noncasual impulse response
h_{id}	Ideal impulse response
A_s	Minimum filter stopband attenuation in dB
A_{ms}	Maximum filter stopband attenuation in dB
$I_0(x)$	Modified Bessel function of first kind of zero order
$w_r(n)$	Rectangular window function
$w_{vh}(n)$	Von Hann window function
$w_h(n)$	Hamming window function
$w_b(n)$	Blackman window function
$w_{dc}(n)$	Dolph-Chebyshev window function
$w_k(n)$	Kaiser window function
$w_s(n)$	Saramaki window function
$w_u(n)$	Ultraspherical window function
$w_e(n)$	Exponential window function
$w_c(n)$	Cosh window function
$w_{mc}(n)$	Modified Cosh window function
$w_{mk}(n)$	Modified Kaiser window function

$\alpha_k, \alpha_e, \alpha_c$	Shape parameter for the Kaiser, Exponential and Cosh windows
$\alpha_{e,Appr}, \alpha_{c,Appr}$	Approximated values of α_e and α_c , respectively
α_{mc}, α_{mk}	Second shape parameter for the modified Cosh and modified Kaiser windows
ρ_{mc}, ρ_{mk}	Third shape parameter for the modified Cosh and modified Kaiser windows
DSP	Digital Signal Processing
FIR	Finite Impulse Response
IIR	Infinite Impulse Response
OPAMP	Operational Amplifier
OTA	Operational Transconductance Amplifier
CR	Contrast Ratio
STR	Sidelobe energy to total energy ratio

CHAPTER-1

INTRODUCTION

1.1 Background

Digital filters can be considered as the most important and frequently used elements in digital signal processing applications. They are classified as finite impulse response (FIR) and infinite impulse response (IIR) filters by the duration of their impulse response. Each FIR and IIR filters have advantages and disadvantages. Therefore, neither of them can be considered as best for all situations.

FIR filters are very popular because they can be designed as always stable and having exact linear phase. A disadvantage of FIR filters over IIR filters is their implementation complexity in case the filter order is very large. The implementations of FIR filters can be done using either recursive or nonrecursive techniques. But, a nonrecursive implementation guarantees a stable filter [1].

To design nonrecursive digital filters, there are many methods in literature such as optimization methods, numerical methods, discrete Fourier transform and Fourier series method [2]. Although optimum designs can be obtained by using the optimization methods, a large amount of computation is required and this makes the optimization methods unsuitable for real time applications [2]. On the other hand, Fourier series method with windowing is the most straightforward technique to design nonrecursive filters and involves a minimal amount of computation compared to other methods. The aim to use a window function (or window for short) in Fourier series method is to truncate and smooth the infinite duration impulse response of the ideal filter.

1.2 Problem Definition

In literature, many windows have been proposed to obtain better nonrecursive digital filters [3-14]. The windows are classified as fixed or adjustable according to having number of independent parameters in their functions [9, 15]. Due to their flexibility properties, the adjustable windows are preferred for practical applications. Despite of existing many windows in literature, the problem is that the filters designed by the windows are suboptimal [2], i.e, the filter order required to satisfy a given prescribed specifications is not the lowest. And, a higher order filter means more computations, more memory, more components and more power. Therefore, the researches focused on providing new adjustable windows to improve the filter spectral characteristics and to reduce the required filter order are ongoing.

1.3 Thesis Objective

The objective of this thesis research is to find a new adjustable window which enables the filter designer to provide a high quality nonrecursive digital filter by using a lower order compared to existing window functions in literature.

The Ultraspherical window has three independent parameters, and is shown to yield the lowest filter order and highest minimum stopband quality [14]. To achieve better results than the Ultraspherical window, the research is focused on providing three-parameter windows.

1.4 Literature Summary

Direct truncation of Fourier series causes the oscillations, and these oscillations were first explained mathematically by Gibbs in 1899 [16] and therefore they became called Gibbs' Oscillations.

To reduce the effects of Gibbs' oscillations for practical applications, one approach was proposed by Fejer in 1900 [17]. Then, Lanczos proposed a better smoothing approach than Fejer averaging approximation in 1956 [18]. These methods considered a function with only one jump discontinuity, but Gibbs' oscillations are characteristic of any truncated Fourier series regardless of the number of discontinuities [19].

Better smoothing operations are obtained by the window functions. Window functions are categorized as fixed or adjustable according to the number of independent parameters in their functions. The simplest one is the rectangular window, but it performs only direct truncation without smoothing effect. Some of the more popular fixed window functions are von Hann, Hamming and Blackman [2]. Since the fixed windows have only one parameter-namely the window length, they provide only one spectral characteristic for every length. Due to having the shortage of flexibility property, they are not useful as much as the adjustable windows for practical applications.

Dolph-Chebyshev window proposed by Dolph in 1946 [3] is an important two-parameter adjustable window. It produces the minimum mainlobe width for a specified maximum sidelobe level among the all windows in literature.

Kaiser window is another one of the most important adjustable windows in literature. In 1966, it was introduced by Kaiser [20]. It has two parameters and achieves close approximations to discrete prolate functions that have maximum energy concentration in the mainlobe. The filter design equations for the Kaiser window were published by Kaiser in 1974 [4]. It provides better results compared to Dolph-Chebyshev window for nonrecursive digital filter design applications.

In 1989 Saramaki proposed another two-parameter adjustable window which is also an approximation to discrete prolate functions like the Kaiser window [7]. The results published in [7] showed that the filters designed by the Saramaki window provided a better stopband attenuation than the filters designed by the Kaiser window. Unlike the Kaiser window, the Saramaki window has the advantage of having analytical expressions in both frequency and time domains and no power series expansions. But as a disadvantage its time domain function is based on the recursive expressions like the Dolph-Chebyshev window.

In literature many two-parameter adjustable windows have been proposed. Some of them are Poisson [21], Cauchy [21], Gaussian [21], Parzen-Cos⁶(πt) window family [13], but they don't provide better results than the Kaiser window for nonrecursive filter design. Therefore, only Dolph-Chebyshev, Kaiser and Saramaki as two-parameter windows will be taken into account for comparisons purpose.

In 2001, Deczky introduced the Ultraspherical windows, which are based on the Ultraspherical (or Gegenbauer) polynomials, for nonrecursive digital filter design [22]. These polynomials took attention after Deczky by some authors as well [23, 24]. But, the use of Ultraspherical windows in nonrecursive digital filter design was investigated in detail by Bergen and Antoniou [14]. They demonstrated that the three-parameter Ultraspherical window family yields a lower-order filter compared to the filters designed by the Saramaki, Kaiser and Dolph-Chebyshev windows. Also, it was shown in the same paper that for a fix filter order the Ultraspherical window family yields better stopband attenuation than the well known two-parameter windows. The Ultraspherical window family has an important property that the Saramaki and Dolph-Chebyshev windows are its special cases.

1.5 Structure of Thesis

The thesis is organized into six chapters, which can be described as follows:

Chapter 1. Introduction – This chapter gives an overview of thesis work, problem definition, research objective, prior works and thesis structure.

Chapter 2. Review of Digital Filters – Some background information about the digital filters and the advantages of the digital filters over the analog filters are explained in Section 2.2. The recursive and nonrecursive digital filters are defined in Section 2.3. The design methods for recursive and nonrecursive are discussed briefly in Section 2.4. The chapter is concluded with the last section that presents the comparison of recursive and nonrecursive digital filters.

Chapter 3. Windowing in Nonrecursive Filters Design – The use of Fourier series method in the design of nonrecursive digital filters is explained in Section 3.2. In the next section, the Gibbs' Phenomena which is the undesirable effect in Fourier series design method is discussed. The use of window functions in Fourier series method is explained in Section 3.4. The definition of a window function with its spectral characteristic is given in Section 3.5. The last section presents the well-known fixed and adjustable windows in literature.

Chapter 4. Proposed Window Functions – This chapter presents four proposed adjustable window functions. In Section 4.2 the Exponential window is defined, and its spectrum design equations are found. Also, the spectrum comparisons with the Kaiser and Ultraspherical windows are achieved. The next proposed window, namely Cosh window, is introduced in Section 4.3. Its spectrum design equations and the comparisons with the Kaiser and Exponential windows are performed in this section. The modified version of the Cosh window is given in Section 4.4. The effect of additional parameter on the window spectrum is analyzed, and then the optimum solutions for $N = 51$ and 101 are obtained. The spectrum comparisons are performed with the Cosh, Exponential and Kaiser windows. The chapter is concluded with the introduction of the modified Kaiser window in Section 4.5. The optimum solutions are obtained for $N = 51$ and 101 , and the comparisons are performed with the previous proposed windows, Kaiser and Ultraspherical windows.

Chapter 5. Nonrecursive Filters Design Using the Proposed Window Functions – This chapter presents the application of the four proposed windows in the design of nonrecursive digital filters. In Section 5.2, the filter design using the Exponential window is explained. The filter design equations are obtained, and comparisons with the Kaiser window in terms of the minimum and maximum stopband attenuations are performed. In the next section, the use of Cosh window is explained with providing the filter design equations. The filters designed by this window are compared with the filters designed by the Exponential and Kaiser windows. In Section 5.4, the filters designed by the modified Cosh window are discussed. The effect of additional parameter on the filter spectrum is given. The optimum solutions that yield best minimum stopband attenuation for the modified Cosh window for $N = 51$ and 127 are found. The filter design comparisons are performed with the Cosh, Exponential and Kaiser windows. The use of modified Kaiser window in the design of nonrecursive digital filters is presented in Section 5.5. Optimum solutions for $N = 51$ and 127 are found, and the comparisons with the three proposed and Kaiser windows are given. The last section presents two comparison examples between the four proposed and four well-known windows in literature in terms of minimum stopband quality and filter order.

Chapter 6. Conclusions and Future Works – This last chapter summarizes the thesis results and gives recommendation for further work.

CHAPTER-2

REVIEW OF DIGITAL FILTERS

2.1 Introduction

The chapter begins with some basics about the digital filters. The comparison with the analog filters is given. Then, recursive and nonrecursive digital filters are introduced. After that, the design methods for recursive and nonrecursive digital filters are discussed briefly. The chapter is concluded with the advantages and disadvantages of nonrecursive digital filters over recursive filters.

2.2 Digital Filters

Filters are circuits or devices such that their output gain and/or phase vary as a function of the frequency of the input. Due to having this frequency sensitivity, they are used to pass signals at selected frequencies and reject signals at other frequencies.

In terms of their operations, the filters can mainly be classified as

- Lowpass filters – allow the low frequency components below the cut-off frequency to pass and the high frequency components above the cut-off frequency to reject
- Highpass filters – allow the high frequency components above the cut-off frequency to pass and the low frequency components below the cut-off frequency to reject
- Bandpass filters – allow the frequency components inside a certain band to pass and the frequency components outside the band to reject
- Bandstop filters – allow the frequency components outside a certain band to pass and the frequency components inside the band to reject

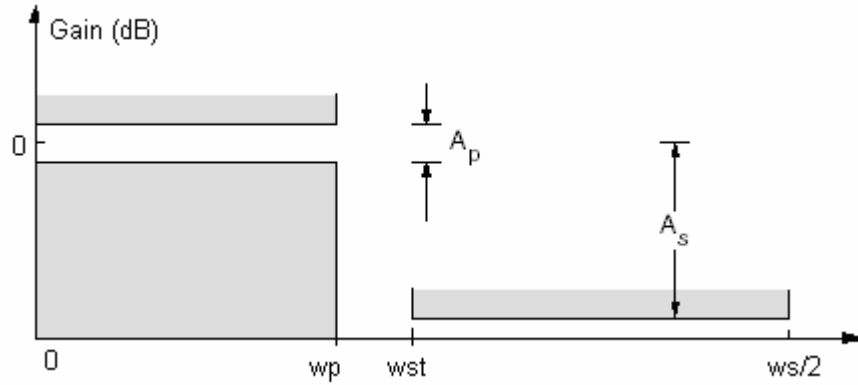


Figure 2.1 Lowpass filter amplitude specifications

Figure 2.1 shows the amplitude specifications of a lowpass filter. The parameters in the figure are

w_p = passband frequency

w_{st} = stopband frequency

w_s = sampling frequency

A_p = maximum allowable attenuation in passband

A_s = minimum allowable attenuation in stopband

Also, the cut-off frequency (w_{ct}) and the transition width (Δw) are two important parameters for a filter specification. They can be found from the following relations

$$w_{ct} = (w_{st} + w_p) / 2 \quad (2.1)$$

$$\Delta w = w_{st} - w_p \quad (2.2)$$

The filters are categorized as analog or digital according to their physical makeup and how they work. In an analog filter, analog electronic circuits which may be made up from passive and active components such as resistors, capacitors, operational amplifiers (OPAMP) or operational transconductance amplifiers (OTA) are used in order to produce the required filtering effect. There are well-established standard techniques to design an analog filter circuit for a given requirement. The signal being filtered in analog filters is an electrical voltage or current, which is the direct analogue of the physical quantity such as a sound signal or transducer output.

As for a digital filter, it uses a digital processor such as a personal computer or special digital signal processing chip to perform the filtering effect. Since the

operation is based on numerical calculations on sampled values of the signal, the analog input signal must first be sampled and digitized using an analog to digital converter. The resulting binary numbers representing the input signal are transferred to the processor, which carries out numerical calculations on them. Note that the signal in a digital filter is represented by a sequence of numbers rather than a voltage or current [25].

Main advantages of digital filters over analog filters can be listed as follows [26].

- A digital filter is *programmable*. This means that its operation is determined by a program stored in the processor's memory. Therefore, without changing the hardware, the digital filter can easily be changed. But, the circuit of an analog filter must be redesigned to change the operation.
- Digital filters are easily *designed, tested and implemented* on a processor.
- Digital filter characteristics are extremely stable with respect to temperature compared to analog filters.
- Digital filters can operate on *low frequency* signals accurately, unlike the analog filters.
- Digital filters are more *versatile* to process signals in a variety of ways. For example, adaptive digital filters can adapt to changes in the characteristics of the signal.

2.3 Types of Digital Filters

According to their implementations, the digital filters are classified as recursive and nonrecursive. Their brief definitions are given in the following subsections.

2.3.1 Recursive digital filters

The response of a causal recursive digital filter is defined by [27]

$$y(nT) = \sum_{k=0}^M a_k x[(n-k)T] - \sum_{k=1}^L b_k y[(n-k)T] \quad (2.3)$$

where $y(nT)$ is the output of the filter at discrete time instance n , a_k is the k -th feed forward filter coefficient, b_k is the k -th feed back filter coefficient, $y(n-k)$ is the filter input delayed by k samples, $x(n-k)$ is the filter input delayed by k samples, M is the order of numerator, and L is the order of denominator. Note that the output of a recursive filter at any instant depends on both the previous inputs and the previous outputs. The feedback mechanism is inherent in any recursive structure.

The transfer function of a causal recursive digital filter is defined as

$$H(z) = \frac{\sum_{k=0}^M a_k z^{-k}}{\sum_{k=1}^L b_k z^{-k}} \quad (2.4)$$

For causality, the degree of the denominator L must be equal or greater than that of the numerator M . The poles of the transfer function can be placed anywhere inside the unit circle.

2.3.2 Nonrecursive digital filters

A causal nonrecursive digital filter is defined mathematically as a convolution of N filter coefficients with a sequence of input data samples

$$y(nT) = \sum_{k=0}^{N-1} a_k x([n-k]T) \quad (2.5)$$

where $y(nT)$ is the output of the filter at discrete time instance n , a_k is the k -th feed forward filter coefficient, $x(n-k)$ is the filter input delayed by k samples, and N is the filter length which is the number of coefficients. Note that unlike the recursive filters, the filter output depends only on the previous inputs. This feature is why a nonrecursive digital filter has a finite duration impulse response.

The transfer function of an N -length causal nonrecursive digital filter is defined

$$H(z) = \sum_{n=0}^{N-1} h(nT) z^{-n} = \sum_{k=0}^{N-1} a_k z^{-k} \quad (2.6)$$

where $h(nT)$ is the impulse response of the filter. The poles of a nonrecursive filter transfer function are fixed at the origin in the unit circle.

The frequency response of the filter is given by

$$H(e^{j\omega T}) = M(\omega)e^{j\theta(\omega)} = \sum_{n=0}^{N-1} h(nT)e^{-j\omega nT} \quad (2.7a)$$

where $M(\omega)$ and $\theta(\omega)$ are the amplitude and phase responses of the filter, respectively. They are described as

$$M(\omega) = |H(e^{j\omega T})| \quad (2.7b)$$

$$\theta(\omega) = \arg H(e^{j\omega T}) \quad (2.7c)$$

2.3.3 Linear-phase nonrecursive digital filters

Nonrecursive filters can be designed to have linear or nonlinear phase responses. Linear phase digital filters allow all the frequency components of an input signal to pass through the filter with the same delay, which means that the group delay through the filter is a constant value independent of the frequency. Linear phase filters are useful in filtering applications in which you want to minimize signal spreading over time.

In order for a nonrecursive filter to be linear phase, its impulse response must be symmetric about its center point. Table 2.1 summarizes the frequency responses of linear phase nonrecursive filters for four cases [2].

Table 2.1 Frequency responses of linear-phase nonrecursive digital filters for various cases

Case	$h(nT)$	N	$H(e^{j\omega T})$
I	Symmetrical	Odd	$e^{-j\omega(N-1)T/2} \sum_{k=0}^{(N-1)/2} a_k \cos \omega kT$
II	Symmetrical	Even	$e^{-j\omega(N-1)T/2} \sum_{k=1}^{N/2} b_k \cos[\omega(k-1/2)T]$
III	Antisymmetrical	Odd	$e^{-j[\omega(N-1)T/2 - \pi/2]} \sum_{k=0}^{(N-1)/2} a_k \sin \omega kT$
IV	Antisymmetrical	Even	$e^{-j[\omega(N-1)T/2 - \pi/2]} \sum_{k=1}^{N/2} b_k \sin[\omega(k-1/2)T]$

The coefficients in Table 2.1 are

$$a_0 = h \left[\frac{(N-1)T}{2} \right], \quad a_k = 2h \left[\left(\frac{N-1}{2} - k \right) T \right], \quad b_k = 2h \left[\left(\frac{N}{2} - k \right) T \right] \quad (2.8)$$

According to the frequency responses given in Table 2.1, each case exhibit different properties with respect to the realizable filter characteristics.

- Case-I : There is no restriction for this case. Lowpass, highpass, bandpass and bandstop filters can be realized.
- Case-II: Only lowpass and bandpass filters can be realized. Since the frequency response at Nyquist frequency (π/T) is zero, highpass and bandstop filters cannot be realized for this case.
- Case-III: Only bandpass filter can be realized. Since the frequency response at Nyquist and dc frequencies is zero, lowpass, highpass and bandstop filters cannot be realized for this case.
- Case-IV: Only highpass and bandpass filters can be realized. Since the frequency response at dc frequency is zero, lowpass and bandstop filters cannot be realized for this case.

2.4 Digital Filters Design Methods

2.4.1 Recursive digital filters design methods

The design methods for recursive filters can be classified as indirect or direct. Indirect design approaches are based on deriving the discrete-time transfer function from a continuous-time transfer function, i.e., converting analog filter into a digital filter. However, direct design methods generate the discrete-time transfer function directly in z-domain.

In the indirect approach, first a continuous-time transfer function that satisfies certain specifications is obtained using one of the standard analog-filter approximations such as Butterworth and Chebyshev. Then a corresponding discrete-time transfer function is obtained using one of the following methods [2].

- Invariant impulse-response method
- Modified invariant impulse-response method
- Matched-z transformation
- Bilinear transformation

The obtained discrete time transfer function must satisfy the following realisability constraints.

- It must be a rational function of z with real coefficients
- Its poles must lie within the unit circle of the z plane
- The degree of the numerator polynomial must be equal to or less than that of the denominator polynomial.

The first constraint is due to the fact that the signal is assumed to be real and the digital filter elements such as unit delays, adders and multipliers perform the real arithmetic. The second constraint is required to have stability. And, the last one is required for causality property.

In the invariant impulse-response method, the objective is to design a recursive filter having unit sample response that is the sampled version of the impulse response of the analog filter. In order for this method to be sufficient the sampling period must be selected sufficiently small to completely avoid or at least minimize the effects of aliasing. Also, this method is inappropriate for designing highpass filters [28] and allpole filters-having only poles in the finite s plane due to spectrum aliasing that results from the sampling process [2].

The modified invariant impulse-response method overcomes the problem of designing allpole filters, and also can be applied to filters that have zeros in the finite s plane. The main problem of this method is the increase in the filter order in order to solve the stability problem. This makes the method uneconomical.

Matched-z transformation method is fairly simple to apply and gives reasonable results provided that a sufficiently large sampling frequency is used. Its main disadvantage is that it introduces a relatively large error in the passband loss.

Bilinear transformation method is one of the most important methods for the design of digital filters due to having some important advantages. This design method preserves the maxima and minima of the amplitude response and, as a consequence, passbands and stopbands in the analog filter translate into corresponding passbands and stopbands in the digital filter. Furthermore, the passband ripple and minimum stopband attenuation in the analog filter are preserved in the digital filter. And, the digital filter is stable if the analog filter is stable. The main problem of this method is warping effect which introduces frequency-scale distortion. Prewarping can be effected by choosing the parameters in the analog filter transformations appropriately [2].

An alternative approach for the design of recursive digital filters is the direct one. In this approach, optimization methods are generally used. In the optimization methods, a discrete-time transfer function is assumed and an error function is formulated on the basis of some desired amplitude and/or phase response. A norm of the error function is then minimized with respect to the transfer function coefficients. As the value of the norm approaches the zero, the resulting amplitude or phase response approaches the desired amplitude or phase response. These methods are iterative and, as a result, they usually involve a large amount of computation. However, unlike the indirect methods, they are suitable for the design of filters having arbitrary amplitude or phase responses. Furthermore, they often yield superior designs [2].

2.4.2 Nonrecursive digital filters design methods

Unlike the recursive filters, only direct methods are used for the design of nonrecursive digital filters. Four well-known methods are used. These methods are [2]:

- Fourier series method using the window method
- Numerical methods
- Discrete Fourier transform method
- Optimization methods

The first method provides closed form solutions and, as a result, it is easy to apply and involves only a minimal amount of computation. Unfortunately, the designs are suboptimal with respect to filter complexity whereby a filter design is said to be optimal if the filter order is the lowest that can be achieved for the required specifications [2]. The detailed explanation for this method is given in Chapter 3.

Numerical methods use numerical formulas to design the nonrecursive filters that can perform interpolation, differentiation or integration. The most fundamental numerical formulas are the formulas for interpolation since they form the basis of many other formulas, including formulas for differentiation and integration. The most commonly used interpolation formulas are the Gregory-Newton, Bessel, Everret, Stirling, and Gauss interpolation formulas. A nonrecursive filter is obtained by expressing one of the above numerical formulas in the form of difference equation [2].

The discrete Fourier transform method, unlike the Fourier series method with the window method, can be used for any given magnitude response. It is useful for the design of non-prototype filters where the desired magnitude response can take any irregular shape. But, there are some disadvantages with this method. For example, the frequency response obtained this method is equal to the desired frequency response only at the sampled points. At the other points, there will be a finite error present [29].

Optimization methods provide optimal solutions for the design of nonrecursive filters. But they perform this work at the expense of a huge amount of computation. The basic idea in the optimization methods is to find the filter coefficients until the particular error is minimized. There are various optimization methods as [29]

- Least squared error frequency domain design
- Weighted Chebyshev approximation
- Nonlinear equation solution for maximal ripple FIR filters
- Polynomial interpolation solution for maximal ripple FIR filters

For example, in weighted-Chebyshev method, an error function is formulated for the desired filter in terms of a linear combination of cosine functions and is then

minimized by using a very efficient multivariable optimization algorithm known as the *Remez exchange algorithm*. When convergence is achieved, the error function becomes equiripple as in other types of Chebyshev solutions [2]. The amplitude of the error in different frequency bands of interest is controlled by applying weighting to the error function. After the well-known *McClellan-parks-Rabiner* computer program [30] was provided for the design of nonrecursive filters, the optimization methods found widespread applications. Although the optimization methods yield optimum designs, they require a large amount of computation which makes them unsuitable for real time applications.

2.5 Comparison of Recursive and Nonrecursive Digital Filters

The main advantages of nonrecursive digital filters over the recursive filters can be listed as follows:

- They are simple to design.
- They are guaranteed to be stable.
- They can be guaranteed to have perfect linear phase. This is a desirable property for many applications such as music and video processing.
- They have a low sensitivity to filter coefficient quantization errors. This is an important property to have when implementing a filter on a DSP processor or on an integrated circuit.

The main disadvantage of nonrecursive digital filters over the recursive filters can be listed as follows:

- They require a higher order to perform the filtering. Higher order means more memory, more power and more processing time.

CHAPTER-3

WINDOWING IN NONRECURSIVE FILTERS DESIGN

3.1 Introduction

This chapter explains the Fourier series method with windowing for the design of nonrecursive digital filters. The chapter begins by examining the use of the Fourier series as a tool in the design of nonrecursive digital filters. It turns out that due to the Gibbs' phenomena Fourier series by itself does not yield good designs, but by applying the window technique in conjunction with the Fourier series some moderately successful approximations can be obtained. After the definition and spectral properties of window functions are introduced, the well known and mostly used windows in literature are given.

3.2 Filter Design Using the Fourier Series

The idea of using Fourier series in the design of filters comes from the fact that the frequency response of a nonrecursive filter is a periodic function of ω with period ω_s . Therefore, applying Fourier series for the frequency-domain representation of filters, it can be written as [2]

$$H(e^{j\omega T}) = \sum_{n=-\infty}^{\infty} h(nT)e^{-j\omega nT} \quad (3.1a)$$

where

$$h(nT) = \frac{1}{\omega_s} \int_{-\omega_s/2}^{\omega_s/2} H(e^{j\omega T}) e^{j\omega nT} d\omega \text{ and } \omega_s = \frac{2\pi}{T} \quad (3.1b)$$

By letting $e^{j\omega T} = z$ in Eq. (3.1a), the transfer function can be obtained as

$$H(z) = \sum_{n=-\infty}^{\infty} h(nT)z^{-n} \quad (3.2)$$

For a given frequency spectrum, $H(e^{j\omega T})$, a corresponding transfer function can be obtained using Eq. (3.1b) and Eq. (3.2). But, the obtained transfer function becomes noncausal and has an infinite order. In order to provide a finite order transfer function, the series in Eq. (3.2) can be truncated as

$$H(z) = \sum_{n=-(N-1)/2}^{(N-1)/2} h(nT)z^{-n} \quad (3.3)$$

where $h(nT) = 0$ is defined for the range $|n| > (N-1)/2$.

By expanding Eq. (3.3), it can be written as

$$H(z) = h(0) + \sum_{n=1}^{(N-1)/2} [h(-nT)z^n + h(nT)z^{-n}] \quad (3.4)$$

In order to make the transfer function causal, $H(z)$ is multiplied by $z^{-(N-1)/2}$. This multiplication changes the group delay by an amount of $(N-1)T/2$, but does not affect the amplitude response of the obtained filter.

3.3 Gibbs' Phenomena

Gibbs' phenomena are the observation of oscillations, known as *Gibbs' oscillations*, in the passband and stopband regions. These oscillations are resulted from the direct truncation of Fourier series for the design of nonrecursive filters. Figure 3.1 shows the amplitude responses of the lowpass filter designed by the Fourier series method for $N = 11, 31$ and 51 .

From Figure 3.1 it is observed that an increase in the window length results in a narrower transition width and an increase in the frequency of the passband and stopband oscillations. Also, the amplitudes of the oscillations are decreased at both low and high frequencies. But, the amplitudes of the last ripple in the passband and the first ripple in the stopband remain unchanged. Therefore, since the obtained filter characteristic is not good due to Gibbs' oscillations, the quality of the filter must be improved by reduction of Gibbs' oscillations.

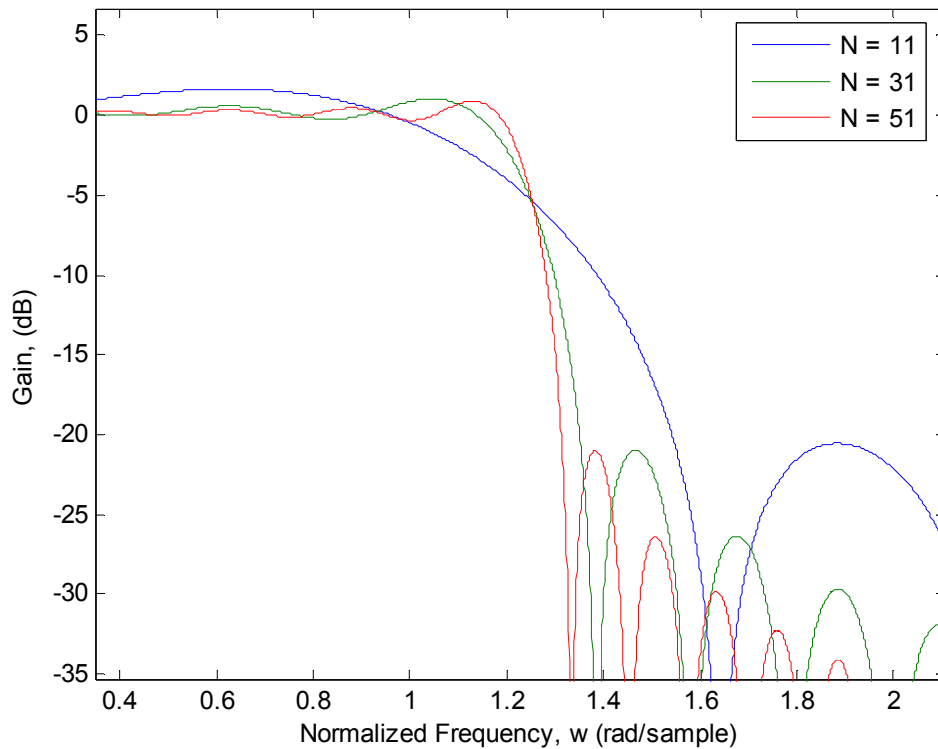


Figure 3.1 Amplitude responses of the lowpass filter for $N = 11, 31,$ and 51

3.4 Nonrecursive Digital Filters Design Using the Windowing Method

In the previous section, it is observed that the Fourier series method with direct truncation introduces the undesired Gibbs' oscillations in the amplitude response of the filters. To reduce these oscillations, the windowing method using the window functions is applied.

The design of nonrecursive digital filters using the window functions involves four general steps as follows:

- First, an idealized frequency response is assumed. Then, using Eq. (3.1) an idealized infinite-duration noncausal filter is obtained.
- To achieve the desired filter specifications, a suitable window is selected.
- The window function is constructed and applied.
- As a last step, the resulting finite-duration noncausal filter is converted into causal filter.

An ideal lowpass filter has a frequency response with a cut-off frequency w_{ct} and sampling frequency w_s as

$$H_{id}(e^{jwT}) = \begin{cases} 1 & \text{for } |w| \leq w_{ct} \\ 0 & \text{for } w_{ct} < |w| \leq w_s / 2 \end{cases} \quad (3.5)$$

The infinite-duration impulse response of the ideal noncausal lowpass filter is obtained by applying the Fourier series to Eq. (3.5). Straightforward analysis gives

$$h_{id}(nT) = \begin{cases} w_{ct}T / \pi & \text{for } n = 0 \\ \frac{\sin w_{ct}nT}{n\pi} & \text{for } n \neq 0 \end{cases} \quad (3.6)$$

Then, a finite-duration noncausal impulse response is obtained by applying a window $w(nT)$

$$h_{nc}(nT) = w(nT)h_{id}(nT) \quad (3.7)$$

Note that the multiplication of two discrete functions in time domain corresponds to the convolution of their spectrums in frequency domain. Therefore the equation above can be written as

$$H_{nc}(e^{jwT}) = W(e^{jwT}) \otimes H_{id}(e^{jwT}) \quad (3.8)$$

As explained in Section 3.2, delaying the noncausal impulse response $h_{nc}(nT)$ by a duration $(N-1)T/2$, a causal filter with N-length can be obtained as

$$h_c(nT) = h_{nc}[(n - (N-1)/2)T] \quad \text{for } 0 \leq n \leq N-1 \quad (3.9)$$

3.5 Window Functions

3.5.1 Definition of window function

The windowing method is used to reduce Gibbs' oscillations resulting from the truncation of a Fourier series by using a class of time-domain functions - known as window functions. A typical normalized window function in discrete time domain is shown in Figure 3.2. A *window function* (or simply *window*), $w(nT)$, with an odd length of N is a time domain function which is nonzero for $|n| \leq (N-1)/2$ and zero for otherwise. Although the formalism in this thesis only report on odd length windows, the results can be generalized to even length windows.

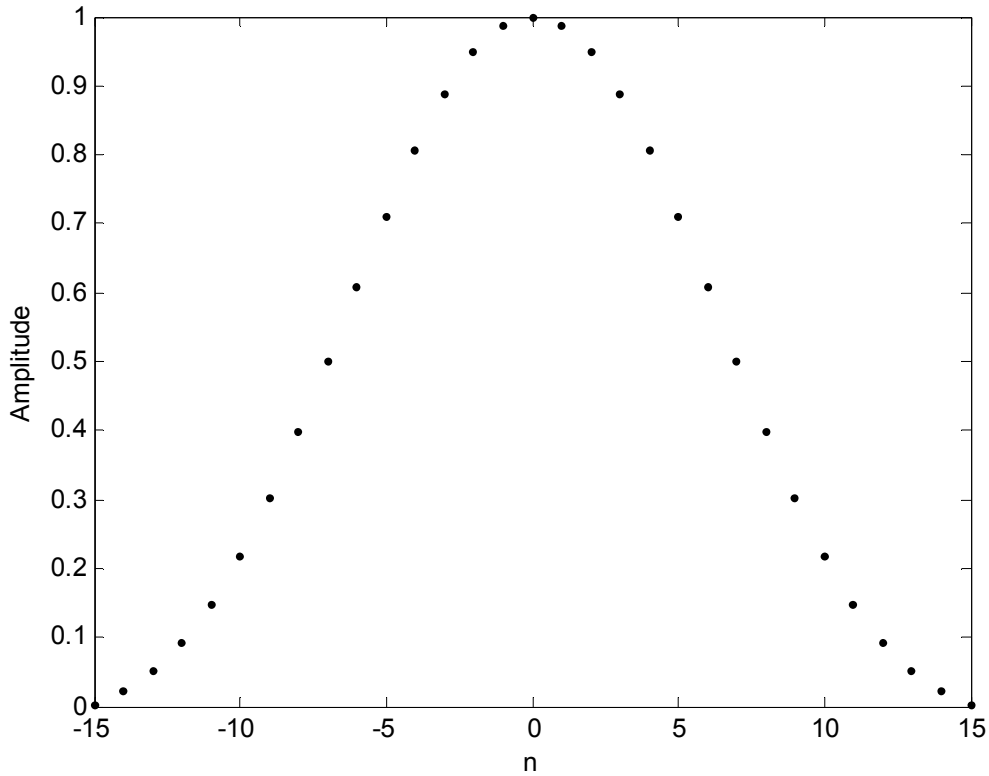


Figure 3.2 A typical normalized window function plotted for $N = 31$

3.5.2 Spectral characteristic of windows

Windows are generally classified and compared in terms of their spectral characteristics. The frequency spectral representation of a window $w(nT)$ of length N over the range $|n| \leq (N-1)/2$ is given by

$$W(e^{j\omega T}) = \sum_{n=-(N-1)/2}^{(N-1)/2} w(nT)e^{-j\omega nT} \quad (3.10)$$

Rearranging Eq. (3.10) for the symmetric windows, the frequency spectrum becomes

$$W(e^{j\omega T}) = A(\omega)e^{j\theta(\omega)} = w(0) + 2 \sum_{n=1}^{(N-1)/2} w(nT) \cos \omega nT \quad (3.11)$$

where $A(\omega)$ and $\theta(\omega)$ are the amplitude and phase spectrums of a window, respectively. And, T is the interval between samples.

A typical window has a normalized amplitude spectrum in dB range as shown in Figure 3.3.

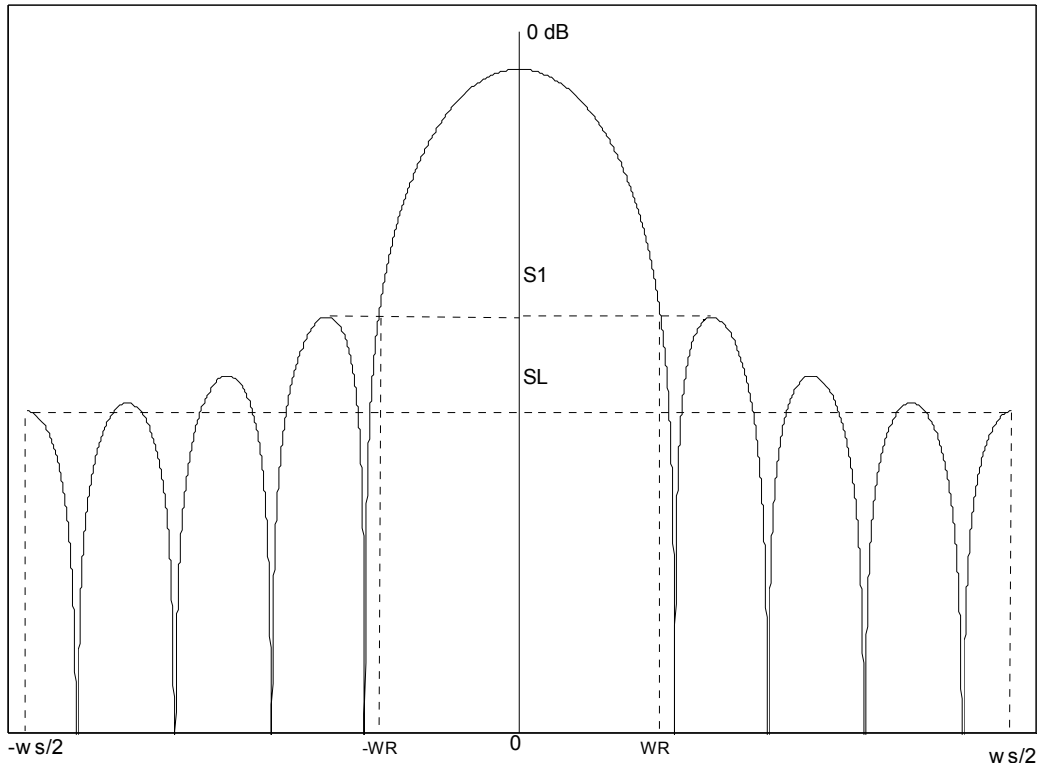


Figure 3.3 A typical window's normalized logarithmic amplitude spectrum

The normalized amplitude spectrum shown by Figure 3.3 can be obtained by the following equation

$$\left| W_N(e^{jwT}) \right| = 20 \log_{10} (|A(w)| / |A(0)|) \quad (3.12)$$

The common spectral characteristic parameters to distinguish the windows performance are mainlobe width (w_M), ripple ratio (R) and sidelobe roll-off ratio (S). From Figure 3.3, these parameters can be defined as

$$w_M = \text{Two times half mainlobe width} = 2w_R$$

$$R = \text{Maximum sidelobe amplitude in dB} - \text{Mainlobe amplitude in dB} = S_1$$

$$S = \text{Maximum sidelobe amplitude in dB} - \text{Minimum sidelobe amplitude in dB} \\ = S_1 - S_L$$

In spectrum analysis applications, the mainlobe width provides a resolution measure between adjacent signals while the ripple ratio determines the worst-case scenario for detecting weak signals in the presence of strong signals. And, the distribution of energy throughout the sidelobes is described by the sidelobe roll-off

ratio, which can be of importance if prior knowledge of the location of an interfering signal is known [19].

As for the filter design applications; the mainlobe width affects the transition width between the passband and stopband, the ripple ratio causes the ripples in the passband and stopband. And, the sidelobe roll-off ratio determines the distribution of stopband energy.

Good windows have the following properties:

- The mainlobe width should be narrow
- Ripple ratio should be small
- Sidelobe roll-off ratio should be large

Unfortunately, the first two requirements are contradictory [2].

Note that for the rest of the report, the sampling period (T) is considered as one.

3.6 Well-Known Windows in Literature

In literature, many windows have been proposed. They are classified as fixed or adjustable according to having number of independent parameters in their functions. Fixed windows have only one parameter, namely, the window length which controls the mainlobe width. Adjustable windows have two or more independent parameters, namely, the window length, as in fixed windows, and one or more additional parameters that can control other window characteristics.

3.6.1 Fixed windows

The most well-known and frequently used fixed windows are Rectangular, Von Hann, Hamming and Blackman. They are still in use for simple signal processing applications.

3.6.1.1 Rectangular window

The Rectangular window is the simplest one among all windows. As the name implies, it has a rectangular shape as shown in Figure 3.4. It is defined as [2]

$$w_r(n) = \begin{cases} 1 & |n| \leq \frac{N-1}{2} \\ 0 & \text{otherwise} \end{cases} \quad (3.13)$$

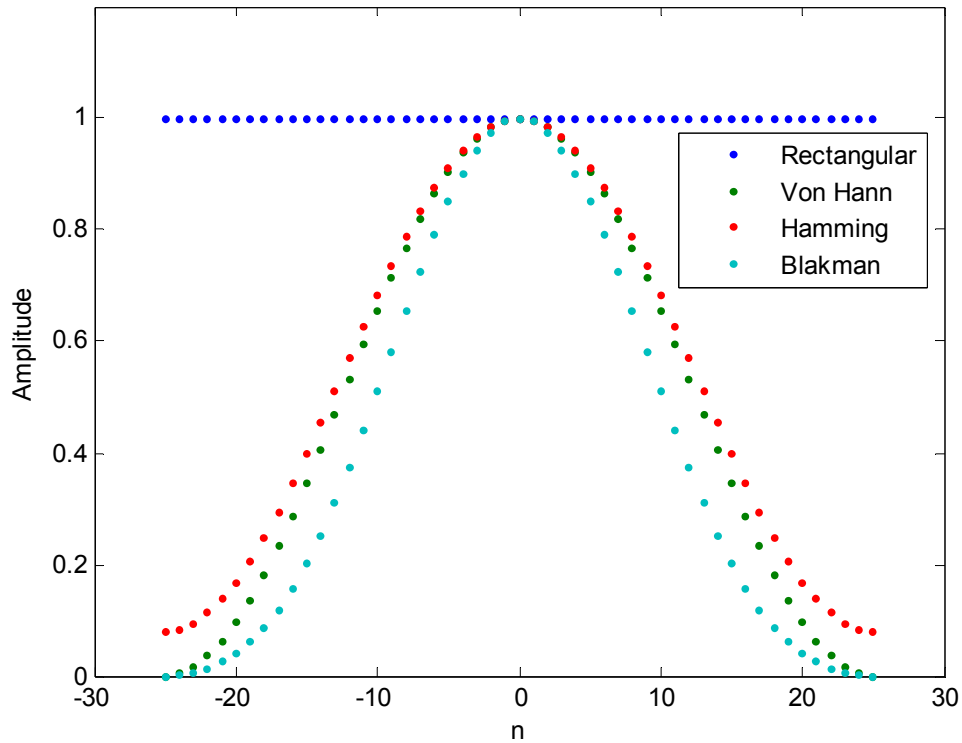


Figure 3.4 Four common fixed windows in time domain for $N = 51$

The frequency spectrum of the Rectangular window is

$$W_r(e^{j\omega T}) = \frac{\sin(\omega NT / 2)}{\sin(\omega T / 2)} \quad (3.14)$$

From Eq. (3.13) it is seen that the Rectangular window can be used for the direct truncation, but has no smoothing effect. The Rectangular window has the narrowest mainlobe width, but also has the largest ripple ratio among the windows.

3.6.1.2 Von Hann window

The Von Hann (or also known as Hanning) is proposed to have a better ripple ratio than the Rectangular window. It is plotted for $N = 51$ as shown in Figure 3.4 and defined by

$$w_{vh}(n) = \begin{cases} 0.5 + 0.5 \cos \frac{2\pi n}{N-1} & |n| \leq \frac{N-1}{2} \\ 0 & \text{otherwise} \end{cases} \quad (3.15)$$

And, the spectrum of Von Hann window is

$$W_{vh}(e^{j\omega T}) = 0.5 \frac{\sin(\omega NT/2)}{\sin(\omega T/2)} + 0.25 \left[\frac{\sin[\omega NT/2 - N\pi/(N-1)]}{\sin[\omega T/2 - \pi/(N-1)]} + \frac{\sin[\omega NT/2 + N\pi/(N-1)]}{\sin[\omega T/2 + \pi/(N-1)]} \right] \quad (3.16)$$

The Von Hann window has better ripple ratio than the Rectangular window, but its mainlobe width is two times wider.

3.6.1.3 Hamming window

The Hamming window shown in Figure 3.4 is similar to the Von Hann window, but the coefficients of the terms are rearranged to have a better ripple ratio. It is defined as

$$w_h(n) = \begin{cases} 0.54 + 0.46 \cos \frac{2\pi n}{N-1} & |n| \leq \frac{N-1}{2} \\ 0 & \textit{otherwise} \end{cases} \quad (3.17)$$

Its spectrum can be found as

$$W_h(e^{j\omega T}) = 0.54 \frac{\sin(\omega NT/2)}{\sin(\omega T/2)} + 0.23 \left[\frac{\sin[\omega NT/2 - N\pi/(N-1)]}{\sin[\omega T/2 - \pi/(N-1)]} + \frac{\sin[\omega NT/2 + N\pi/(N-1)]}{\sin[\omega T/2 + \pi/(N-1)]} \right] \quad (3.18)$$

The Hamming window provides better ripple ratio than the Von Hann window, and their mainlobe widths are almost the same.

3.6.1.4 Blackman window

The Blackman window shown in Figure 3.4 has an additional cosine term compared to the Von Hann and Hamming windows in order to have a better ripple ratio. It is defined as

$$w_b(n) = \begin{cases} 0.42 + 0.5 \cos \frac{2\pi n}{N-1} + 0.08 \cos \frac{4\pi n}{N-1} & |n| \leq \frac{N-1}{2} \\ 0 & \text{otherwise} \end{cases} \quad (3.19)$$

The frequency spectrum of the Blackman window can be found from

$$W_b(e^{j\omega T}) = 0.42W_r(e^{j\omega T}) + 0.25W_r(e^{j[\omega T - 2\pi/(N-1)]}) + 0.25W_r(e^{j[\omega T + 2\pi/(N-1)]}) \\ + 0.04W_r(e^{j[\omega T + 2\pi/(N-1)]}) + 0.04W_r(e^{j[\omega T - 2\pi/(N-1)]}) \quad (3.20)$$

The Blackman window has better ripple ratio than the previous fixed windows at the expense of having widest mainlobe width.

3.6.1.5 Spectral comparison of fixed windows

To observe the spectral differences of the fixed windows in terms of the mainlobe width, ripple ratio and sidelobe roll-off ratio, their spectrums are plotted for $N = 51$ as shown in Figure 3.5. From Figure 3.5 and Table 3.1 which summarizes the figure, it is seen that the Rectangular window has the narrowest mainlobe width, but has also the largest ripple ratio and smallest sidelobe roll-off ratio. The Von Hann

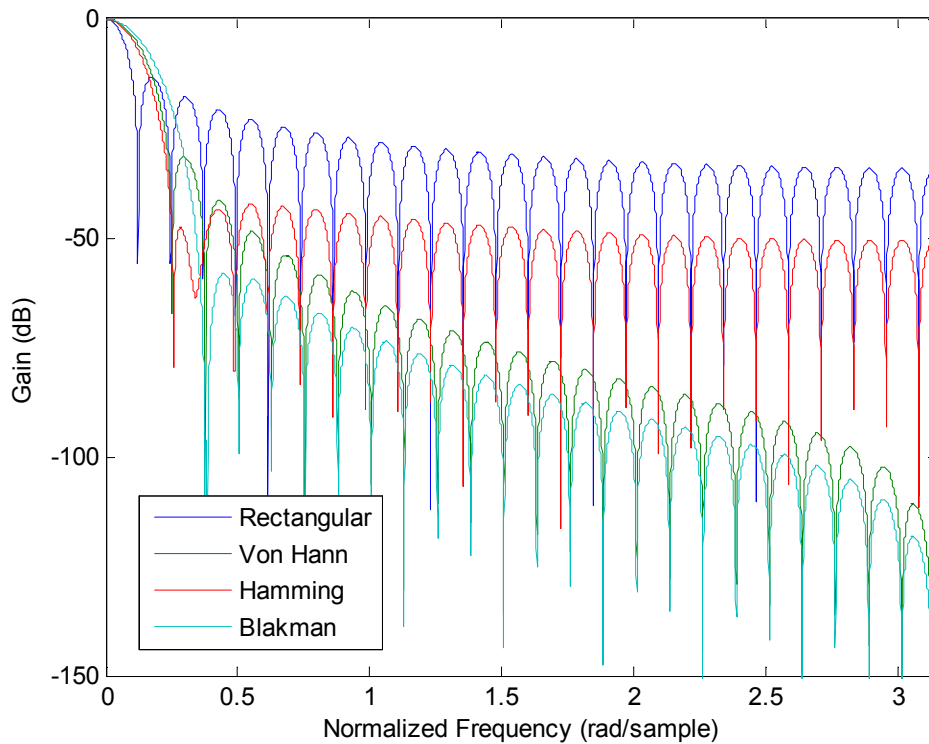


Figure 3.5 Spectrums of four common fixed windows for $N = 51$

window has better ripple ratio and sidelobe roll-off ratio than the Rectangular window, but its mainlobe width is wider. Hamming window has better ripple ratio compared to the Von Hann window at the expense of having a little wider mainlobe width. From Figure 3.5 it is observed that the largest sidelobe amplitude occurs at the first sidelobe for each window except the Hamming window in which it happens at the third sidelobe. Since the sidelobe pattern of the Hamming window is not monotonic, it is not suitable to define the sidelobe roll-off ratio for that window. As for the Blackman window, it has the best ripple ratio, but has also the worst mainlobe width. This example demonstrates that having a narrower mainlobe width and smaller ripple ratio for a window is contradictory as mentioned in Section 3.5.

Table 3.1 Comparison of four common fixed windows for $N = 51$

Window	N	w_R	R	S
Rectangular	51	0.1001	-13.25	20.90
Von Hann	51	0.2352	-31.47	79.32
Hamming	51	0.2440	-42.31	-
Blackman	51	0.3549	-58.11	60.16

To see the effect of the window length on the fixed windows, a simulation example is given below. It is observed that an increase in the window length results in a narrower mainlobe width for all fixed windows. Also, it is seen that the ripple ratio is almost independent from the window length.

Table 3.2 Comparison of four fixed windows in terms of the ripple ratio and mainlobe width for $N = 51$ and 101

Window type	R for $N = 51$	R for $N = 101$	w_R for $N = 51$	w_R for $N = 101$
Rectangular	-13.25	-13.26	0.1001	0.0506
Von Hann	-31.47	-31.47	0.2352	0.1176
Hamming	-42.31	-42.58	0.2440	0.1212
Blackman	-58.11	-58.11	0.3549	0.1774

3.6.2 Adjustable windows

The most well-known and frequently used adjustable windows are Dolph-Chebyshev, Kaiser, Saramaki and Ultraspherical. Only the Ultraspherical window has three independent parameters, while others have two.

3.6.2.1 Dolph-Chebyshev window

This window based on the Chebyshev polynomials is proposed by Dolph [3]. The independent parameters are the window length and the ripple ratio. The Dolph-Chebyshev window is defined as [2]

$$w_{dc}(n) = \frac{1}{N} \left[\frac{1}{r} + 2 \sum_{i=1}^{(N-1)/2} T_{N-1} \left(x_0 \cos \frac{i\pi}{N} \right) \cos \frac{2ni\pi}{N} \right] \quad (3.21a)$$

for $n = 0, 1, 2, \dots, (N-1)/2$ where

$$r = 10^{-R/20} \quad \text{and} \quad x_0 = \cosh \left(\frac{1}{N-1} \cosh^{-1} \frac{1}{r} \right) \quad (3.21b)$$

Function $T_k(x)$ is the k th-order Chebyshev polynomial of the first kind and is described as

$$T_k(x) = \begin{cases} \cos(k \cos^{-1} x) & |x| \leq 1 \\ \cosh(\cosh^{-1} x) & |x| \geq 1 \end{cases} \quad (3.21c)$$

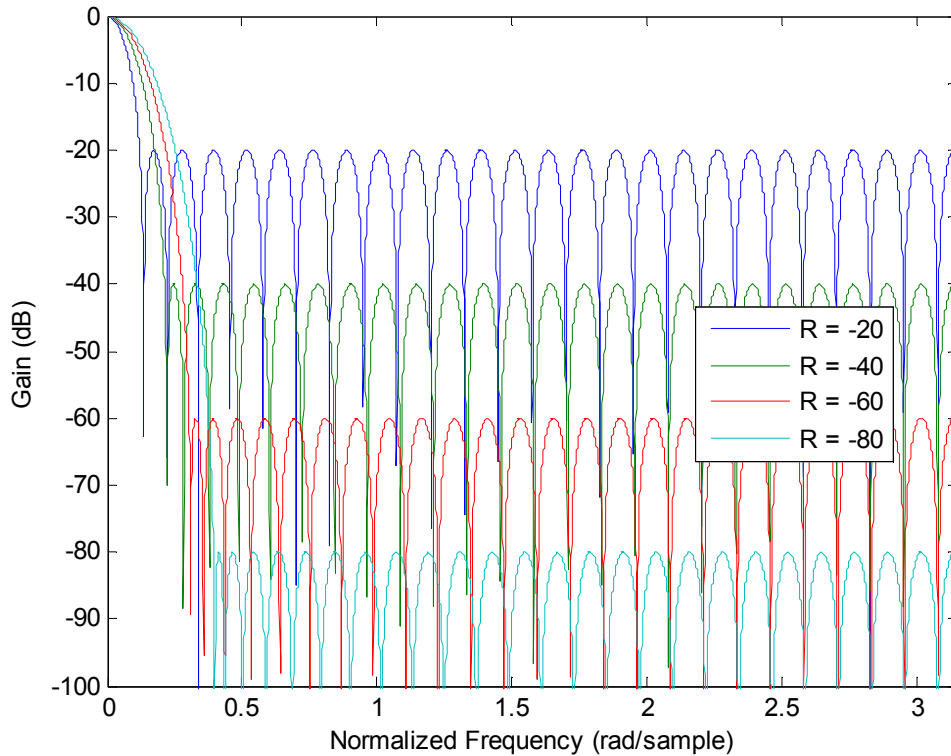


Figure 3.6 Dolph-Chebyshev window spectrums for various R with N = 51
The Dolph-Chebyshev window's spectrum can be found from

$$W_{DC}(e^{jwT}) = T_{N-1} \left[x_0 \cos \left(\frac{wT}{2} \right) \right] \quad (3.22)$$

Figure 3.6 shows the Dolph-Chebyshev window spectrums for different ripple ratio $R = -20, -40, -60$ and -80 dB for $N = 51$. It is obviously seen from the figure that the sidelobe pattern is fixed, that is, all sidelobes have the same amplitude for each window length. This window has an important property compared to the windows in literature that a minimum mainlobe width is achieved for a specified ripple ratio. Therefore, it is widely used for the beamforming applications in antenna theory.

3.6.2.2 Kaiser window

This window is proposed by Kaiser [20]. It has two independent parameters, namely the window length and the adjustable shape parameter α_k . The Kaiser window is defined by

$$w_k(n) = \begin{cases} \frac{I_0(\alpha_k \sqrt{1 - \left(\frac{2n}{N-1}\right)^2})}{I_0(\alpha_k)} & |n| \leq \frac{N-1}{2} \\ 0 & otherwise \end{cases} \quad (3.23a)$$

where α_k is the adjustable parameter, and $I_0(x)$ is the modified Bessel function of the first kind of order zero. The function $I_0(x)$ can be described by the power series expansion as

$$I_0(x) = 1 + \sum_{k=1}^{\infty} \left[\frac{1}{k!} \left(\frac{x}{2} \right)^k \right]^2 \quad (3.23b)$$

The Kaiser window for $\alpha_k = 0$ corresponds to the rectangular window. While an approximation closed formula for the Kaiser window spectrum exists [2], the exact Kaiser window spectrum can be obtained using Eq. (3.11).

Figure 3.7 shows the effect of the Kaiser window parameter, α_k , on the ripple ratio characteristic for $N = 51$ and 101 . It is clearly seen that as α_k becomes larger, the ripple ratio becomes smaller. Also, it is observed that the ripple ratio remains almost the same for a change in the window length. As known from the fixed windows,

while the window length increases, the mainlobe width of the Kaiser window decreases.

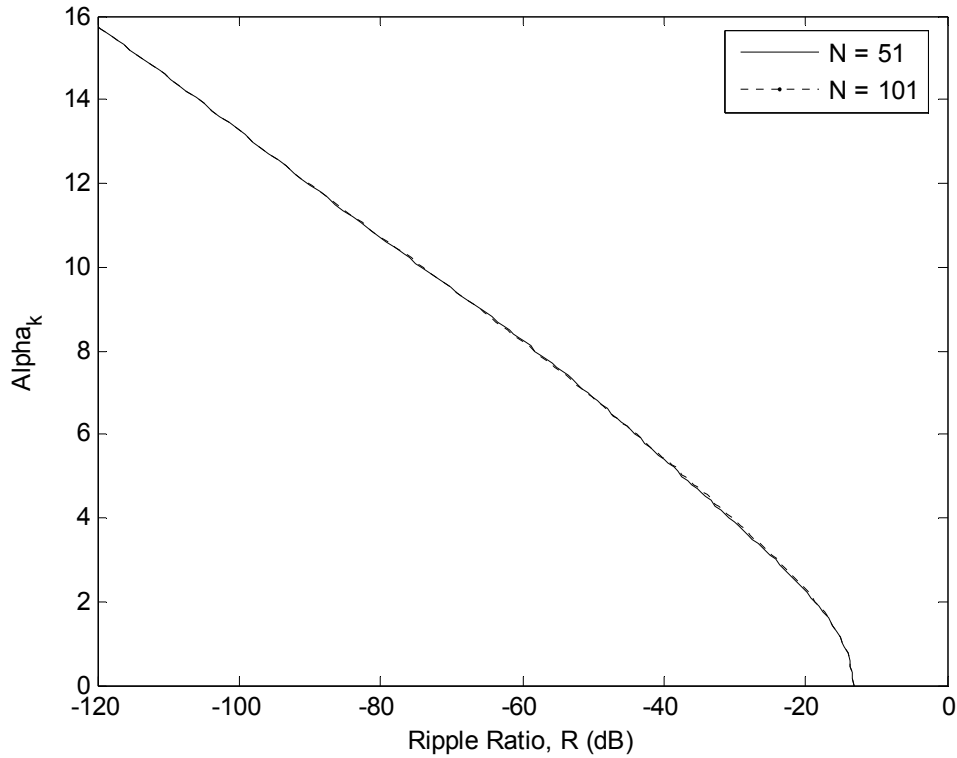


Figure 3.7 Relation between α_k and R for the Kaiser window with $N = 51$ and 101

Kaiser developed the relation between the shape parameter α_k and the ripple ratio as [31]

$$\alpha_k = \begin{cases} 0 & \text{for } R \leq 13.26 \\ 0.76609(R-13.26)^{0.4} + 0.09834(R-13.26) & \text{for } 13.26 < R \leq 60 \\ 0.12348(R+6.3) & \text{for } 60 < R \leq 120 \end{cases} \quad (3.24)$$

3.6.2.3 Saramaki window

This window is proposed by Saramaki [7] and like the Kaiser window it is a close approximation to the discrete prolate functions which minimize the sidelobe energy. In time domain, it is defined by the following recursive relations

$$w_s(n) = \begin{cases} \hat{w}(n) / \hat{w}(0) & |n| \leq (N-1)/2 \\ 0 & \text{otherwise} \end{cases} \quad (3.25a)$$

where

$$\hat{w}(n) = v_0(n) + 2 \sum_{k=1}^{(N-1)/2} v_k(n) \quad (3.25b)$$

$$v_0(n) = \begin{cases} 1 & n = 0 \\ 0 & \text{otherwise} \end{cases} \quad (3.25c)$$

$$v_1(n) = \begin{cases} \gamma - 1 & n = 0 \\ \gamma / 2 & |n| = 1 \\ 0 & \text{otherwise} \end{cases} \quad (3.25d)$$

$$v_k(n) = \begin{cases} 2(\gamma - 1)v_{k-1}(n) - v_{k-2}(n) + \gamma[v_{k-1}(n-1) + v_{k-1}(n+1)] & |n| \leq k \\ 0 & \text{otherwise} \end{cases} \quad (3.25e)$$

And, its frequency spectrum is

$$W_s(e^{jwT}) = \frac{\sin\left[\frac{(2M+1)}{2} \cos^{-1}[\gamma \cos w + (\gamma - 1)]\right]}{\sin\left[\frac{1}{2} \cos^{-1}[\gamma \cos w + (\gamma - 1)]\right]} \quad (3.26)$$

It is demonstrated in [7] that the Saramaki window minimizes the sidelobe energy better than Kaiser window. The main advantage of the Saramaki window over the Kaiser window is that it has analytic expressions in both time and frequency domains and no power series expansions are required in evaluating window function. But, it has also a disadvantage that its time domain function is based on the recursive equations whereas the Kaiser window is not.

3.6.2.4 Ultraspherical window

The coefficients of the N-length Ultraspherical window can be calculated by [32]

$$w_u(nT) = \frac{A}{p-n} \binom{\mu+p-n-1}{p-n-1} \sum_{m=0}^n \binom{\mu+n-1}{n-m} \binom{p-n}{m} B^m \quad \text{for } n = 0, 1, \dots, N-1 \quad (3.27a)$$

where

$$A = \begin{cases} \mu x_\mu^p & \text{for } \mu \neq 0 \\ x_\mu^p & \text{for } \mu = 0 \end{cases}, \quad B = 1 - x_\mu^{-2}, \quad p = N-1 \quad (3.27b)$$

This window has three independent parameters which are μ , x_μ , and N . With the appropriate selection of these parameters, Ultraspherical windows can be designed to achieve prescribed specifications for the sidelobe roll-off ratio, the ripple ratio and mainlobe width simultaneously. Parameter μ alters the sidelobe roll-off ratio, x_μ provides a trade-off between the ripple ratio and a width characteristic, and N allows different ripple ratios to be obtained for a fixed width characteristic and vice versa. The relationship between Ultraspherical window parameters μ , x_μ , and N and the prescribed specifications for the sidelobe roll-off ratio, the ripple ratio, and the width characteristic can be found in [32].

A normalized window function is obtained as

$$\hat{w}(nT) = w_u(nT) / w(CT) \quad (3.28a)$$

where

$$C = \begin{cases} \frac{N-1}{2} & \text{for odd } N \\ \frac{N}{2-1} & \text{for even } N \end{cases} \quad (3.28b)$$

The binomial coefficients in Eq. (3.27a) can be calculated as

$$\binom{\alpha}{0} = 1 \quad \binom{\alpha}{p} = \frac{\alpha(\alpha-1)\dots(\alpha-p+1)}{p!} \quad \text{for } p \geq 1 \quad (3.29)$$

The frequency spectrum of the Ultraspherical window is given by

$$W_u(e^{jwT}) = C_{N-1}^\mu \left[x_\mu \cos\left(\frac{wT}{2}\right) \right] \quad (3.30a)$$

where $C_n^\mu(x)$ is the Ultraspherical polynomial which can be calculated using the recurrence relationship

$$C_r^\mu(x) = \frac{1}{r} \left[2x(r+\mu-1)C_{r-1}^\mu(x) - (r+2\mu-2)C_{r-1}^\mu(x) \right] \quad (3.30b)$$

For $r = 2, 3, \dots, n$, where $C_0^\mu(x) = 1$ and $C_1^\mu(x) = 2\mu x$

The Dolph-Chebyshev window is the special case for $\mu = 0$, which results in

$$W_{dc}(e^{jwT}) = T_{N-1}\left[x_0 \cos\left(\frac{wT}{2}\right)\right] \quad (3.31)$$

where $T_n(x) = \cos(n \cos^{-1} x)$ is the Chebyshev polynomial of the first kind.

The Saramaki window is the special case for $\mu = 1$, which results in

$$W_s(e^{jwT}) = U_{N-1}\left[x_1 \cos\left(\frac{wT}{2}\right)\right] \quad (3.32a)$$

where

$$U_n(x) = \frac{\sin\left[(n+1)\cos^{-1} x\right]}{\sin\left(\cos^{-1} x\right)} \quad (3.32b)$$

is the Chebyshev polynomial of the second kind.

Bergen and Antoniou showed in [14] that the Ultraspherical window yields lower order filters (improved cost) relative to other windows. And, alternatively, the Ultraspherical window gives reduced passband ripple and increased attenuation (better performance) relative to other windows for a fixed filter length.

CHAPTER-4

PROPOSED WINDOW FUNCTIONS

4.1 Introduction

In this chapter, four proposed windows are introduced. Each window has been analyzed in detail. The spectrum design equations for the two-parameter proposed windows are obtained empirically with error analyses results. Moreover, the comparisons especially with the Kaiser and Ultraspherical windows are performed in terms of the spectral parameters.

4.2 Exponential Window

4.2.1 Definition

The simplest proposed window is based on the exponential function using the Kaiser approach. From Figure 4.1, it is seen that the functions $\exp(x)$ and $I_0(x)$ have

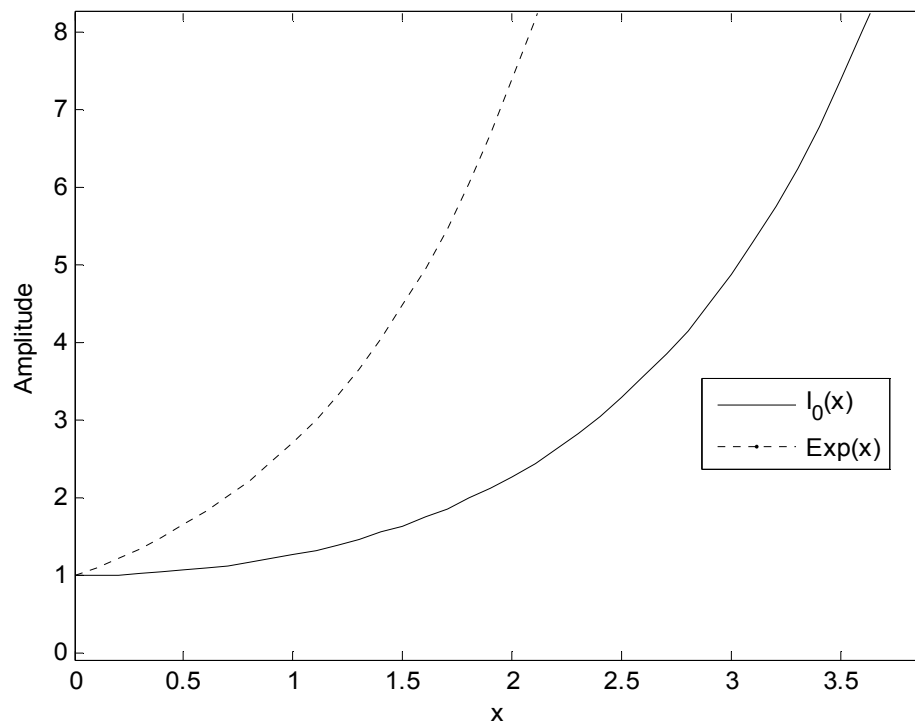


Figure 4.1 Amplitude characteristics of the functions $\exp(x)$ and $I_0(x)$

the same amplitude characteristic. Therefore, a new window - namely “*Exponential window*” for this report, is proposed as [33]

$$w_e(n) = \begin{cases} \frac{\exp\left(\alpha_e \sqrt{1 - \left(\frac{2n}{N-1}\right)^2}\right)}{\exp(\alpha_e)} & |n| \leq \frac{N-1}{2} \\ 0 & \text{otherwise} \end{cases} \quad (4.1)$$

Like the Kaiser window, the Exponential window has two independent parameters, namely the window length (N) and the adjustable shape parameter (α_e). Figure 4.2 shows the time domain characteristic of the Exponential window for various values of the parameter α_e with N = 51. It is seen that $\alpha_e = 0$ corresponds to the Rectangular window as in the case for the Kaiser window. For larger values of α_e , the Exponential window becomes to have a Gaussian shape.

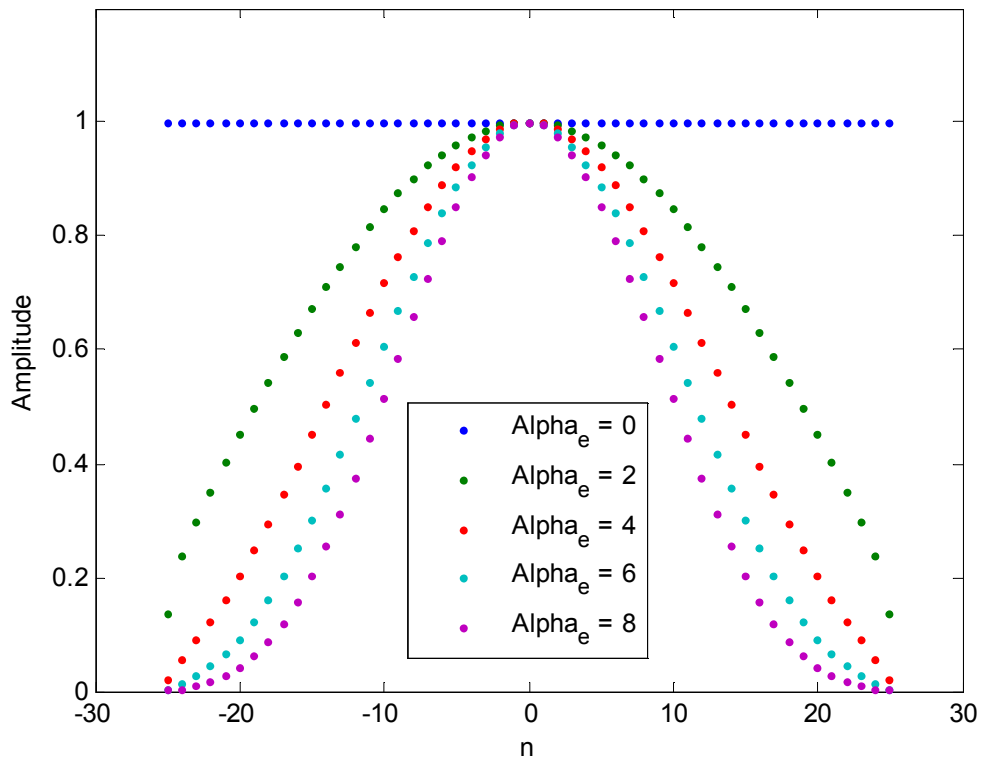


Figure 4.2 Exponential window in time domain for $\alpha_e = 0, 2, 4, 6,$ and 8 with $N = 51$

The spectrum of Exponential window can be found using Eq. (3.11). Figure 4.3 shows the effect of α_e on the Exponential window spectrum for a fixed value of length $N = 51$. And, Table 4.1 summarizes the numerical data in Figure 4.3. As it is seen from the figure and table, an increase in α_e results in a wider mainlobe width and a smaller ripple ratio.

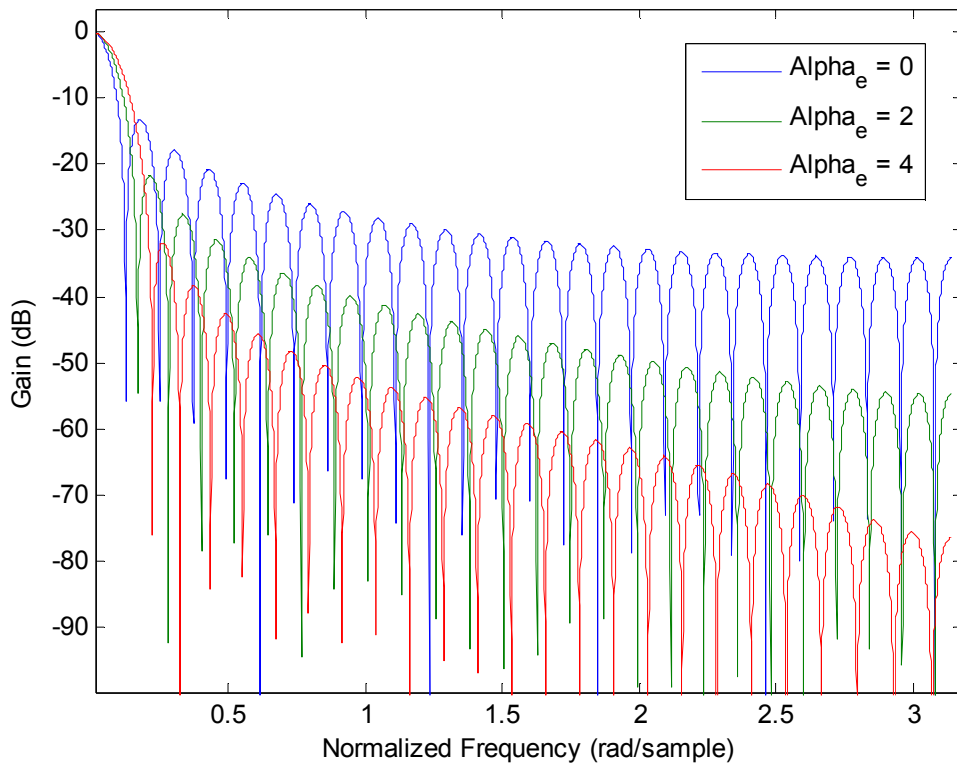


Figure 4.3 Exponential window spectrums in dB for $\alpha_e = 0, 2,$ and 4 with $N = 51$

Table 4.1 Data for the Exponential window spectrum for various α_e with $N = 51$

Window	N	α_e	w_R	R	S
Exponential-1	51	0	0.100	-13.25	20.90
Exponential-2	51	2	0.145	-21.73	32.95
Exponential-3	51	4	0.209	-31.84	44.54

4.2.2 Spectrum design equations

For some applications such as the spectrum analysis [2], the design equations which define the window parameters in terms of the spectral parameters are very useful to find the suitable window for given prescribed specifications. To obtain the spectrum design equations for the Exponential window, it is necessary to find the relations between the window parameters and spectral parameters empirically. Figure 4.4 shows the relation between α_e and the ripple ratio for the window lengths $N = 51$ and 101 .

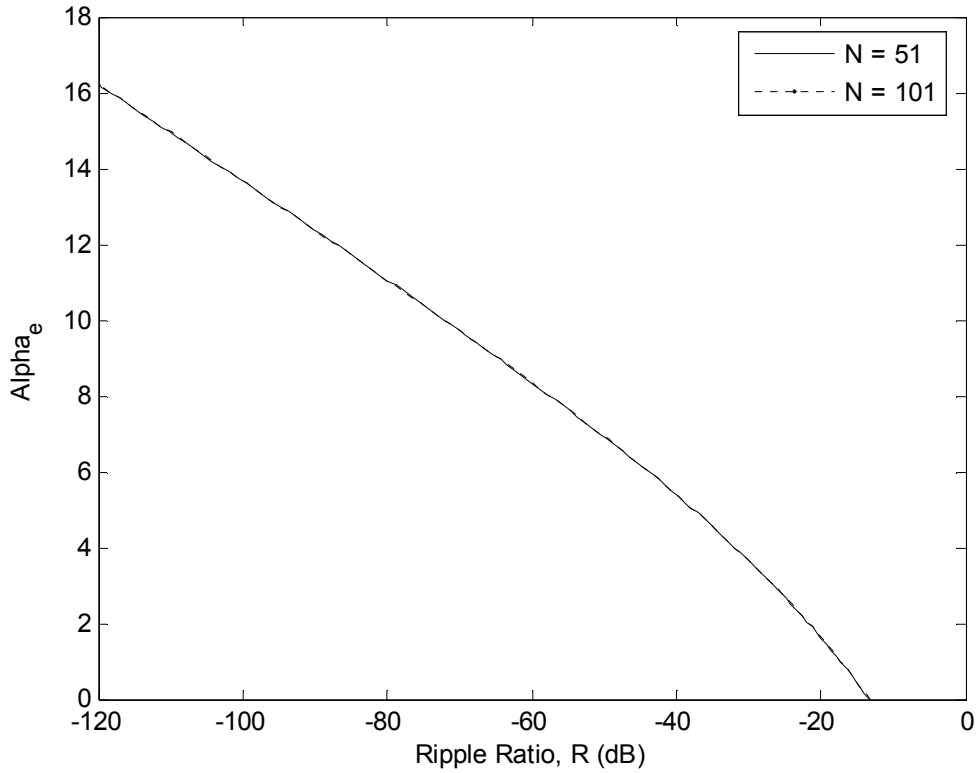


Figure 4.4 Relation between α_e and R for the Exponential window with N = 51 and 101

It is seen from Figure 4.4 that the window length parameter doesn't affect the relation between the adjustable parameter α_e and the ripple ratio. Therefore, using the curve fitting method in MATLAB, the first design equation for α_e in terms of the ripple ratio can be obtained as

$$\alpha_{e,Appr} = \begin{cases} 0 & R > -13.26 \\ -1.513 \times 10^{-3} R^2 - 0.2809 R - 3.398 & -50 < R \leq -13.26 \\ -1.085 \times 10^{-4} R^2 - 0.1506 R - 0.304 & -120 \leq R \leq -50 \end{cases} \quad (4.2)$$

The quadratic approximation model given by Eq. (4.2) for the adjustable parameter α_e is plotted in Figure 4.5. It is seen that the proposed model provides a good approximation for N = 101. Moreover, the approximation error for the first design equation for N = 101 is plotted in Figure 4.6. It is observed that the amplitude of deviations in the alpha is lower than 0.06 which corresponds to very small error in the ripple ratio. More accurate results can be obtained by restricting the range or using higher order approximations, but the proposed model for the Exponential window is adequate for most applications like the Kaiser model.

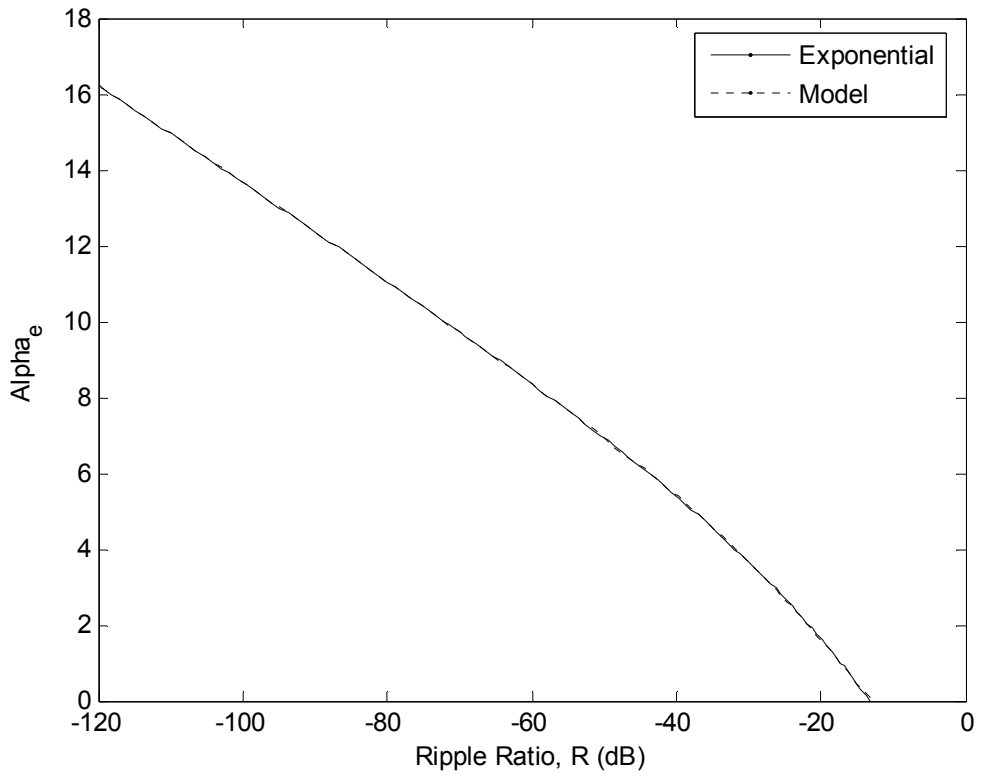


Figure 4.5 Approximated model for α_e of the Exponential window with $N = 101$

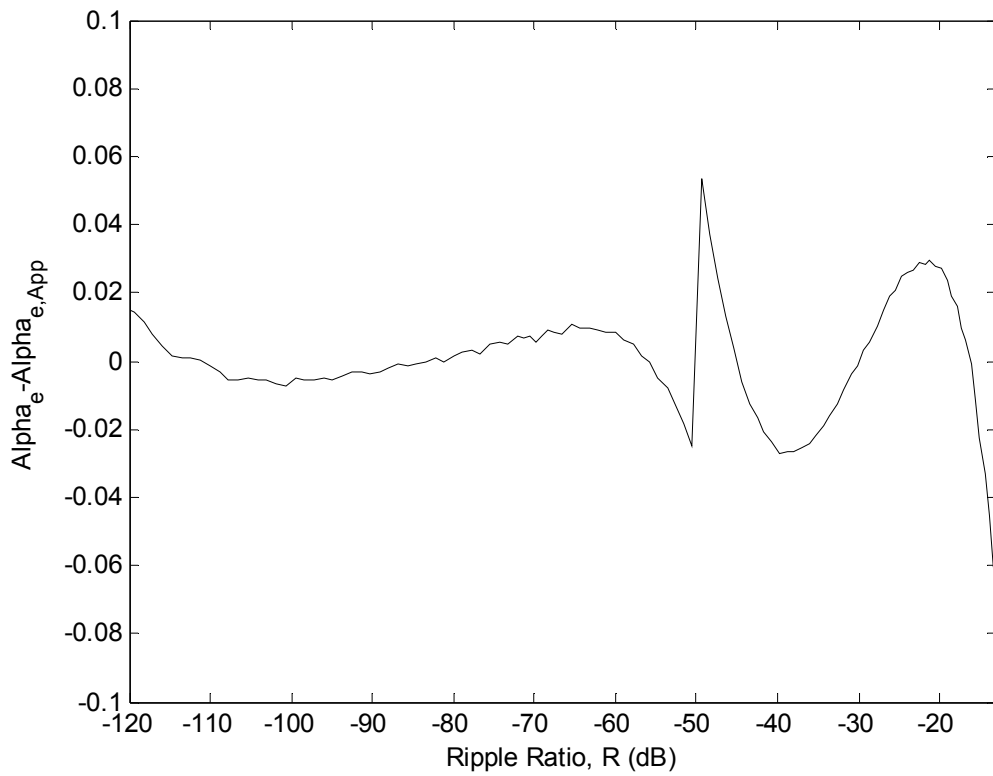


Figure 4.6 Error curve of approximated α_e versus R for $N = 101$

The second design equation is the relation between the window length and the ripple ratio. To predict the window length for a given quantities R and w_R , the normalized width parameter $D_w = 2w_R(N-1)$ is used [32]. The relation between D_w and R for the Exponential window with $N = 51$ and 101 is plotted in Figure 4.7.

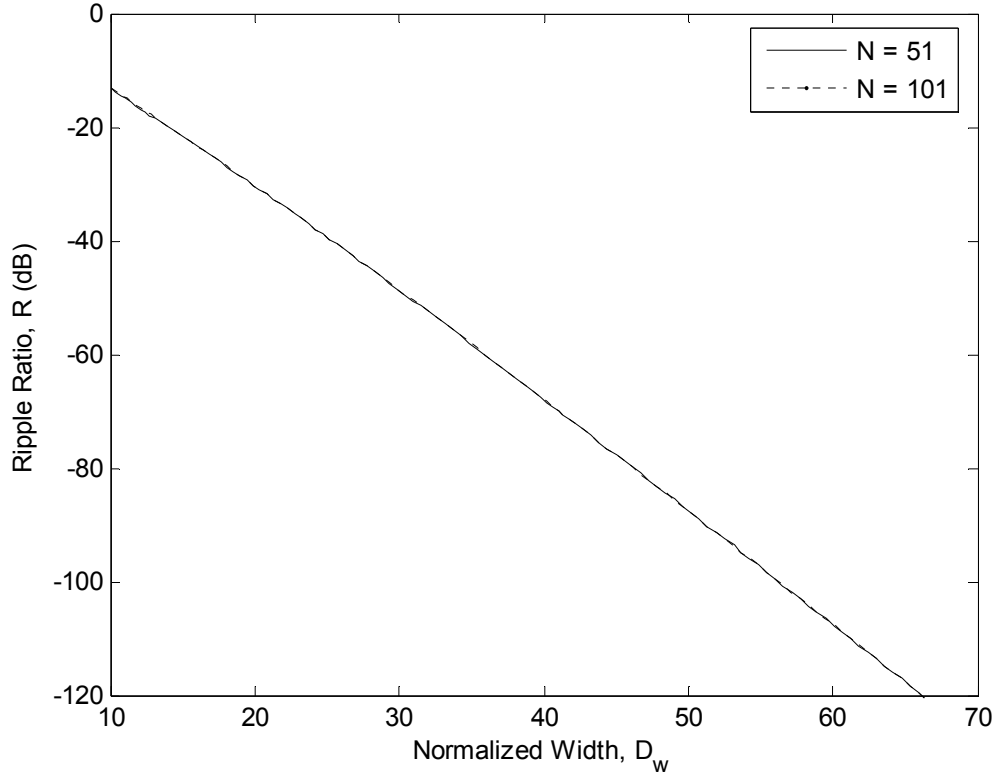


Figure 4.7 Relation between D_w and R for the Exponential window with $N = 51$ and 101

It is seen from Figure 4.7 that as the ripple ratio becomes smaller the mainlobe width becomes wider. Also, it is observed from the same figure that the window length has no effect on the relation between the ripple ratio and normalized mainlobe width. By using the curve fitting method, an approximate design relationship between the normalized width (D_w) and the ripple ratio (R) can be established as

$$D_{w,Appr} = \begin{cases} 0 & R > -13.26 \\ -7.58 \times 10^{-5} R^3 + 7.22 \times 10^{-3} R^2 - 0.3566R + 4.312 & -50 < R \leq -13.26 \\ -1.297 \times 10^{-4} R^2 - 0.5281R + 4.708 & -120 \leq R \leq -50 \end{cases} \quad (4.3)$$

The approximation model given by Eq. (4.3) for the normalized mainlobe width is plotted in Figure 4.8. It is seen that the proposed model provides a good approximation for $N = 101$.

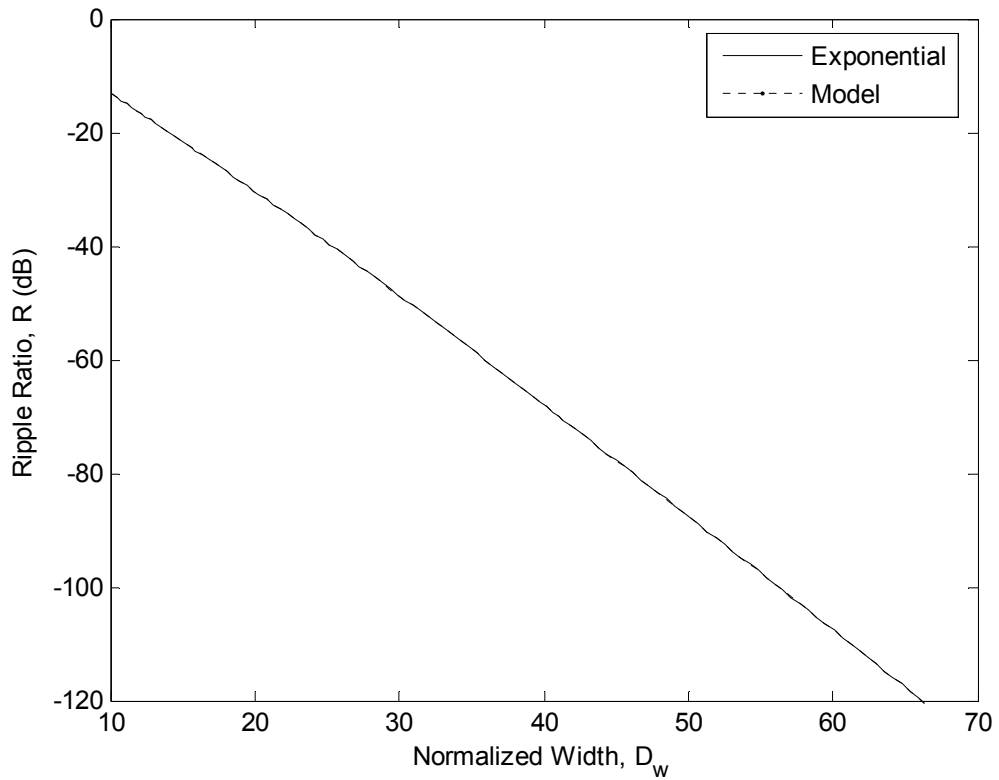


Figure 4.8 Approximated model for D_w of the Exponential window with $N = 101$

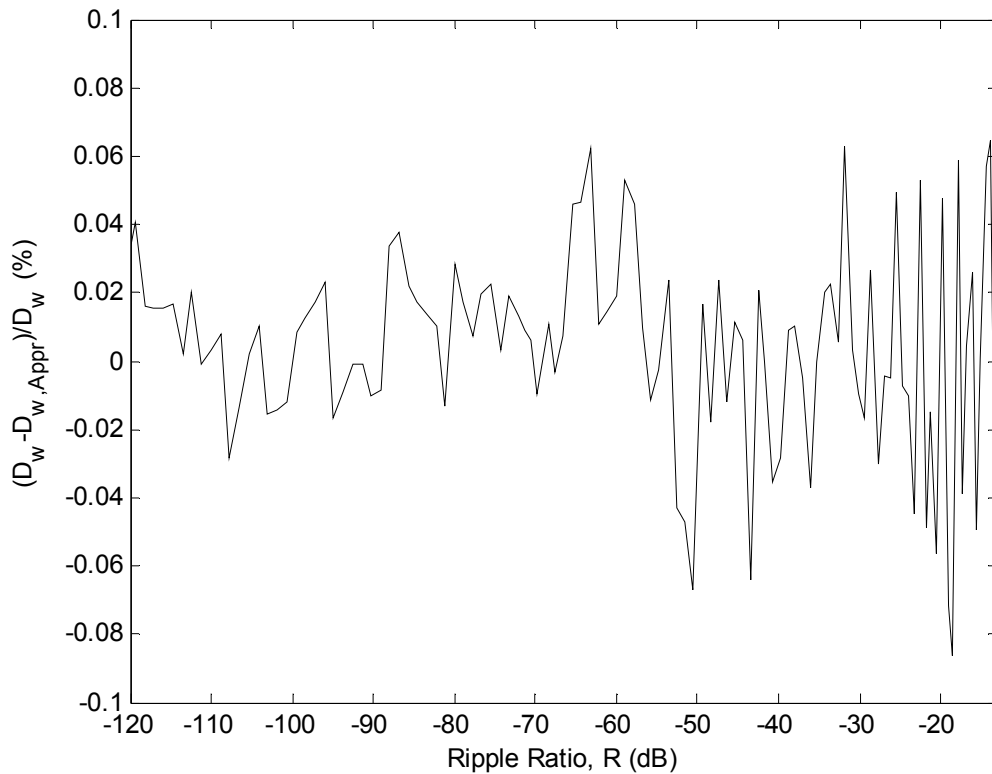


Figure 4.9 Relative error of approximated D_w for the Exponential window in percent versus R with $N = 101$

The relative error of approximated normalized width in percent versus the ripple ratio for $N = 101$ is plotted in Figure 4.9. The percentage error in the model changes

between 0.065 and -0.086. This error range satisfies the error criterion in [32] which states that the predicted error in the normalized width must be smaller than 1 %.

An integer value of the window length N can be predicted from [32]

$$N \geq \frac{D_w, Appr}{2w_R} + 1 \quad (4.4)$$

Using the equations (4.2) through (4.4), an Exponential window can be designed for satisfying the given prescribed values of the ripple ratio and mainlobe width.

In some applications [34], larger sidelobe roll-off ratio may be desired. Figure 4.10 shows the change in the sidelobe-roll off ratio in terms of the normalized mainlobe width parameter for $N = 51$ and 101 . From the figure it can be seen that the sidelobe roll off ratio becomes larger as normalized width increases until one of the sidelobes is dropped due to higher value of alpha. Unlike in the case of ripple ratio, a change in the window length affects significantly the sidelobe roll-off ratio characteristic of the Exponential window.

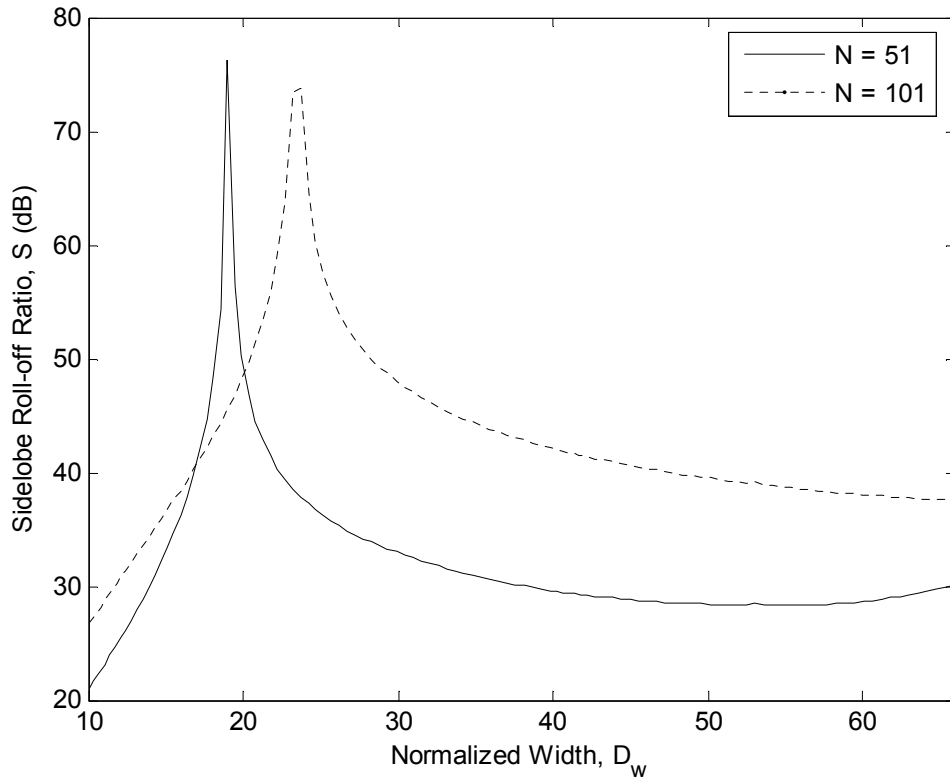


Figure 4.10 Relation between D_w and S for the Exponential window with $N = 51$ and 101

4.2.3 Spectrum comparisons

4.2.3.1 Comparisons with Kaiser window

To be able to make a comparison between the Exponential and Kaiser windows, it is necessary to plot their spectrums and compare their spectral characteristic parameters in terms of the ripple ratio, mainlobe width and sidelobe roll-off ratio. Figure 4.11 shows the comparison of the Exponential and Kaiser windows in terms of the ripple ratio versus normalized mainlobe width for $N = 101$. The figure can be read as follows: Kaiser window provides smaller ripple ratio than the Exponential window for the same mainlobe width, and the difference becomes larger as normalized width increases. Or, the Kaiser window yields narrower mainlobe width for the same ripple ratio.

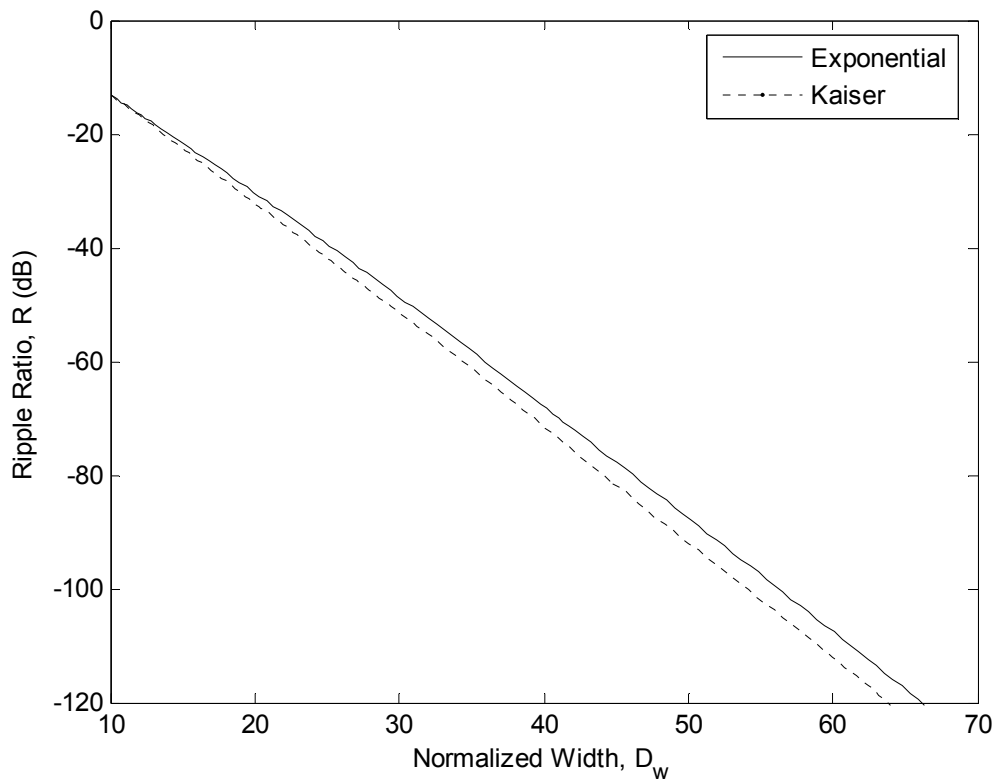


Figure 4.11 Ripple ratio comparison between the Exponential and Kaiser windows for $N = 101$

As for the sidelobe roll-off ratio comparison between the Exponential and Kaiser windows, the simulation result for $N = 101$ is given in Figure 4.12. It is seen that the Exponential window performs higher sidelobe roll-off ratio than the Kaiser window for the same mainlobe width until one sidelobe is lost where the peak values occur.

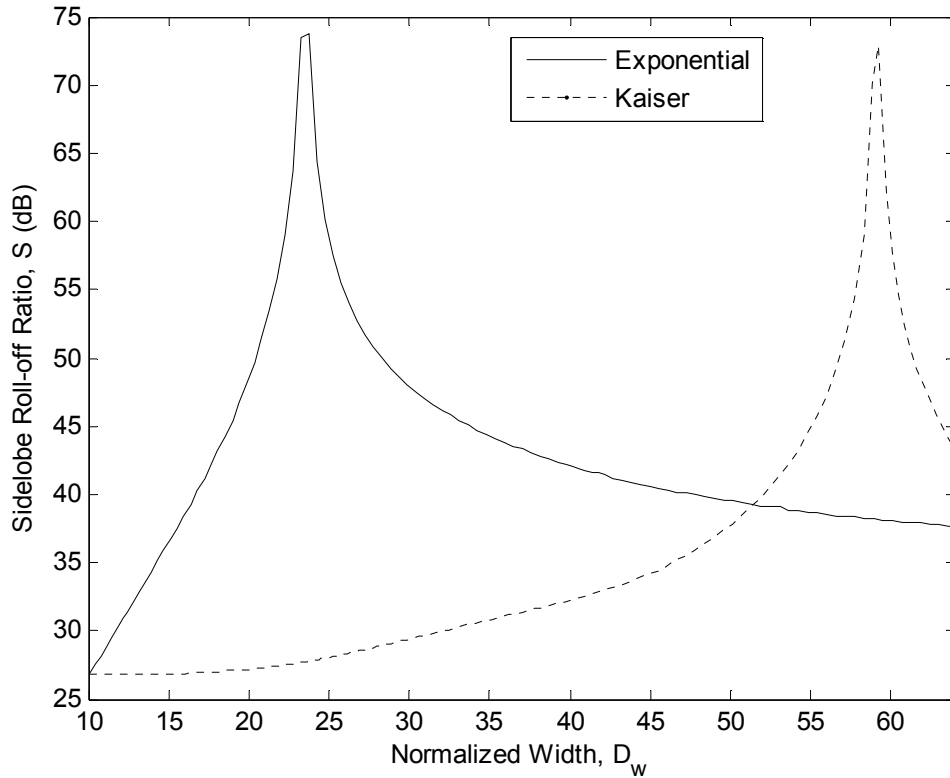


Figure 4.12 Sidelobe roll-off ratio comparison between the Exponential and Kaiser windows for $N = 101$

4.2.3.2 Comparisons with Ultraspherical window

Two specific examples are given for the comparison between the Exponential and Ultraspherical windows. The first comparison example is performed for the narrower mainlobe width and larger sidelobe roll-off ratio with $N = 51$. The simulation result given in Figure 4.13 and Table 4.2 which summarizes the figure shows that the three-parameter Ultraspherical window provides a better ripple ratio than the Exponential window for the same window length, mainlobe width and sidelobe roll-off ratio. The Ultraspherical window parameters for this example are $\mu = 1.99999$ and $x_\mu = 1.00039$. The Matlab programs to find the parameters of the Ultraspherical window can be seen at Appendix.

Table 4.2 Data for the Exponential and Ultraspherical windows used in the first comparison example

Window	N	α_e	w_R	S	R
Exponential	51	2.5	0.164	37.81	-24.10
Ultraspherical	51	-	0.164	37.81	-23.02

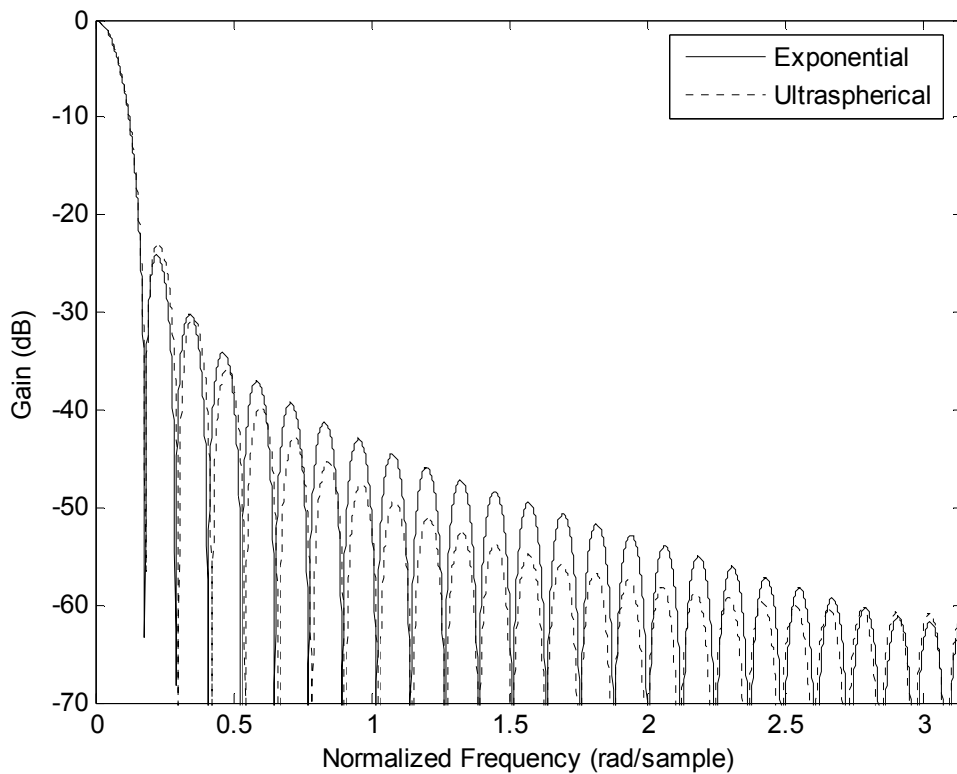


Figure 4.13 Comparison of the Exponential and Ultraspherical windows for narrower mainlobe width and larger sidelobe roll-off ratio with $N = 51$

The second comparison example is given for the wider mainlobe width and smaller sidelobe roll-off ratio for $N = 51$. The simulation result given in Figure 4.14 and Table 4.3 shows that the Exponential window provides a better ripple ratio than the Ultraspherical window in this case. The Ultraspherical window parameters for this example are $\mu = 1.66635$ and $x_\mu = 1.00973$.

From Figures 4.13 and 4.14, the ripples between the maximum and the minimum sidelobe amplitudes can also be observed to be higher for the Exponential window.

Table 4.3 Data for the Exponential and Ultraspherical windows used in the second comparison example

Window	N	α_e	w_R	S	R
Exponential	51	7	0.31	32.48	-50.53
Ultraspherical	51	-	0.31	32.48	-51.75

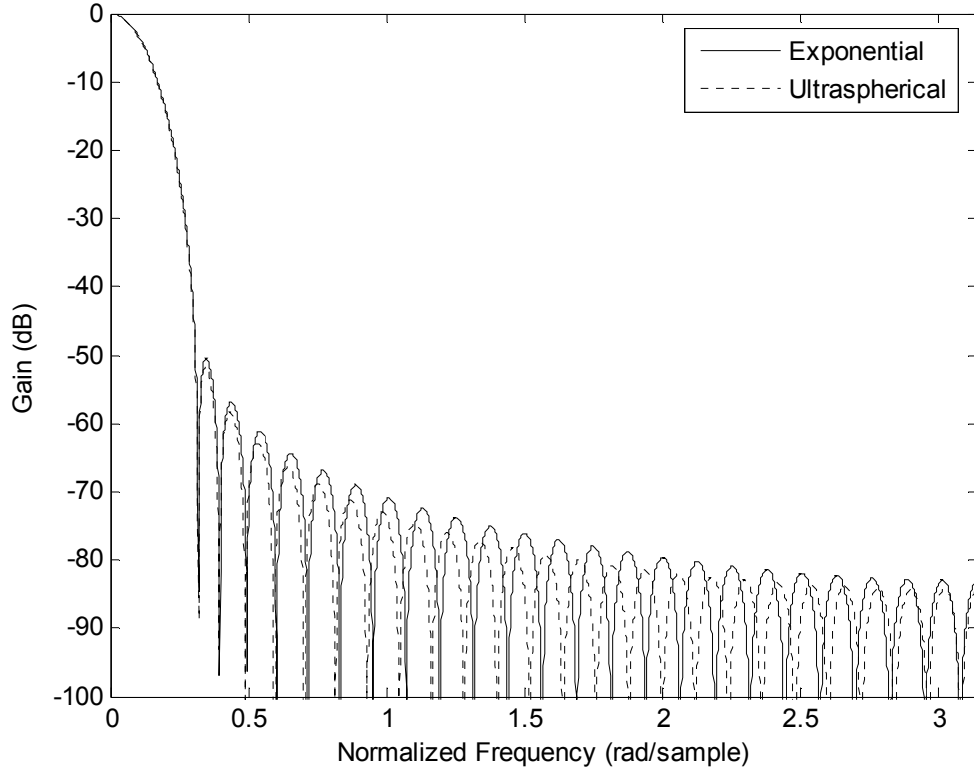


Figure 4.14 Comparison of the Exponential and Ultraspherical windows for wider mainlobe width and smaller sidelobe roll-off ratio with $N = 51$

4.3 Cosh Window

4.3.1 Definition

In Section 4.2, by using the Kaiser approach a simple window based on the exponential function is proposed. In this section, using the same approach, another window based on the cosine hyperbolic function is proposed. The hyperbolic cosine of a variable x is expressed as

$$\cosh(x) = \frac{e^x + e^{-x}}{2} \quad (4.5)$$

From Figure 4.15, like the exponential function it is seen that the cosine hyperbolic function has the same amplitude characteristic with the function $I_0(x)$. Therefore, a new window - namely “Cosh window” for this report, can be proposed as [35]

$$w_c(n) = \begin{cases} \frac{\cosh(\alpha_c \sqrt{1 - \left(\frac{2n}{N-1}\right)^2})}{\cosh(\alpha_c)} & |n| \leq \frac{N-1}{2} \\ 0 & \text{otherwise} \end{cases} \quad (4.6)$$

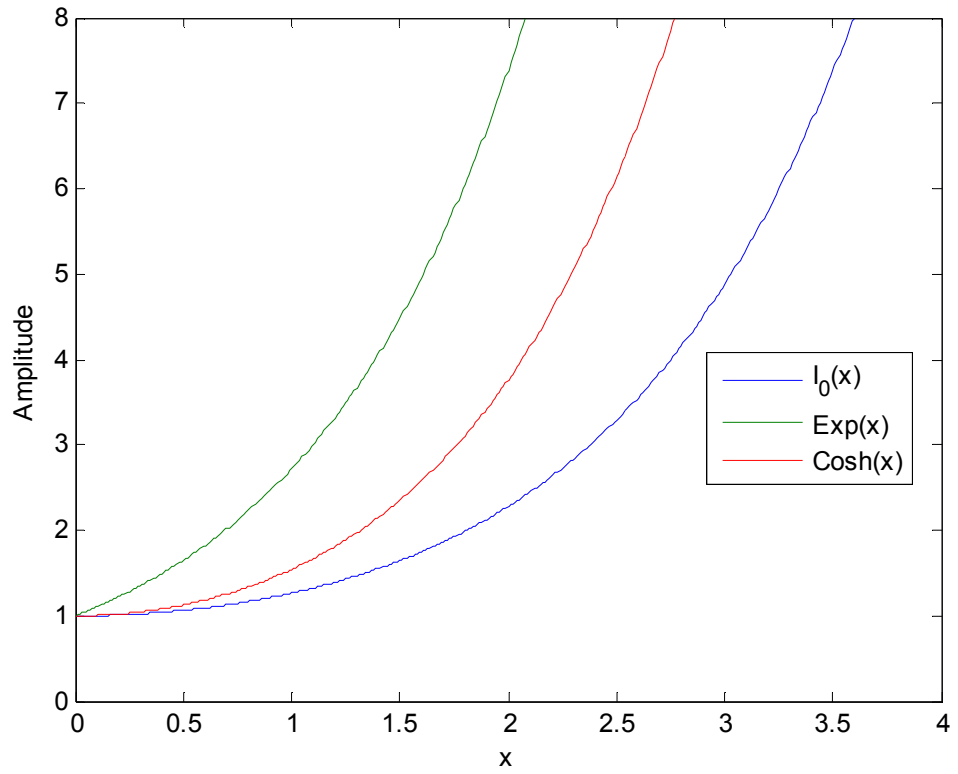


Figure 4.15 Amplitude characteristics of the functions $\cosh(x)$, $\exp(x)$ and $I_0(x)$

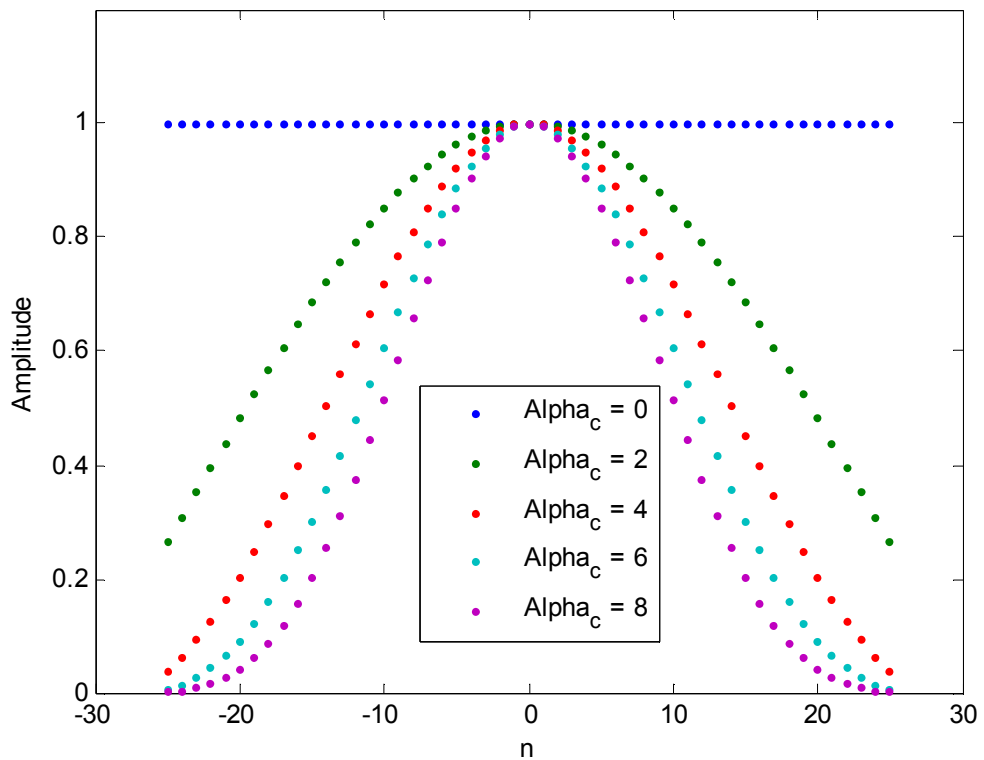


Figure 4.16 Cosh window in time domain for $\alpha_c = 0, 2, 4, 6,$ and 8 with $N = 51$

Figure 4.16 shows the time domain characteristic of the Cosh window for various values of the parameter α_c for $N = 51$. It is seen from the figure that $\alpha_c = 0$ corresponds to the Rectangular window. The exact spectrum of the Cosh window can be obtained using Eq. (3.11).

Like the Kaiser and Exponential windows, the Cosh window has two independent parameters, namely the window length (N) and the adjustable parameter (α_c). As an advantage like the Exponential window, the Cosh window does not have any power series expansion as the Kaiser window does.

Figure 4.17 shows the time required to compute the window coefficients for the Cosh and Kaiser windows. The elapsed time for the Cosh window changes from 0.04 to 0.48 ms, while it changes from 28 to 124 ms for the Kaiser window. As it is obvious from this figure, the Cosh window is computationally efficient compared to the Kaiser window due to having no power series expansion in its time domain representation.

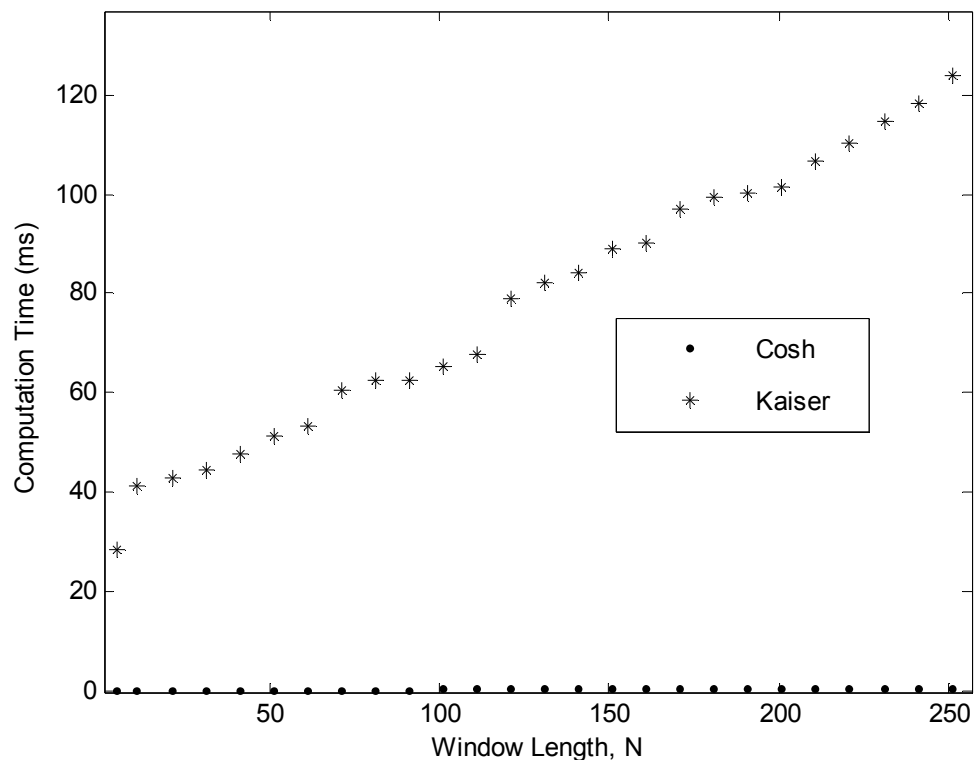


Figure 4.17 Computation time comparison between the Cosh and Kaiser windows for various window length

Figure 4.18 shows the frequency domain plots of the Cosh window for various values of α_c and $N = 51$. As it is seen from this figure and Table 4.4, which summarizes the numerical data in Figure 4.18, that an increase in α_c results in a wider mainlobe width and a smaller ripple ratio.

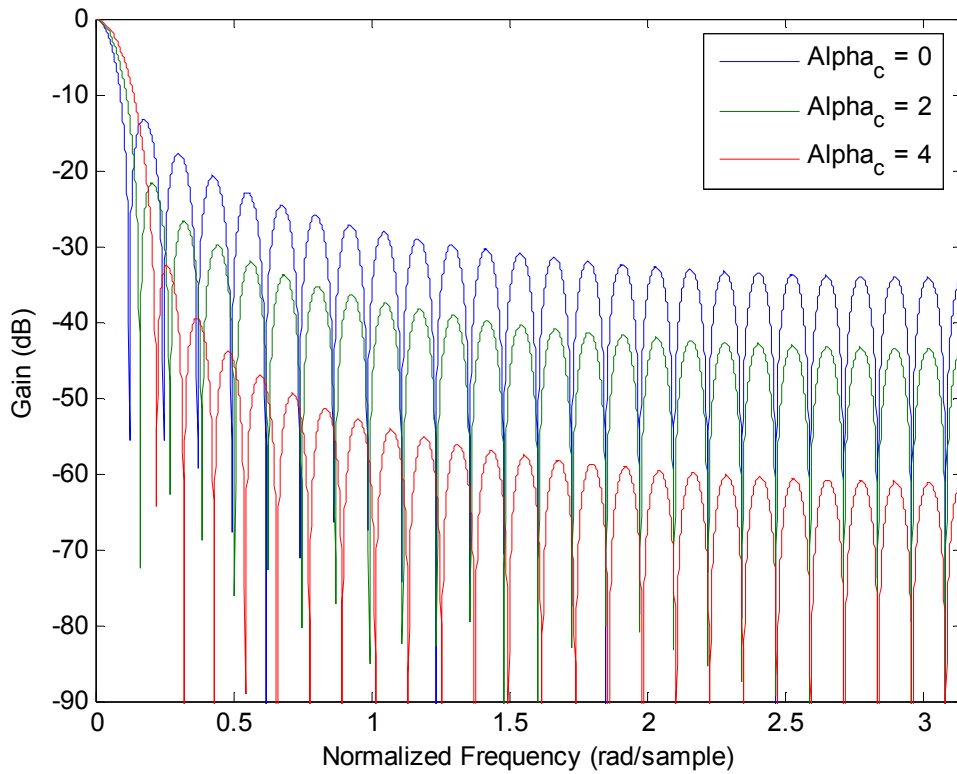


Figure 4.18 Cosh window spectrums in dB for $\alpha_c = 0, 2,$ and 4 with $N = 51$

Table 4.4 Data for the Cosh window spectrum for various α_c with $N = 51$

Window	N	α_c	w_R	R	S
Cosh-1	51	0	0.1	-13.25	20.9
Cosh-2	51	2	0.145	-21.63	21.9
Cosh-3	51	4	0.209	-32.6	28.49

4.3.2 Spectrum design equations

Figure 4.19 shows the relation between α_c and the ripple ratio for the Cosh window for $N = 51$ and 101 . As seen from this figure, the ripple ratio remains almost constant for a change in the window length. Therefore, using curve fitting method an

approximate design equation for the adjustable parameter α_c in terms of the ripple ratio can be obtained as [36]

$$\alpha_{c,Appr} = \begin{cases} 0 & R > -13.26 \\ 0.4611(-R-13.26)^{0.4} - 0.1165(R+13.26) & -50 < R \leq -13.26 \\ -8.763 \times 10^{-5} R^2 - 0.1469R - 0.1461 & -120 \leq R \leq -50 \end{cases} \quad (4.7)$$

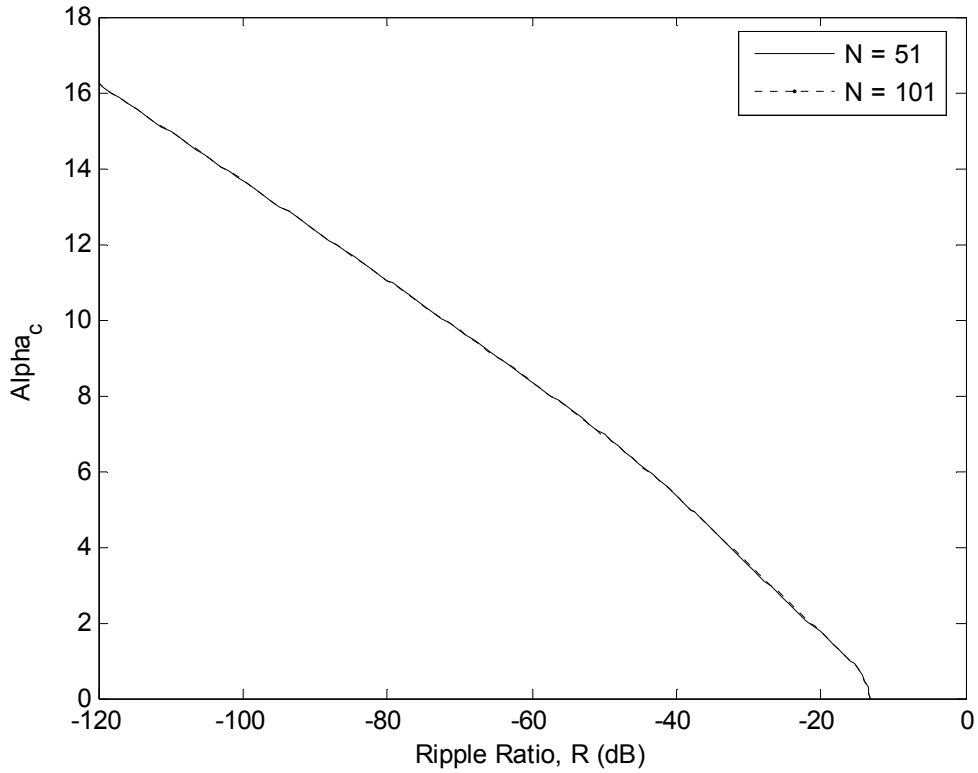


Figure 4.19 Relation between α_c and R for the Cosh window with $N = 51$ and 101

The approximation model given by Eq. (4.7) for the adjustable parameter α_c is plotted in Figure 4.20. It is seen that the proposed model provides a good fitting for $N = 101$. Moreover, the approximation error for $N = 101$ is plotted in Figure 4.21. It is observed that the largest deviation in alpha is 0.1 which corresponds to an error of 0.4 dB in actual ripple ratio. As for the Kaiser model given in [31], the largest deviation in alpha is 0.07, but this corresponds to an error of 0.44 dB in actual ripple ratio. More accurate results can be obtained by restricting the range or using higher order approximations, but the proposed model for the Cosh window is adequate for most applications like the Kaiser model.

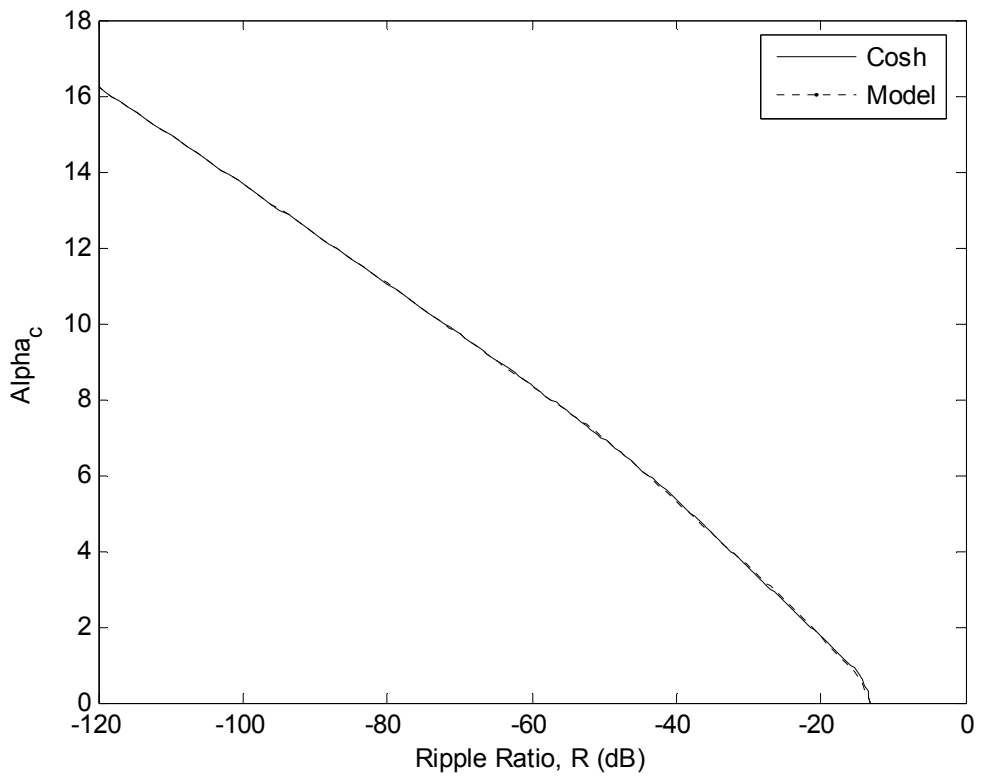


Figure 4.20 Approximated model for α_c of the Cosh window with $N = 101$

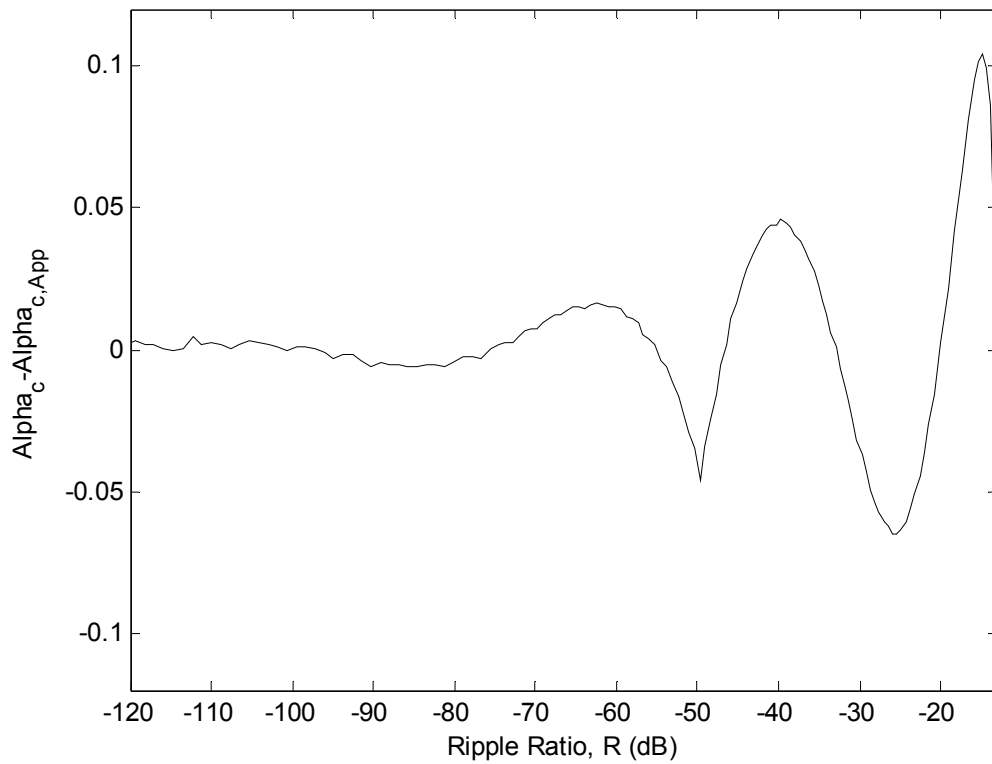


Figure 4.21 Error curve of approximated α_c versus R for $N = 101$

The relation between D_w and R for the Cosh window for $N = 51$ and 101 is plotted in Figure 4.22. It is seen that the ripple ratio becomes smaller as the mainlobe becomes wider. Also, it is observed from the same figure that the window length has no effect on the relation between the ripple ratio and normalized mainlobe width. By using the curve fitting method, an approximate design relationship between the normalized width and the ripple ratio can be established as [36]

$$D_{w,Appr} = \begin{cases} 0 & R > -13.26 \\ -7.58 \times 10^{-5} R^3 + 7.22 \times 10^{-3} R^2 + 4.312R - 0.3566 & -50 < R \leq -13.26 \\ -1.297 \times 10^{-4} R^2 - 0.5281R + 4.708 & -120 \leq R \leq -50 \end{cases} \quad (4.8)$$

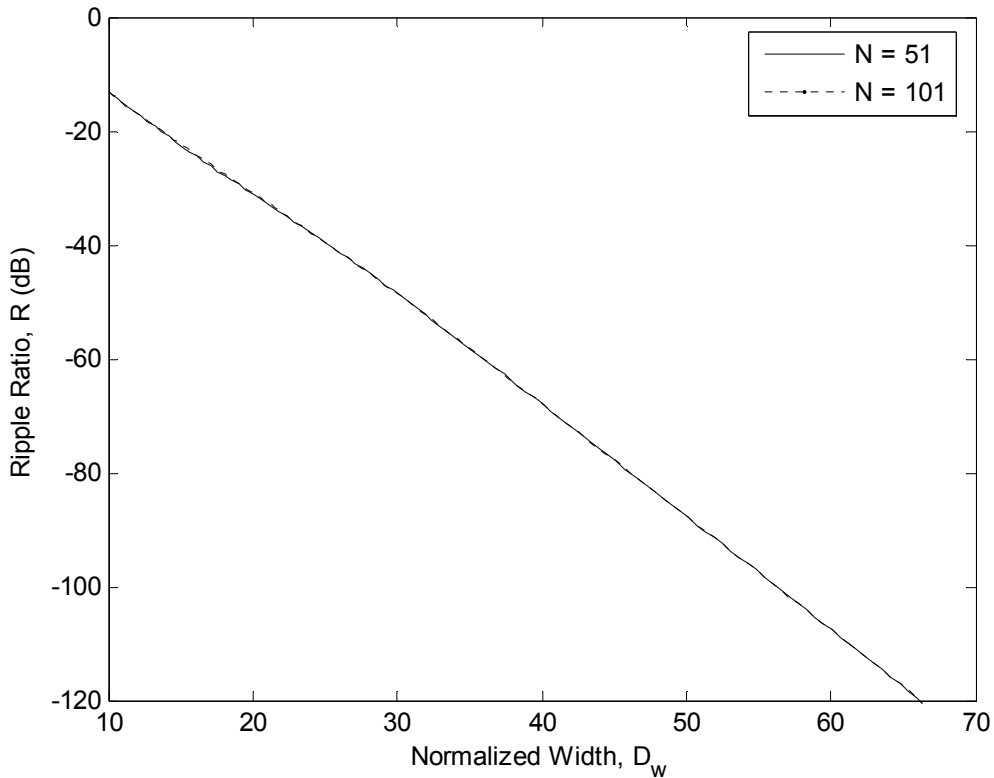


Figure 4.22 Relation between D_w and R for the Cosh window with $N = 51$ and 101

The approximation model given by Eq. (4.8) for the normalized width is plotted in Figure 4.23. It is seen that the proposed model for D_w of the Cosh window provides a good approximation for $N = 101$. The relative error of approximated normalized width in percent versus the ripple ratio for $N = 101$ is plotted in Figure 4.24. The percentage error in the model changes between 0.204 and -0.234 . This error range satisfies the error criterion in [32] which states that the predicted error in the normalized width must be smaller than 1% .

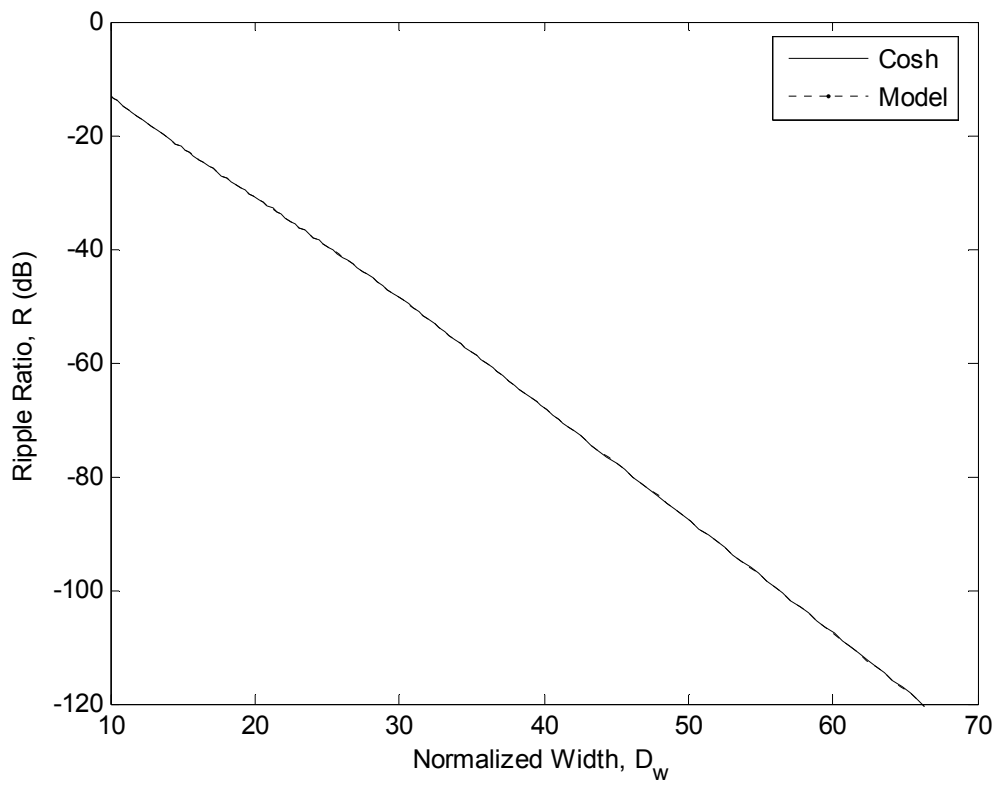


Figure 4.23 Approximated model for D_w of the Cosh window with $N = 101$

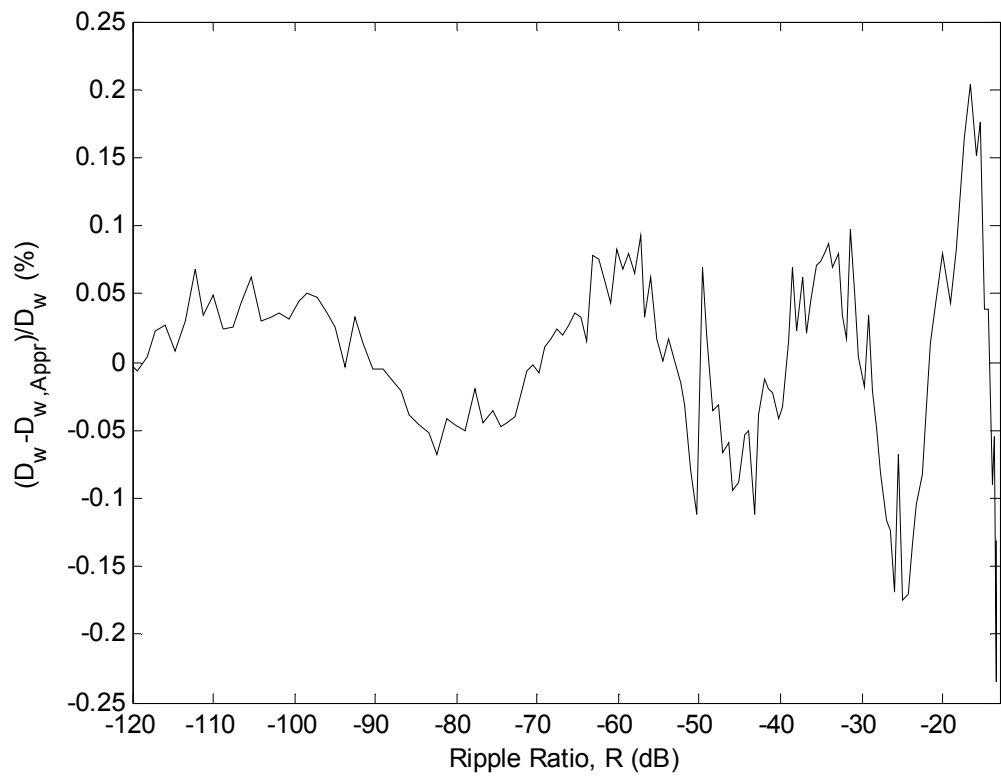


Figure 4.24 Relative error of approximated D_w for the Cosh window in percent versus R with $N = 101$

Figure 4.25 shows the change in the sidelobe-roll off ratio versus the normalized width for $N = 51$ and 101 . It can be concluded that the sidelobe roll-off ratio increases as the normalized width increases until one of the sidelobes is dropped due to higher value of α . Unlike in the case of ripple ratio, a change in the window length affects significantly the sidelobe roll-off ratio.

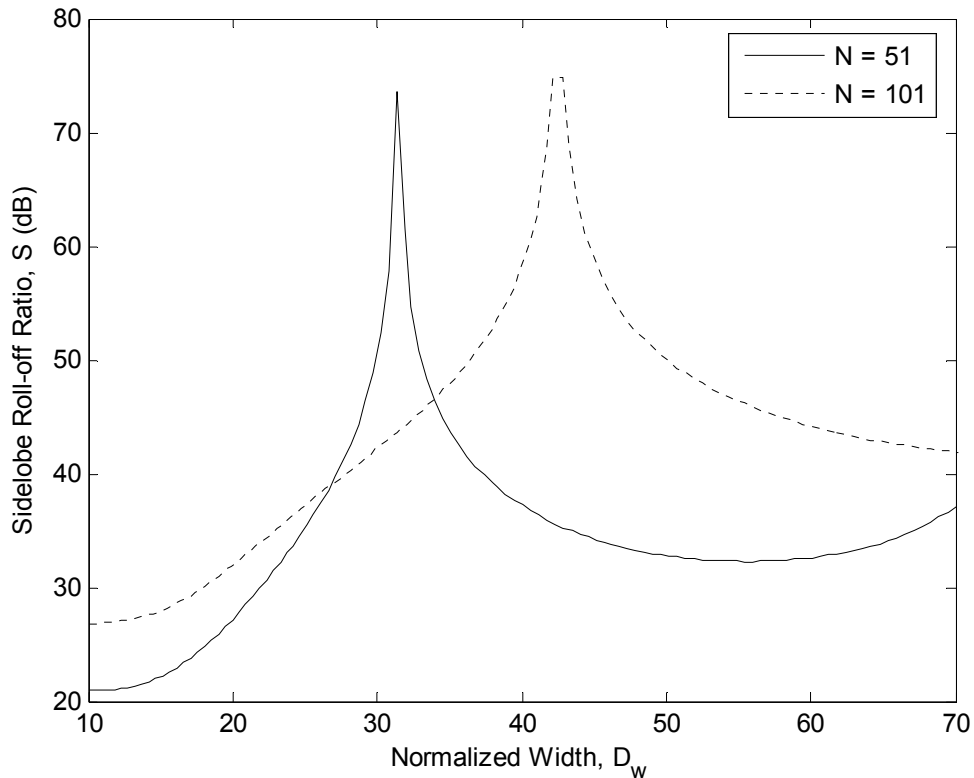


Figure 4.25 Relation between D_w and S for the Cosh window with $N = 51$ and 101

4.3.3 Spectrum comparisons

4.3.3.1 Comparisons with Exponential and Kaiser windows

Figure 4.26 shows a general comparison of the Cosh window in a wide range with the Exponential and Kaiser windows in terms of the ripple ratio versus normalized mainlobe width for $N = 101$. The figure demonstrates that the Kaiser window provides smaller ripple ratio than the others for the same mainlobe width. For the range $D_w < 25$, the Cosh window produces smaller ripple ratio than the Exponential window. And, for the range $25 < D_w$ the Cosh and Exponential windows perform the same ripple ratio characteristic.

The simulation results for the sidelobe roll-off ratio comparison is given for $N = 101$ in Figure 4.27. It is seen that the Cosh window performs better than the Kaiser

window but worse than the Exponential window in terms of the sidelobe roll-off ratio for the same mainlobe width until one sidelobe is lost where the peak values occur.

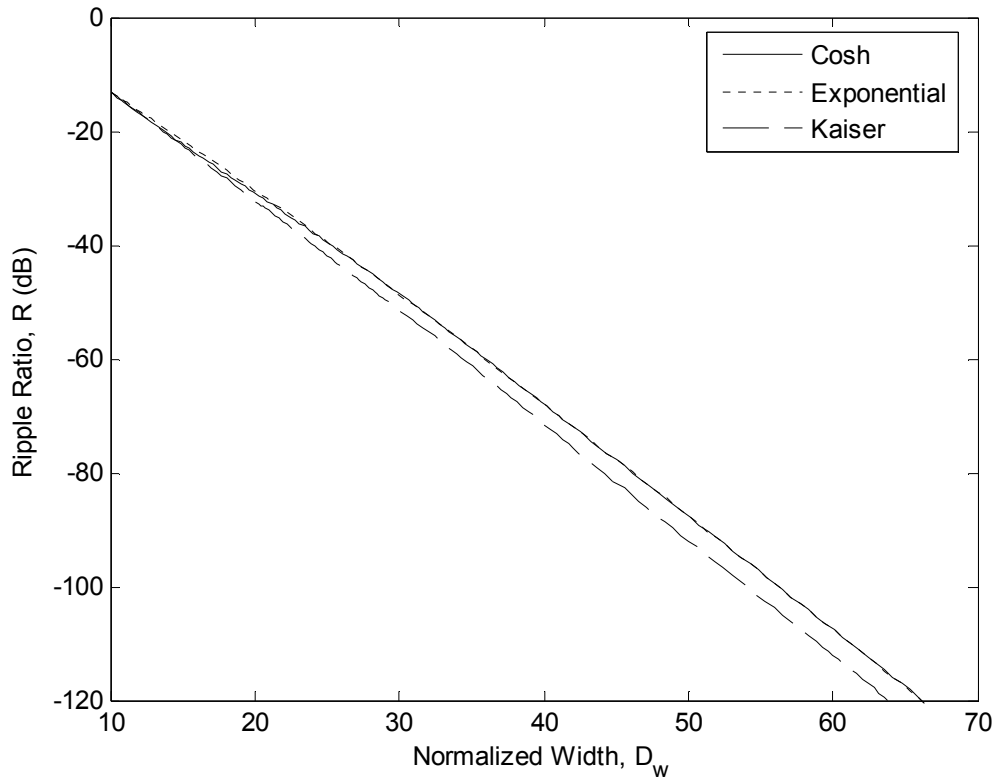


Figure 4.26 Ripple ratio comparison between the Cosh, Exponential and Kaiser windows for $N = 101$

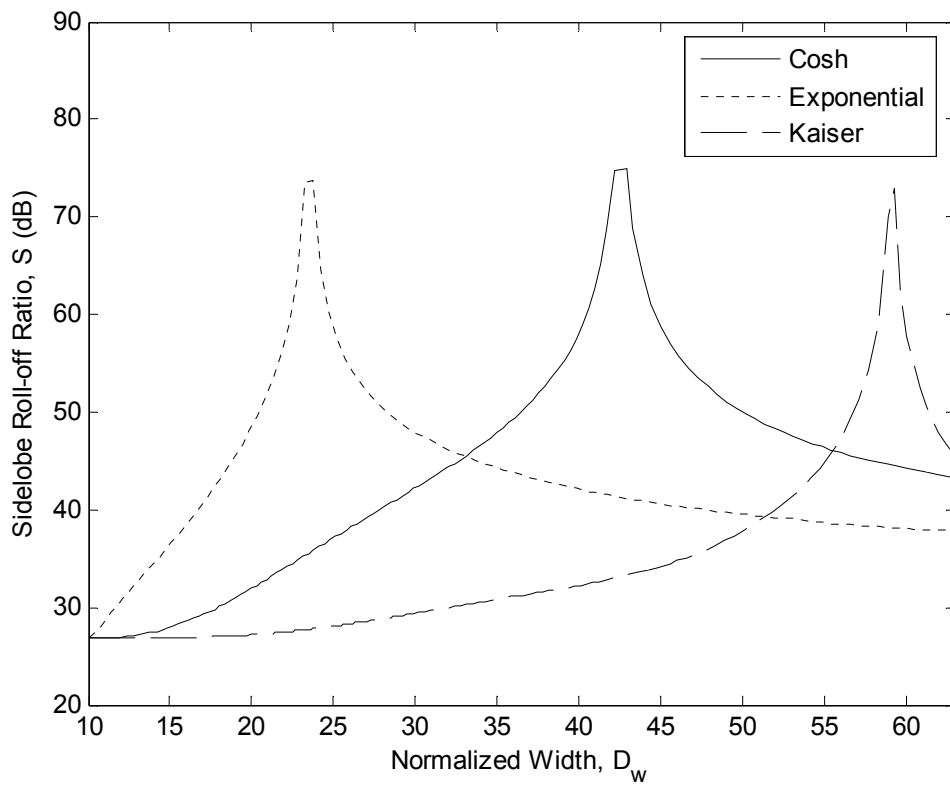


Figure 4.27 Sidelobe roll-off ratio comparison between the Cosh, Exponential and Kaiser windows for $N = 101$

4.3.3.2 Comparisons with Ultraspherical window

As for the comparison with Ultraspherical window, two examples for $N = 51$ are given below. For fixed values of w_R and S , the ripple ratio characteristic of the Cosh and Ultraspherical windows is compared.

The first comparison example is performed for the narrower mainlobe width and smaller sidelobe roll-off ratio. The simulation result is shown in Figure 4.28 and the data is summarized in Table 4.5. The results show that the Ultraspherical window provides a better ripple ratio than the Cosh window for the same window length, mainlobe width and sidelobe roll-off ratio. The Ultraspherical window parameters for this example are $\mu = 1.99997$ and $x_\mu = 1.00039$.

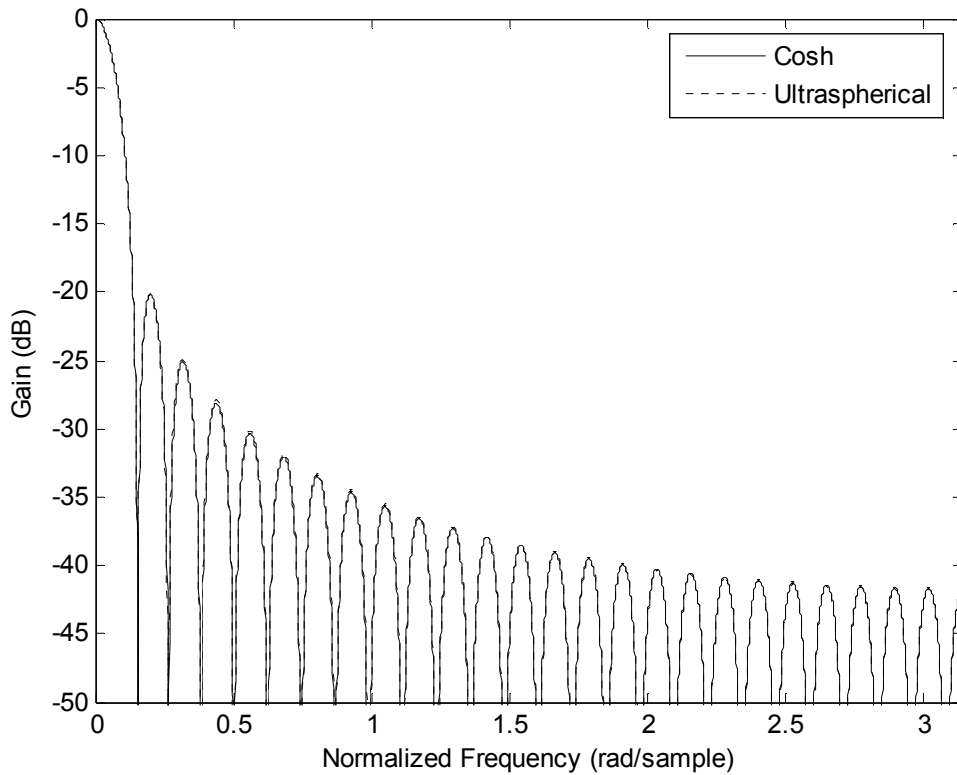


Figure 4.28 Comparison of the Cosh and Ultraspherical windows for narrower mainlobe width and smaller sidelobe roll-off ratio with $N = 51$

Table 4.5 Data for the Cosh and Ultraspherical windows used in the first comparison example

Window	N	α_c	w_R	S	R
Cosh	51	2.2	0.1515	22.242	-22.81
Ultraspherical	51	-	0.1515	22.242	-22.95

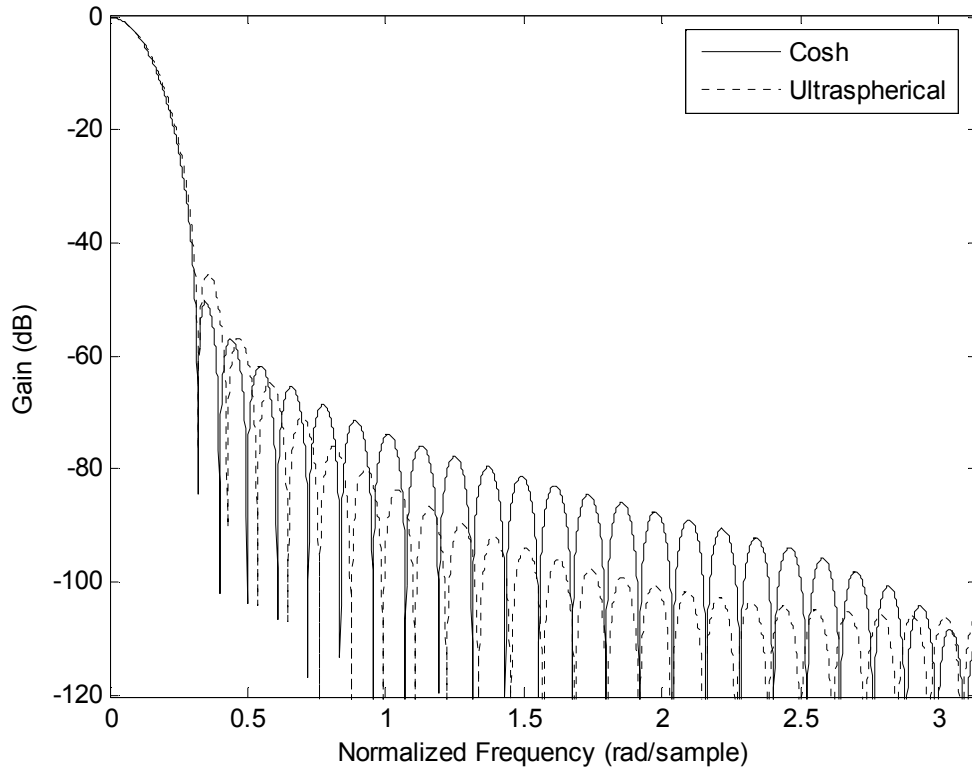


Figure 4.29 Comparison of the Cosh and Ultraspherical windows for wider mainlobe width and larger sidelobe roll-off ratio with $N = 51$

The second comparison example is performed for the wider mainlobe width and larger sidelobe roll-off ratio. The simulation result is shown in Figure 4.29 and the data is summarized in Table 4.6. The results show that the Cosh window provides significantly better ripple ratio than the Ultraspherical window for the same window length, mainlobe width and sidelobe roll-off ratio. The ultraspherical window parameters for this example are $\mu = 3.65266$ and $x_\mu = 1.00547$.

Table 4.6. Data for the Cosh and Ultraspherical windows used in the second comparison example

Window	N	α_c	w_R	S	R
Cosh	51	7	0.3095	60.35	-50.35
Ultraspherical	51	-	0.3095	60.35	-45.53

From two specific examples above, we can conclude that for narrower mainlobe width and smaller sidelobe roll-off ratio the Ultraspherical window is better, for wider mainlobe width and larger sidelobe roll-off ratio the Cosh window performs better results in terms of the ripple ratio.

4.3.3.3 Comparison with the combinational windows including Hamming window

The aim to combine windows is to provide a better window spectral characteristic than that of each window used in the combination. From the previous sections, it is observed that the Cosh window has a worse ripple ratio than the Kaiser window. To improve its ripple ratio, the combination with the Hamming window [1] is suggested.

Figure 4.30 shows the comparison of the Cosh, Kaiser and combinational windows including the Hamming window for a fixed window length and mainlobe width. In this figure, it should be noticed that the highest sidelobe amplitude - which gives the ripple ratio, for the Cosh and Kaiser windows occurs in the first sidelobe but it occurs in the third sidelobe for the combinational windows. The numerical results of Figure 4.30 with the additional information for the Hamming window are summarized in Table 4.7

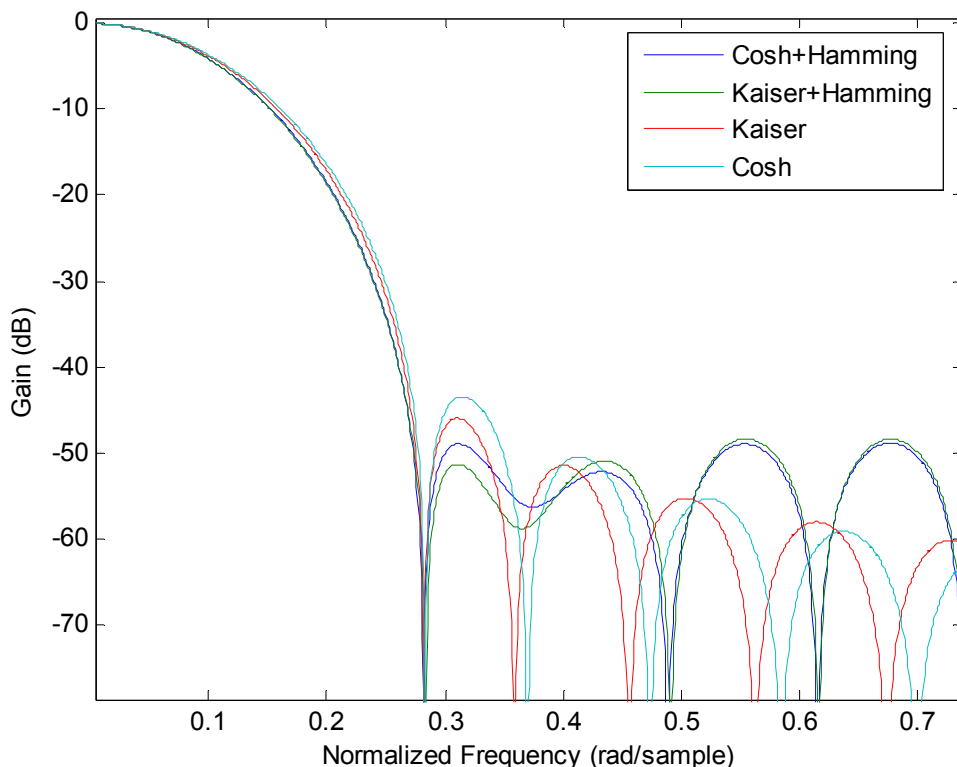


Figure 4.30 Comparison of the Cosh, Kaiser and combinational windows with the Hamming window for $N = 51$ and $w_R = 0.272$ rad/sample

From Table 4.7, it is seen that the combination of the Cosh and Hamming windows has the smallest ripple ratio. But this improved ripple ratio comes at the expense of reduced sidelobe roll-off ratio.

Table 4.7 Data for the comparison of the Cosh, Kaiser and combinational windows with the Hamming window for $N = 51$

Window	N	w_R	α	R	S
Cosh + Hamming	51	0.272	6.17	-48.98	50.59
Kaiser + Hamming	51	0.272	6.66	-48.38	55.93
Kaiser	51	0.272	6.295	-45.98	71.02
Cosh	51	0.272	5.931	-43.47	83.54
Hamming	51	0.244	-	-42.31	55.59

This example shows that the Cosh window can perform better results than the Kaiser window in terms of the ripple ratio if it can be used with a suitable window such as the Hamming window.

4.4 Modified Cosh Window

4.4.1 Definition

In Section 4.3, it is demonstrated that the Cosh window with two independent parameters - N and α_c , doesn't give the satisfactory results compared to the Kaiser window in terms of the ripple ratio. To improve its ripple ratio characteristic, a third parameter - denoted as ρ_{mc} is proposed. The new three parameter window - which is called "*modified Cosh window*" through this report, is defined as [37]

$$w_{mc}(n) = \begin{cases} \left(\frac{\cosh(\alpha_{mc} \sqrt{1 - \left(\frac{2n}{N-1}\right)^2})}{\cosh(\alpha_{mc})} \right)^{\rho_{mc}} & |n| \leq \frac{N-1}{2} \\ 0 & \text{otherwise} \end{cases} \quad (4.9)$$

From Eq. (4.9) it is seen that the modified Cosh windows for $\rho_{mc} = 0$ and $\rho_{mc} = 1$ correspond to the Rectangular and Cosh windows, respectively. Therefore, this modified window can provide good sidelobe roll-off ratio characteristic of the Cosh window if necessary.

To observe the effect of the new parameter on the window spectrum, a simulation example for various ρ_{mc} with $N = 51$ and $\alpha_{mc} = 2$ is given below. The exact spectrum for the modified Cosh window can be obtained using Eq. (3.11). The effect of the new parameter on the window spectrum can be observed from Figure 4.31 with the data summarized in Table 4.8. As seen from the figure and table, an increase in the proposed window parameter ρ_{mc} results in a wider mainlobe width and a smaller ripple ratio. Therefore, it can be concluded that ρ_{mc} has the same effect like the parameter α of the Cosh and Kaiser windows.

Table 4.8 Data for the effect of ρ_{mc} on the modified Cosh window with $\alpha_{mc} = 2$ and $N = 51$

Window	α_{mc}	ρ_{mc}	w_R	R	S
Cosh	2	1	0.145	-21.63	21.87
Mod.Cosh-1	2	2	0.205	-34.04	19.75
Mod.Cosh-2	2	3	0.284	-52.70	12.00

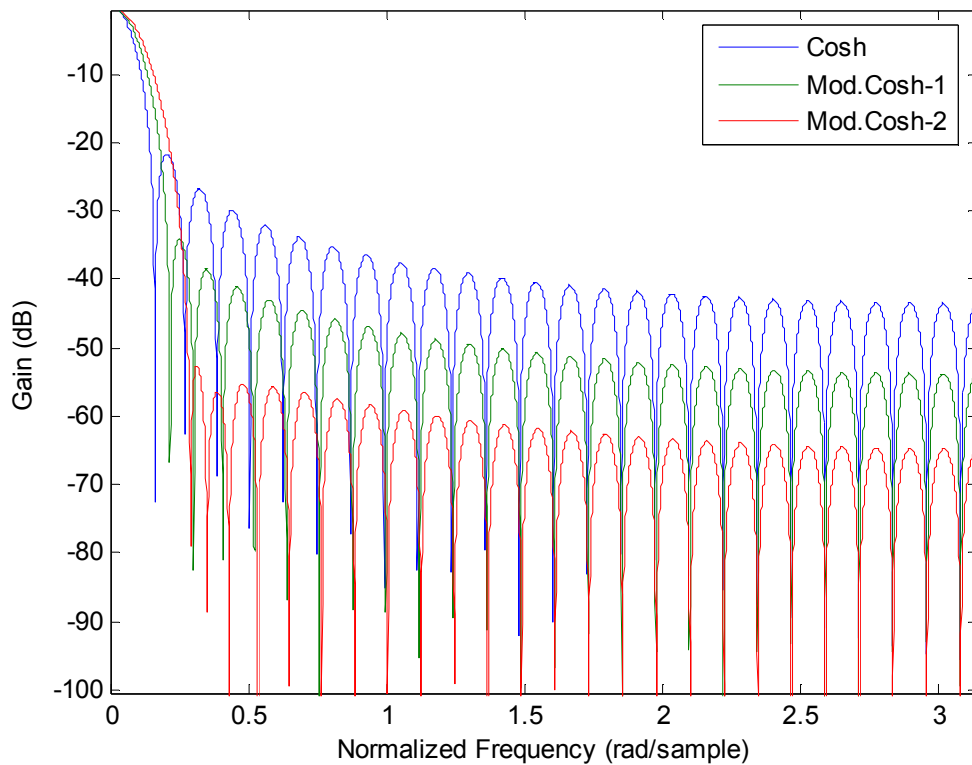


Figure 4.31 Effect of ρ_{mc} on the modified Cosh window for $N = 51$ and $\alpha_{mc} = 2$

4.4.2 Spectrum design equations

Figure 4.32 shows the comparison of the Cosh and modified Cosh windows in terms of the ripple ratio for a wide range of the normalized width for $N = 51$. The

plots in Figure 4.32 are obtained as follows: The first plot in blue line is drawn for the Cosh window, and it is found by changing its adjustable parameter α_c from 0 to 9.45 for $N = 51$. The second plot in green line is drawn for the modified Cosh window for $\alpha_{mc} = 1$, and it is found by changing its adjustable parameter ρ_{mc} from 0 through 10.75. The data for obtaining other plots can be found in Table 4.9.

Table 4.9 Data for the effect of adjustable parameters on the modified Cosh window for $N = 51$

Window	N	α_{mc}	ρ_{mc}
Cosh	51	0-9.45	1
Mod. Cosh-1	51	1	from 0 to 10.75
Mod. Cosh-2	51	1.5	from 0 to 6.25
Mod. Cosh-3	51	2	from 0 to 4.65
Mod. Cosh-4	51	3	from 0 to 3.15
Mod. Cosh-5	51	4	from 0 to 2.40

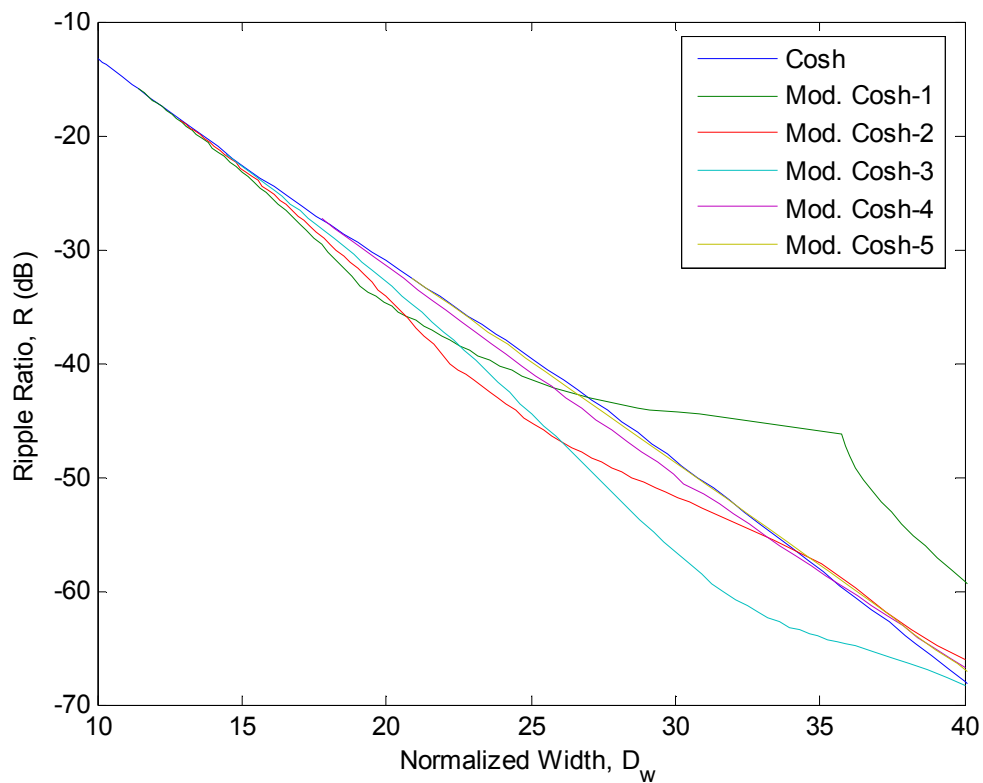


Figure 4.32 Effect of the adjustable parameters on the modified Cosh window for $N = 51$

It can be observed from Figure 4.32 that the new parameter makes the modified Cosh window more flexible than the two-parameter Cosh window. While the Cosh window provides only one ripple ratio for a fixed window length and mainlobe width, the modified Cosh window can yield many ripple ratio. From the figure, it is seen that the modified Cosh window for $\alpha_{mc} = 1$ in green line provides better ripple

ratio than the others for the range $D_w < 21$, but also worse ripple ratio than the others for the range $D_w > 27$. The modified Cosh window for $\alpha_{mc} = 1.5$ in red line provides best ripple ratio values for the range $21 < D_w < 26$, but this window provides the second worst ripple ratio values for the range $D_w > 34.83$.

Since many modified Cosh windows with the combinations of α_{mc} and ρ_{mc} can be designed to satisfy a given mainlobe width for a fixed window length, it is important to be able to find the optimum window which yields the minimum ripple ratio. It is observed from many simulation examples that the minimum ripple ratio for a fixed N value occurs when two sidelobes including the first one in the spectrum have equal amplitude. Figure 4.33 shows the ripple ratio characteristics of the optimum modified Cosh window for $N = 51$ and 101 . As opposed to the Cosh window, it can be seen that a change in the window length affects the ripple ratio for the same normalized mainlobe width.

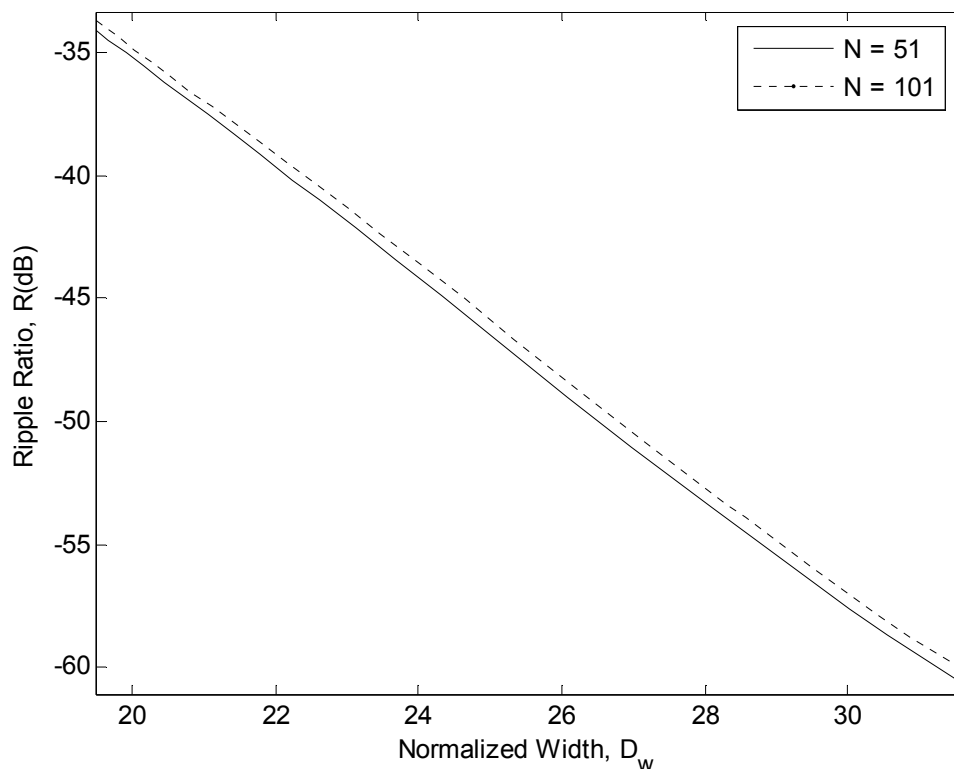


Figure 4.33 Optimum modified Cosh windows for $N = 51$ and 101

Figure 4.34 gives the optimum combinations of α_{mc} and ρ_{mc} to provide the minimum ripple ratio for $N = 51$ and 101 .

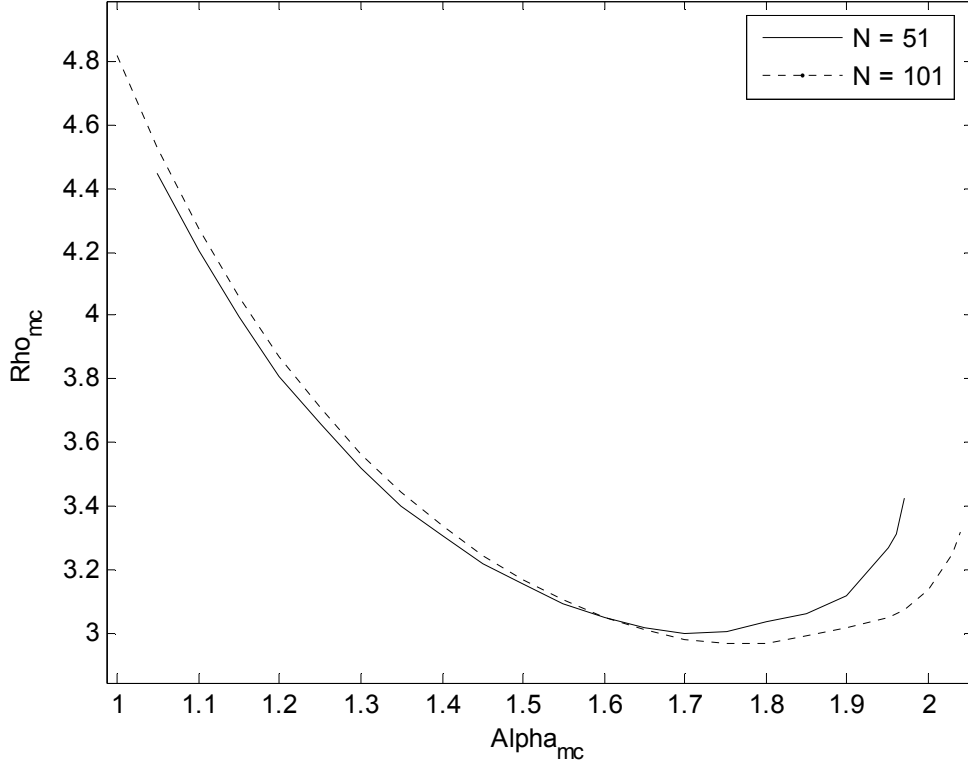


Figure 4.34 Relation between α_{mc} and ρ_{mc} of the optimum modified Cosh windows for $N = 51$ and 101

The design equations for the optimum modified Cosh window for $N = 51$ are found by using curve fitting method in MATLAB

$$\alpha_{mc} = \begin{cases} 0 & R > -13.26 \\ -5.532 \times 10^{-5} R^3 - 9.276 \times 10^{-3} R^2 - 0.531 R - 8.446 & -65 \leq R \leq -30 \end{cases} \quad (4.10a)$$

$$\rho_{mc} = \begin{cases} 0 & R > -13.26 \\ 2.526 \times 10^{-5} R^4 + 5.065 \times 10^{-3} R^3 + 3.801 \times 10^{-1} R^2 + 12.64 R + 160.1 & -65 \leq R \leq -30 \end{cases} \quad (4.10b)$$

Note that the above result is valid only for $N = 51$.

And, the same relations for the optimum modified Cosh window for $N = 101$ can be found

$$\alpha_{mc} = \begin{cases} 0 & R > -13.26 \\ -5.908 \times 10^{-5} R^3 - 9.869 \times 10^{-3} R^2 - 0.564 R - 9.027 & -65 \leq R \leq -30 \end{cases} \quad (4.11a)$$

$$\rho_{mc} = \begin{cases} 0 & R > -13.26 \\ 3.197 \times 10^{-5} R^4 + 6.353 \times 10^{-3} R^3 + 0.47 R^2 + 15.33 R + 193.8 & -65 \leq R \leq -30 \end{cases} \quad (4.11b)$$

Using Eq. (4.10) and Eq. (4.11), the modified Cosh window which yields the narrowest mainlobe width can be designed for a given ripple ratio for $N = 51$ and 101. For other window lengths, the design equations can be found by obtaining the optimum combinations of α_{mc} and ρ_{mc} empirically with applying the same procedure above. Then, applying the suitable curve fitting polynomial, the desired relations can be obtained.

4.4.3 Spectrum comparisons with Cosh and Kaiser windows

The ripple ratio comparisons between the optimum modified Cosh, Kaiser and Cosh windows for $N = 51$ and 101 are shown in Figure 4.35 and Figure 4.36, respectively. In both figures, it can be observed that the proposed modified cosh window provides a significantly better ripple ratio than the Kaiser and cosh windows. And, the difference in the ripple ratio becomes larger for higher values of the normalized width parameter. From figures, it can also be observed that as the window length increases, the ripple ratio difference between modified cosh windows and the other two windows decreases. It can be concluded that as the window length increases, the optimum modified Cosh window approaches to 2-parameter Cosh window.

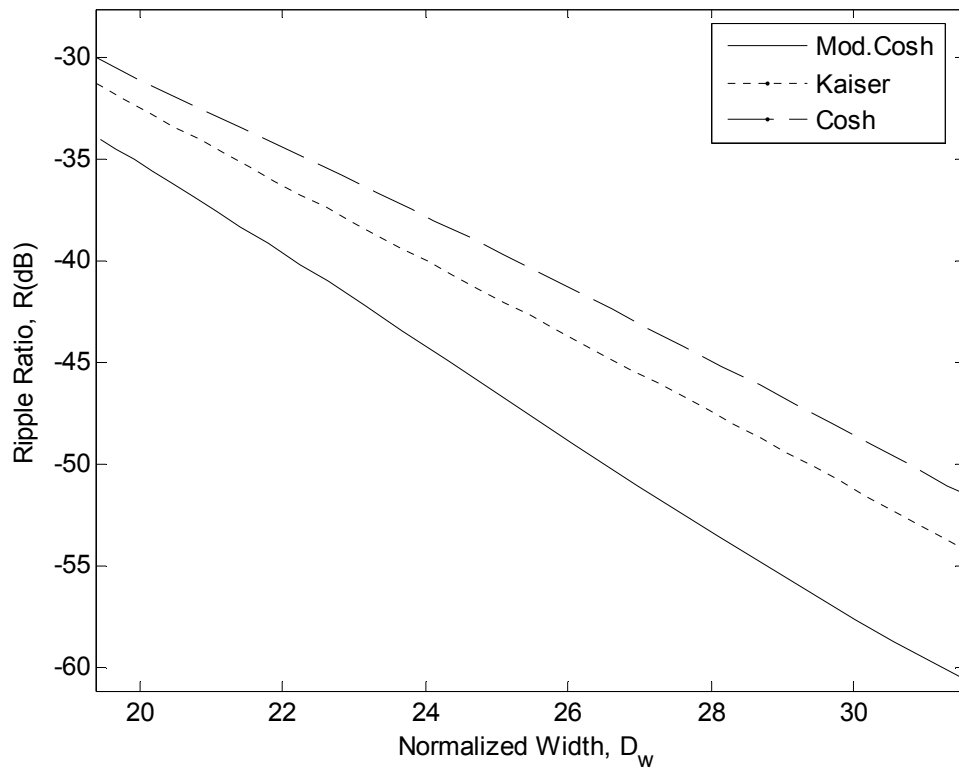


Figure 4.35 Ripple ratio comparison between the optimum modified Cosh, Kaiser and Cosh windows for $N = 51$

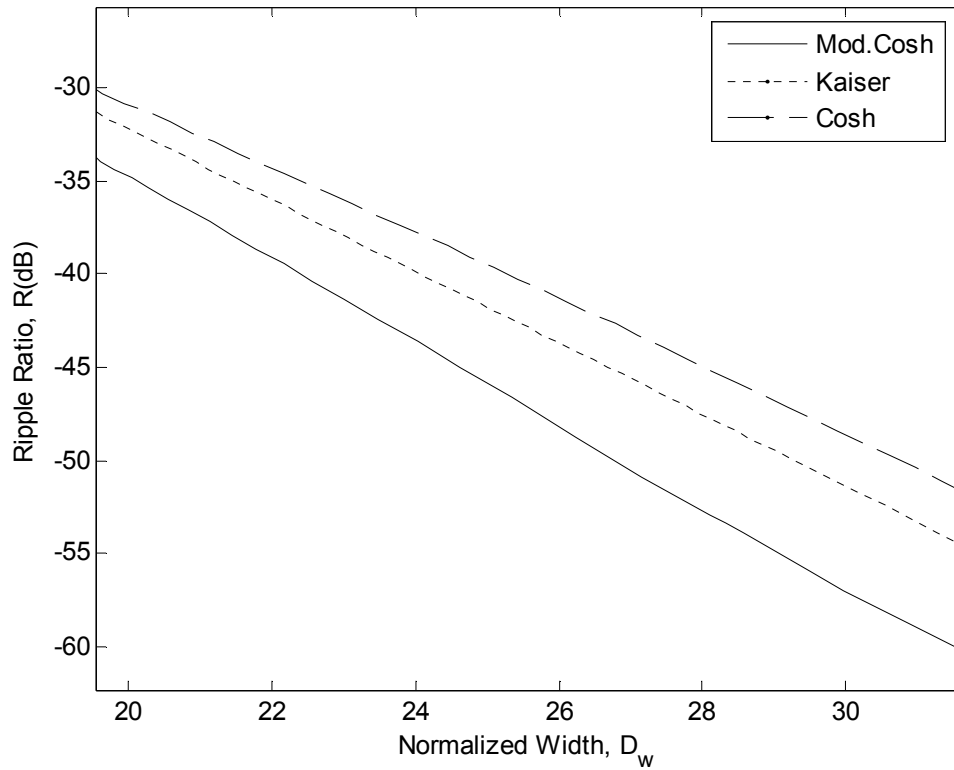


Figure 4.36 Ripple ratio comparison between the optimum modified Cosh, Kaiser and Cosh windows for $N = 101$

The number of window length is important for the practical applications. It is desired for a window to satisfy a given prescribed specifications with the minimum number of the window coefficients for the computational efficiency.

Figure 4.37 shows the spectrums of the modified Cosh, Kaiser and Cosh windows for $R = -60$ dB and $w_R = 0.158$ rad/sample. From Table 4.10, it is seen that the minimum window length to satisfy the given ripple ratio and mainlobe width is obtained by the proposed modified Cosh window. And, the worst case occurs for 2-parameter Cosh window which also provides a wider width with an amount of 0.001 rad/sample compared to other windows.

Table 4.10 Data for the window length comparison between Kaiser, Cosh and the modified Cosh windows for $R = -60$ dB and $w_R = 0.158$ rad/sample

Window	N	ρ_{mc}	α	w_R	R
Mod. Cosh	101	3.3166	2.0407	0.158	-60.00
Kaiser	109	-	8.2164	0.158	-60.00
Cosh	115	1	8.3662	0.159	-60.00

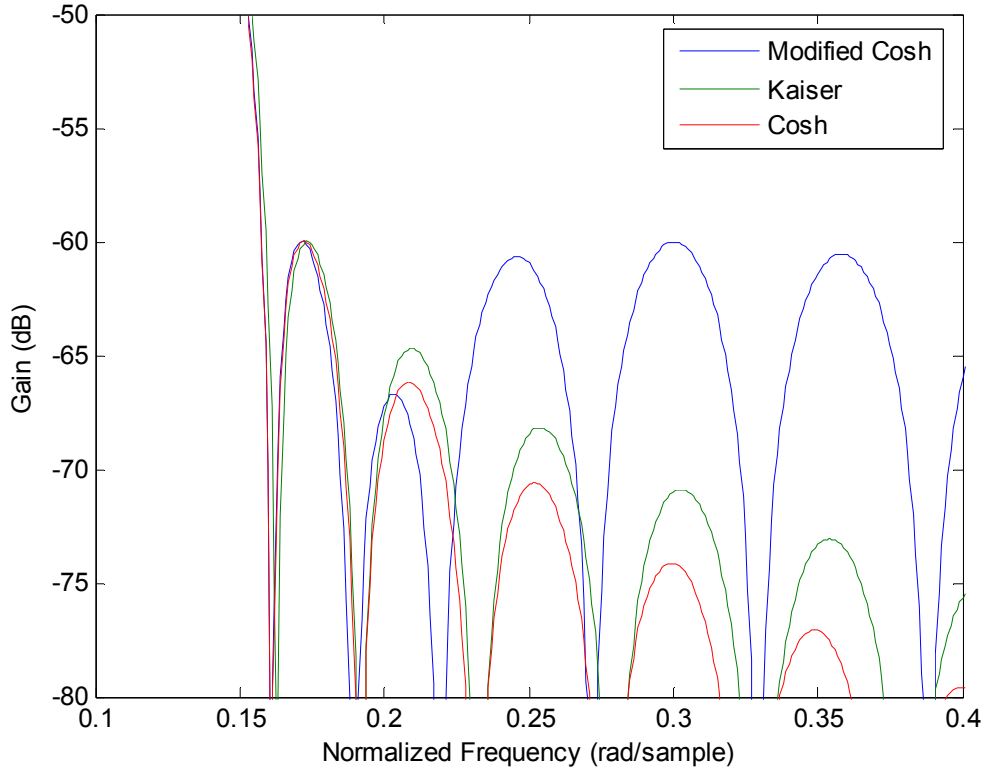


Figure 4.37 Spectrums of the modified Cosh, Kaiser and Cosh windows for $R = -60$ dB and $w_R = 0.158$ rad/sample with enlarged figure around the first sidelobe

Contrast ratio (CR) in an image is defined as the difference in light intensity between the darkest black and brightest white shades within an image. A high CR value is desired since it provides to discern detailed differences between colors producing a crisp and sharp image [2].

The contrast ratio is defined as

$$CR = \frac{E_s + E_m}{E_s} = 1 + MSR \quad (4.12a)$$

where the sidelobe and main-lobe energies are given by

$$E_m = \int_0^{w_r} |W(e^{jwT})|^2 dw \quad (4.12b)$$

$$E_s = \int_{w_r}^{w_s/2} |W(e^{jwT})|^2 dw \quad (4.12c)$$

Without computing from the window spectrum, CR value can also be calculated from

$$CR = \frac{w^T w}{w^T Q w} \quad (4.13a)$$

where w is the window coefficient vector, and the elements of matrix Q can be found from [2]

$$q(n, m) = \begin{cases} -\frac{w_R}{\pi} \sin c[w_R(m-n)] & m \neq n \\ 1 - \frac{w_R}{\pi} & m = n \end{cases} \quad (4.13b)$$

A comparison example for several windows in terms of the ripple ratio and contrast ratio parameters for $N = 101$ and $w_R = 0.121$ rad/sample is given with the results summarized in Table 4.11. It is seen that while the best ripple ratio is obtained from the Dolph-Chebyshev window, it provides the worst CR value. As for two-parameter Cosh window, it provides worse results than the Kaiser window for both the ripple ratio and contrast ratio. But it performs better results than the Hamming and Dolph-Chebyshev windows in terms of the contrast ratio. Using the suitable adjustable parameters, the proposed modified Cosh window can perform good results in terms of the ripple ratio and contrast ratio compared to other windows.

Table 4.11 Data for the comparison of the windows in terms of the ripple ratio and contrast ratio with $N = 101$ and $w_R = 0.121$ rad/sample

Window	α	ρ_{mc}	R	CR
Hamming	-	-	-34.30	34.38
Cosh	5.04	-	-38.16	39.31
Dolph-Chebyshev	-	-	-46.70	31.17
Kaiser	5.48	-	-40.33	40.09
Modified Cosh-1	2.65	1.88	-40.00	40.10
Modified Cosh-2	1.81	2.8	-43.49	38.78

4.5 Modified Kaiser Window

4.5.1 Definition

In Section 4.4, it is demonstrated that with the proposed additional parameter (ρ_{mc}) the spectral characteristic of two-parameter Cosh window is improved significantly in terms of the ripple ratio. Since the Cosh window is derived in the same way as the Kaiser window, it is expected that proposing a similar parameter to the Kaiser window as a third parameter will improve its spectral characteristic. Therefore, by introducing a new parameter (ρ_{mk}) to the Kaiser window, a new three-parameter window, which is called “*modified Kaiser window*” through this report, is defined as [38]

$$w_{mk}(n) = \begin{cases} \frac{\left[I_0\left(\alpha_{mk} \sqrt{1 - \left(\frac{2n}{N-1}\right)^2}\right) \right]^{\rho_{mk}}}{I_0(\alpha_{mk})} & |n| \leq \frac{N-1}{2} \\ 0 & otherwise \end{cases} \quad (4.12)$$

From Eq. (4.12) it is seen that the modified Kaiser windows for $\rho_{mk} = 0$ and $\rho_{mk} = 1$ correspond to the Rectangular and Kaiser windows, respectively. Therefore, this modified window covers good spectral properties of the Kaiser window.

To observe the effect of ρ_{mk} on the modified Kaiser window spectrum, a simulation example for various ρ_{mk} with $N = 51$ and $\alpha_{mk} = 2$ is given below. It is seen from Figure 4.38 with the data summarized in Table 4.12 that when the parameter ρ_{mk} increases the mainlobe width increases and the ripple ratio decreases. Therefore, it can be concluded that ρ_{mk} has the same effect as the parameter ρ_{mc} of the modified Cosh window.

Table 4.12 Data for the effect of ρ_{mk} on the modified Kaiser window with $\alpha_{mk} = 2$ and $N = 51$

Window	α_{mk}	ρ_{mk}	w_R	R	S
Kaiser	2	1	0.129	-18.69	20.91
Mod. Kaiser-1	2	2	0.166	-26.50	18.99
Mod. Kaiser-2	2	3	0.215	-37.63	14.11

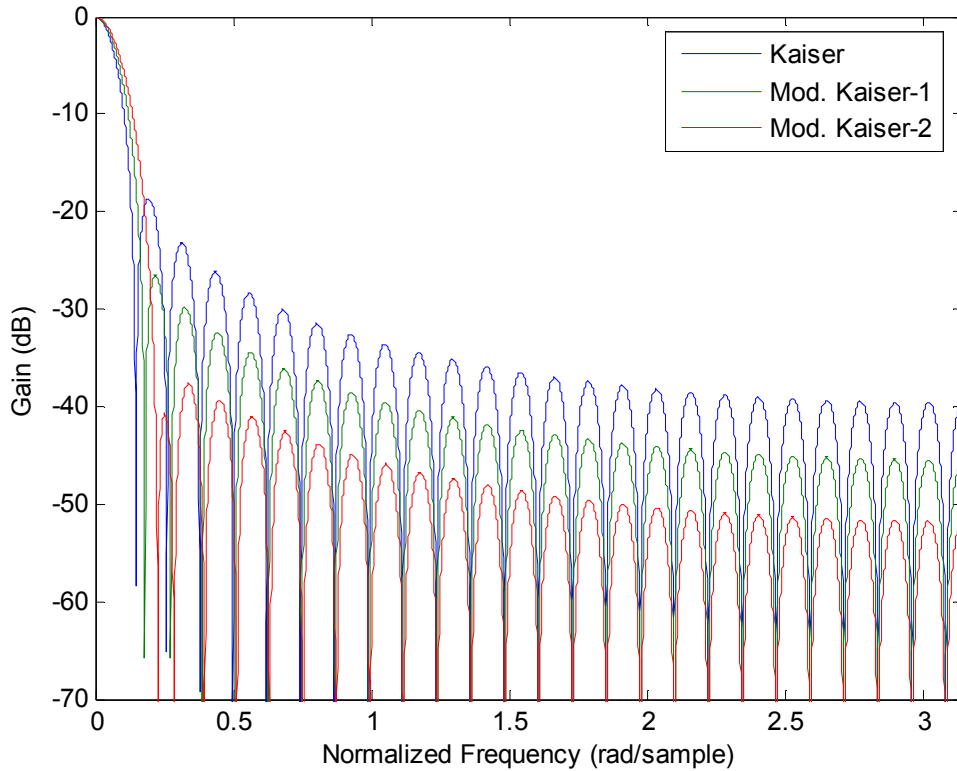


Figure 4.38 Effect of ρ_{mk} on the modified Kaiser window for $N = 51$ and $\alpha_{mk} = 2$

4.5.2 Spectrum design equations

Figure 4.39 shows the comparison of the Kaiser and modified Kaiser windows in terms of the ripple ratio for a wide range of the normalized width for $N = 51$. The plots in Figure 4.39 are found in the same way as the plots in Figure 4.32 in Section 4.4.2. The first plot in blue line is drawn for the Kaiser window, and it is found by changing its adjustable parameter α_k from 0 to 9.70 for $N = 51$. The second plot in green line is drawn for the modified Kaiser window for $\alpha_{mk} = 1$, and it is found by changing its adjustable parameter ρ_{mk} from 0 through 18.25. The data for obtaining all plots in Figure 4.39 can be found in Table 4.13.

Table 4.13 Data for the effect of adjustable parameters on the modified Kaiser window for $N = 51$

Window	N	α_{mk}	ρ_{mk}
Kaiser	51	0-9.70	1
Mod. Kaiser-1	51	1	from 0 to 18.25
Mod. Kaiser-2	51	1.5	from 0 to 9.10
Mod. Kaiser-3	51	2	from 0 to 5.86
Mod. Kaiser-4	51	3	from 0 to 3.44
Mod. Kaiser-5	51	4	from 0 to 2.50

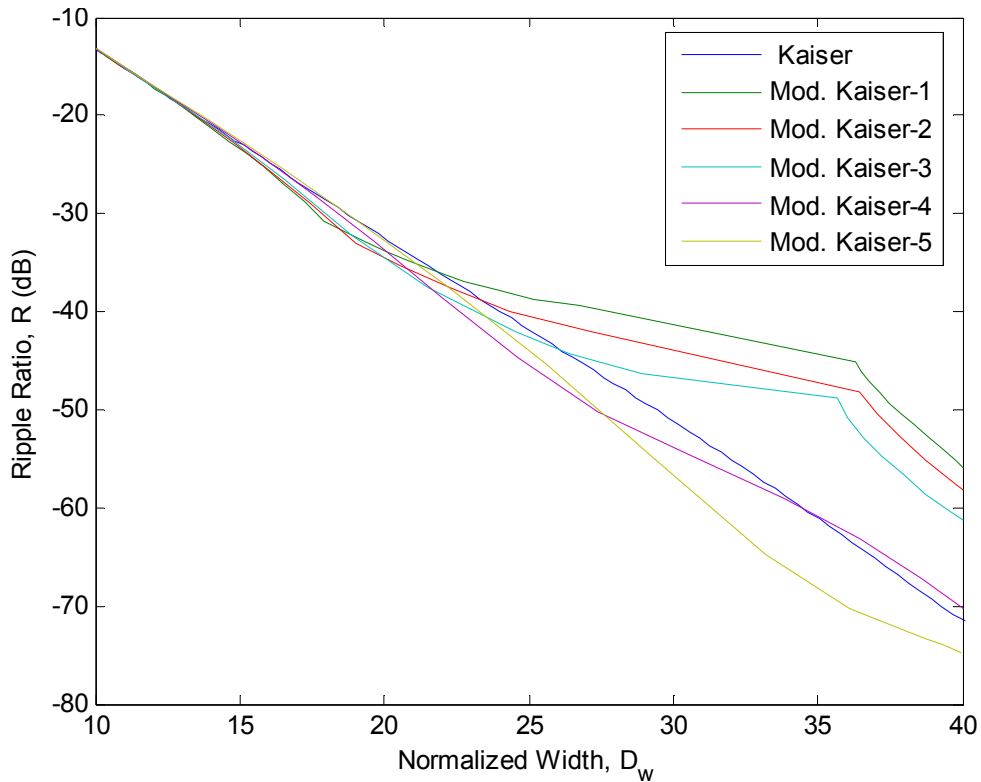


Figure 4.39 Effect of the adjustable parameters on the modified Kaiser window for $N = 51$

It can be observed from Figure 4.39 that the new parameter makes the modified Kaiser window more flexible than the Kaiser window. While two parameter Kaiser window provides only one ripple ratio for a fixed window length and mainlobe width, the modified Kaiser window can yield many ripple ratio like the modified Cosh window. From the figure, it is seen that the modified Kaiser window for $\alpha_{mk} = 1$ in green line provides better ripple ratio than the others for the range $D_w < 18.46$, but also worse ripple ratio than the others for the range $D_w > 21.85$. The modified Kaiser window for $\alpha_{mk} = 1.5$ in red line provides best ripple ratio values for the range $18.46 < D_w < 19.96$, but this window provides the second worst ripple ratio values for the range $D_w > 20.43$.

Since many windows with the combinations of α_{mk} and ρ_{mk} can be designed to satisfy a given mainlobe width for a fixed window length, it is important to be able to find the optimum window which yields the minimum ripple ratio. It is observed from many simulation examples that the minimum ripple ratio for modified Kaiser window for a fixed N value occurs when two sidelobes including the first one in the spectrum have equal amplitude. Figure 4.40 shows the ripple ratio characteristics of the optimum modified Kaiser window for $N = 51$ and 101 . As opposed to the Kaiser window, it can be seen that a change in the window length affects the ripple ratio for

the same normalized mainlobe width. And, Figure 4.41 gives the optimum combinations of α_{mk} and ρ_{mk} to provide the minimum ripple ratio for $N = 51$ and 101 .

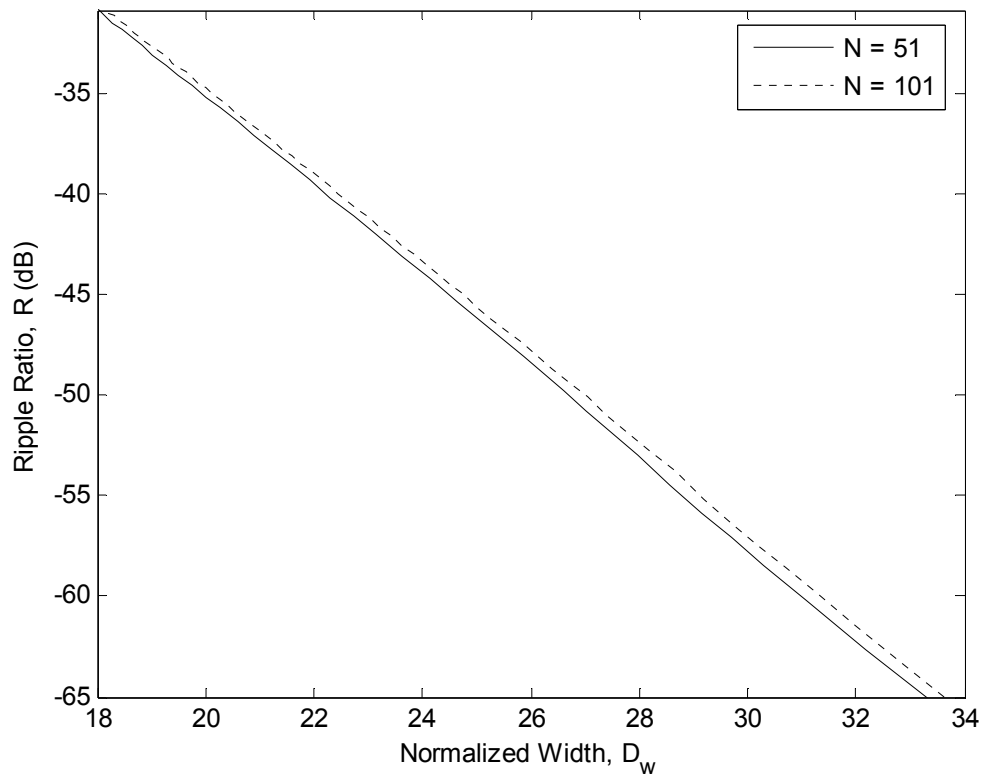


Figure 4.40 Optimum modified Kaiser windows for $N = 51$ and 101

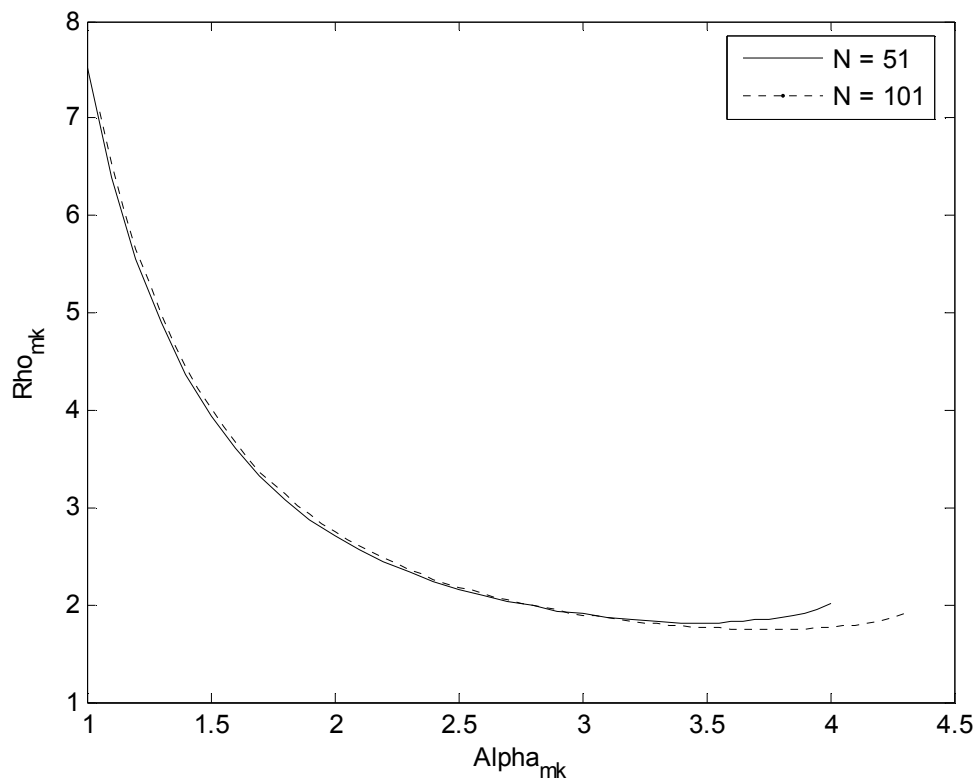


Figure 4.41 Relation between α_{mk} and ρ_{mk} of the optimum modified Kaiser window for $N = 51$ and 101

The design equations for the optimum modified Kaiser window for $N = 51$ are found by using curve fitting method in MATLAB

$$\alpha_{mk} = \begin{cases} 0 & R > -13.26 \\ -5.822 \times 10^{-5} R^3 - 11.05 \times 10^{-3} R^2 - 0.723 R - 12.29 & -65 \leq R \leq -30 \end{cases} \quad (4.13a)$$

$$\rho_{mk} = \begin{cases} 0 & R > -13.26 \\ 7.264 \times 10^{-6} R^4 + 1.576 \times 10^{-3} R^3 + 1.8282 \times 10^{-1} R^2 + 4.629 R + 64.33 & -65 \leq R \leq -30 \end{cases} \quad (4.13b)$$

And, the same relations can be found for $N = 101$ as

$$\alpha_{mk} = \begin{cases} 0 & R > -13.26 \\ -5.822 \times 10^{-5} R^3 - 11.05 \times 10^{-3} R^2 - 0.723 R - 12.29 & -65 \leq R \leq -30 \end{cases} \quad (4.14a)$$

$$\rho_{mk} = \begin{cases} 0 & R > -13.26 \\ 7.264 \times 10^{-6} R^4 + 1.576 \times 10^{-3} R^3 + 1.8282 \times 10^{-1} R^2 + 4.629 R + 64.33 & -65 \leq R \leq -30 \end{cases} \quad (4.14b)$$

Using Eq.(4.13) and Eq.(4.14), the modified Kaiser window which yields the narrowest mainlobe width can be designed for a given ripple ratio for $N = 51$ and 101. For other window lengths, the design equations can be found by obtaining the optimum combinations of α_{mk} and ρ_{mk} empirically with applying the same procedure above. Then, applying the suitable curve fitting polynomial, the desired relations can be obtained.

4.5.3 Spectrum comparisons

4.5.3.1 Comparisons with modified Cosh and Kaiser windows

The ripple ratio comparisons between the modified Kaiser, modified Cosh and two-parameter Kaiser windows for $N = 51$ and 101 are shown in Figure 4.42 and Figure 4.43, respectively. In both figures, it can be observed that the proposed modified Kaiser window provides a significantly better ripple ratio than the Kaiser windows. And, the difference in the ripple ratio becomes larger for higher values of the normalized width parameter. As for the comparison with the modified Cosh window, the modified Kaiser window provides worse results for $21 \leq D_w \leq 28$, and better results for $D_w > 28$.

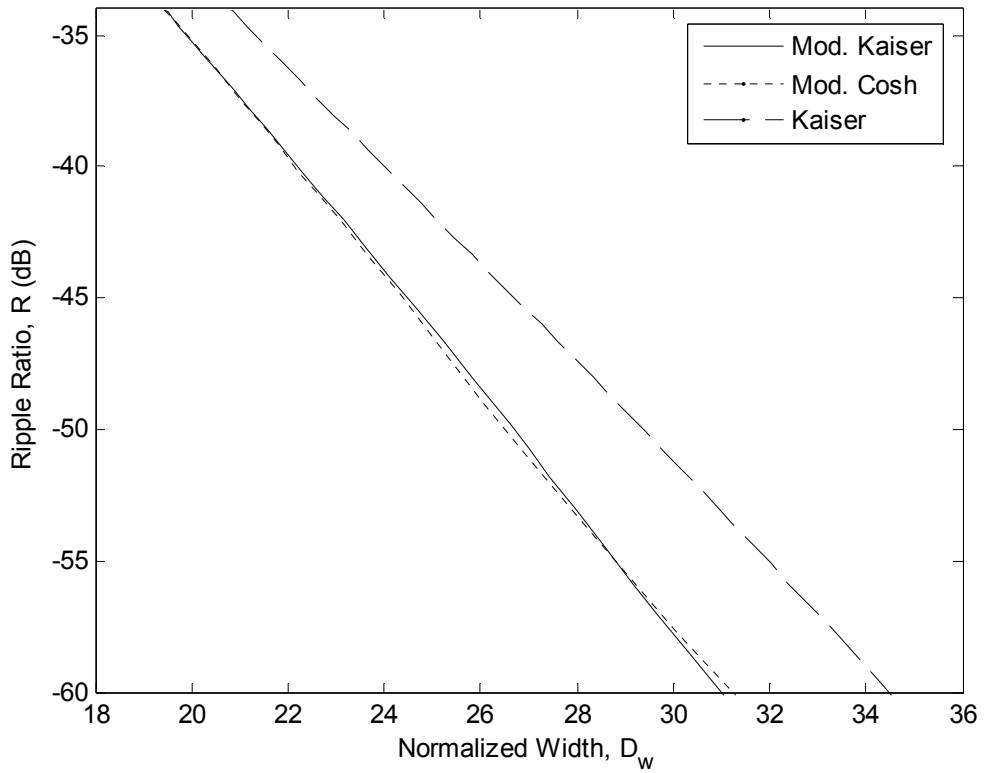


Figure 4.42 Ripple ratio comparison between the optimum modified Kaiser, modified Cosh and Kaiser windows for $N = 51$

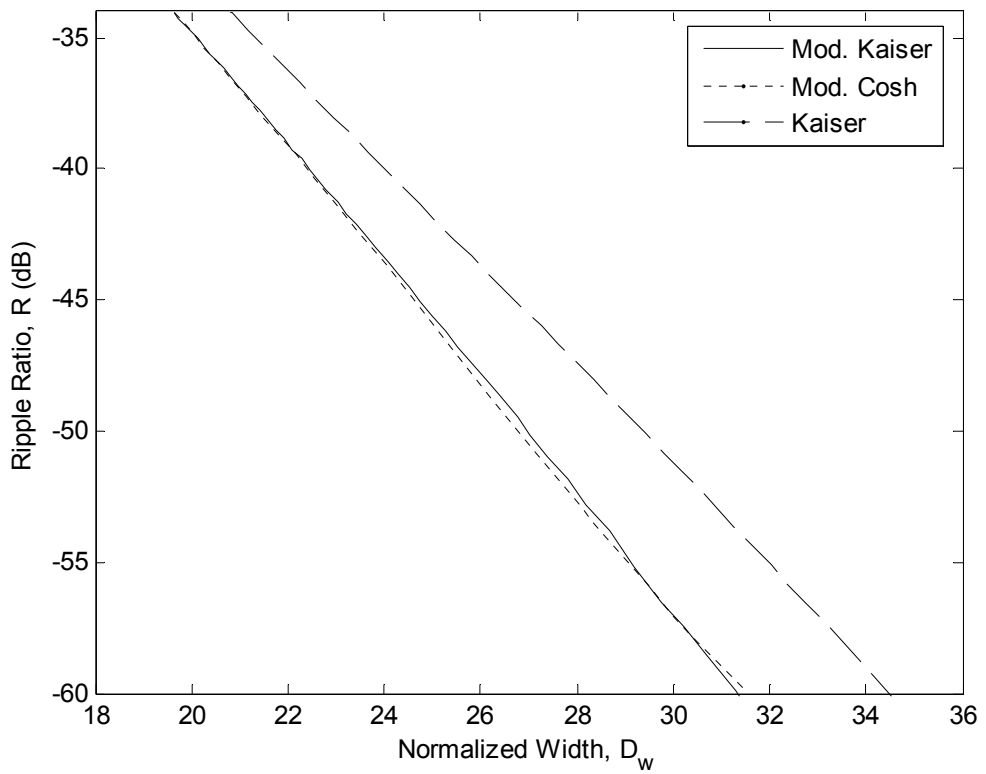


Figure 4.43 Ripple ratio comparison between the optimum modified Kaiser, modified Cosh and Kaiser windows for $N = 101$

4.5.3.2 Comparison with Ultraspherical window

The proposed modified Kaiser window with its optimum values and other three-parameter window known as the Ultraspherical is compared in terms of the ripple ratio for the same mainlobe width and sidelobe roll-off ratio with $N = 51$ [39]. The simulation result of the comparison is shown in Figure 4.44. The left y-axis gives the difference between the ripple ratio of the modified Kaiser window (R_{mk}) and that of Ultraspherical window (R_u). And, the right y-axis gives the sidelobe roll-off ratio. It can be observed that as the mainlobe width increases, the sidelobe roll-off ratio of the proposed window decreases. For wider normalized mainlobe width than $D_w = 33$ rad/sample, the sidelobe roll-off of the proposed modified window loses its monotonicity. From this figure, it is seen that for the given normalized width the proposed modified Kaiser window provides better ripple ratio than the Ultraspherical window with an amount between 1.19 dB and 1.62 dB.

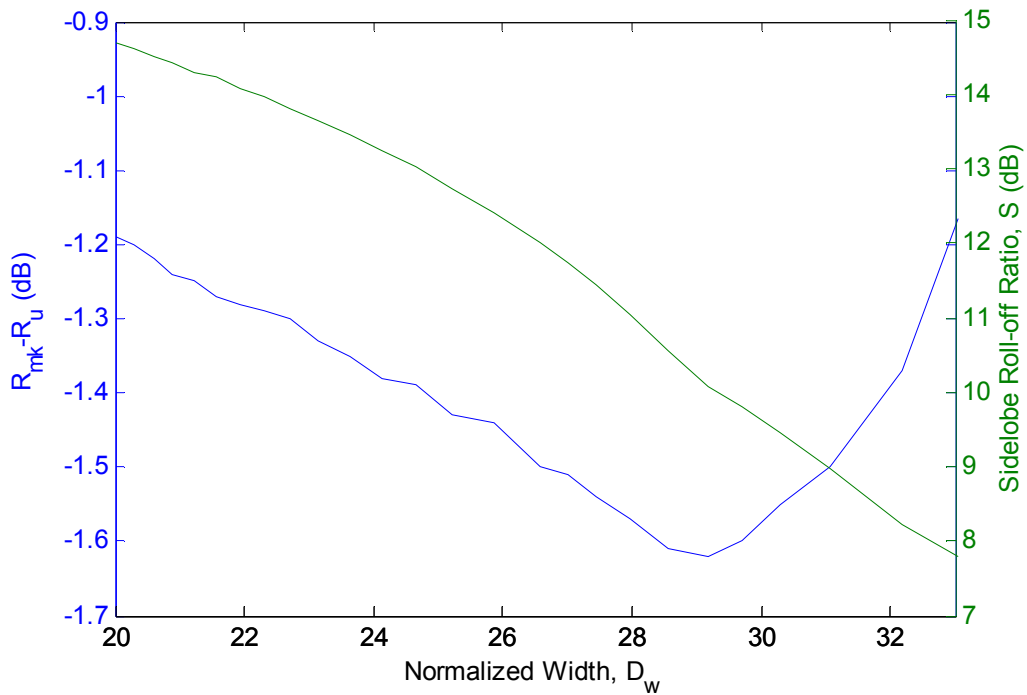


Figure 4.44 Ripple ratio comparison between the modified Kaiser and Ultraspherical windows for the same mainlobe width and sidelobe roll-off ratio with $N = 51$

CHAPTER-5

NONRECURSIVE FILTERS DESIGN USING THE PROPOSED WINDOW FUNCTIONS

5.1 Introduction

In this section, the use of four adjustable proposed windows is studied for the design of nonrecursive digital filters. First, the use of two-parameter Exponential and Cosh windows is analyzed, and the filter design equations are obtained with the error analyses. Then, three parameter modified Cosh and modified Kaiser windows are investigated for filter design. In the next part, two examples are given to demonstrate that our proposed windows provide low order and high quality filters compared to the other well known windows such as the Ultraspherical, Saramaki, Kaiser and Dolph-Chebyshev.

5.2 Nonrecursive Filters Design Using the Exponential Window

In Section 4.2 the Exponential window is introduced, and the simulation results demonstrate that it provides worse ripple ratio but has superior sidelobe roll-off ratio characteristic than the Kaiser window. Therefore, it may be useful for some filter applications [40] since the sidelobe roll-off ratio has a correlation with the far end attenuation.

Figure 5.1 shows the effect of the adjustable shape parameter, α_e , on the filter spectrum. From Figure 5.1 and Table 5.1 it is seen that an increase in the parameter α_e results in a wider transition width and a larger minimum stopband attenuation. This is an expected result because the transition width and minimum stopband attenuation are determined by the mainlobe width and ripple ratio parameters, respectively.

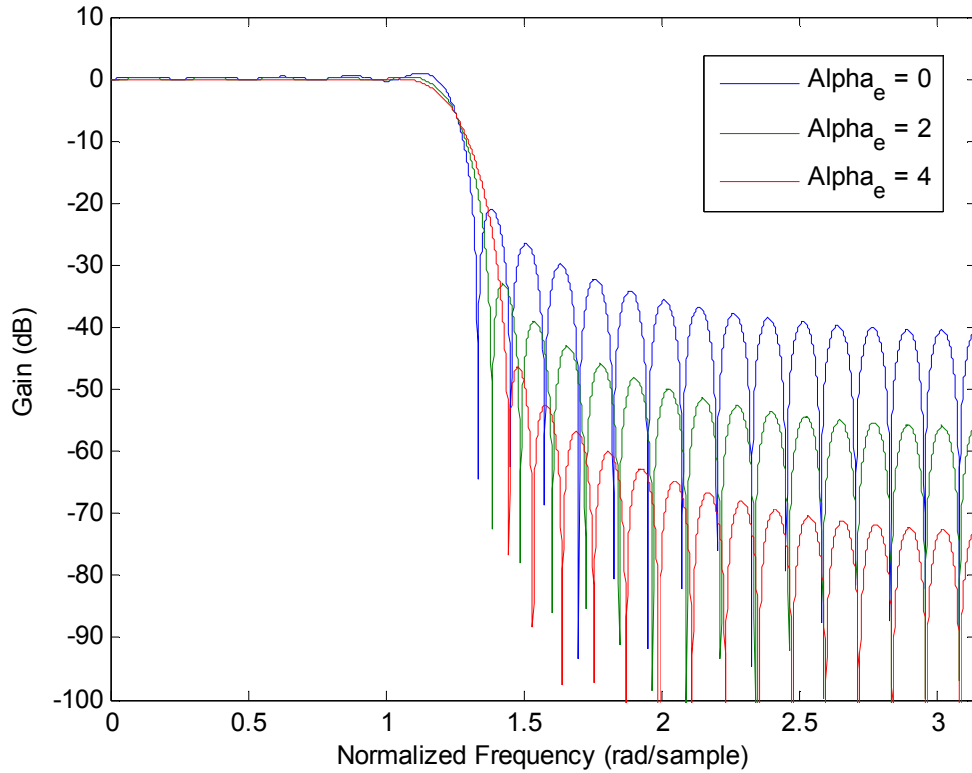


Figure 5.1 Lowpass filters designed by the Exponential window for $\alpha_e = 0, 2,$ and 4 with $N = 51$

Table 5.1 Data for the lowpass filters designed by the Exponential window for various α_e with $N = 51$

Window	N	α_e	Δw	A_s	A_{ms}
Exponential-1	51	0	0.1235	20.98	40.53
Exponential-2	51	2	0.2333	32.96	55.99
Exponential-3	51	4	0.3627	46.38	72.61

5.2.1 Filter design equations

To obtain the filter design equations for the Exponential window, it is necessary to find the relations between the window parameters and filter spectral parameters. Figure 5.2 shows the relation between α_e and the minimum stopband attenuation for $N = 127$. Therefore, using the curve fitting method in MATLAB a design equation for the adjustable parameter (α_e) in terms of the minimum stopband attenuation can be obtained as [41]

$$\alpha_{e,Appr} = \begin{cases} 0 & A_s > 20.8 \\ 4.053 \times 10^{-6} A_s^3 - 1.11 \times 10^{-3} A_s^2 + 0.2161 A_s - 4.047 & 20.8 \leq A_s \leq 120 \end{cases} \quad (5.1)$$

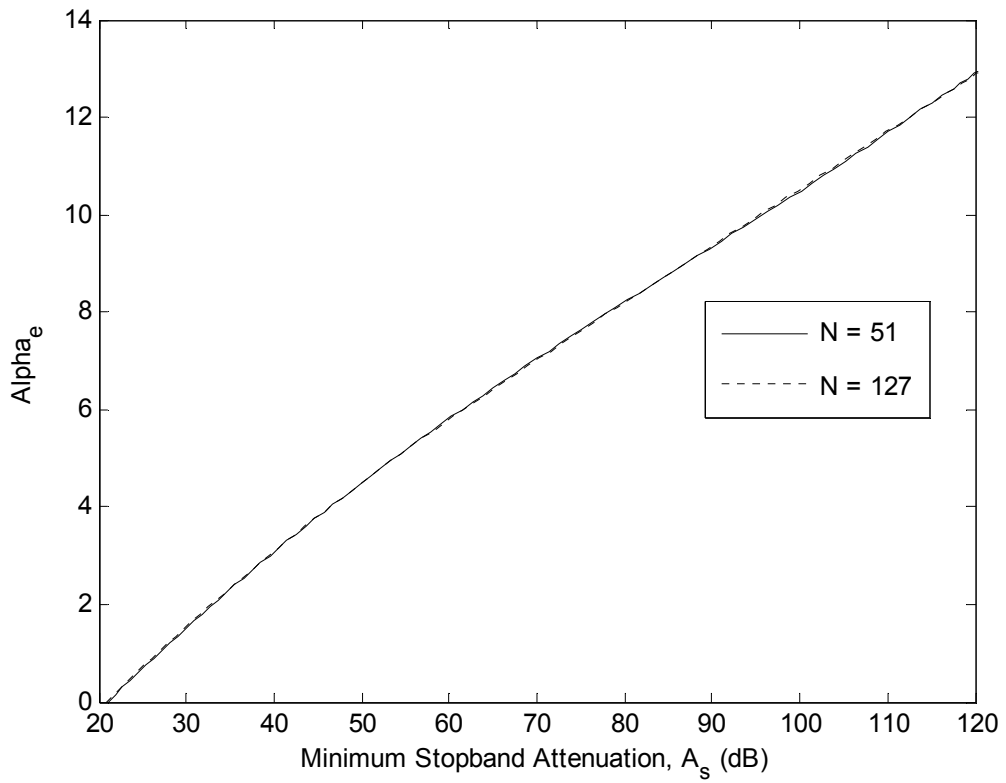


Figure 5.2 Relation between α_e and A_s for the Exponential window with $N = 51$ and 127

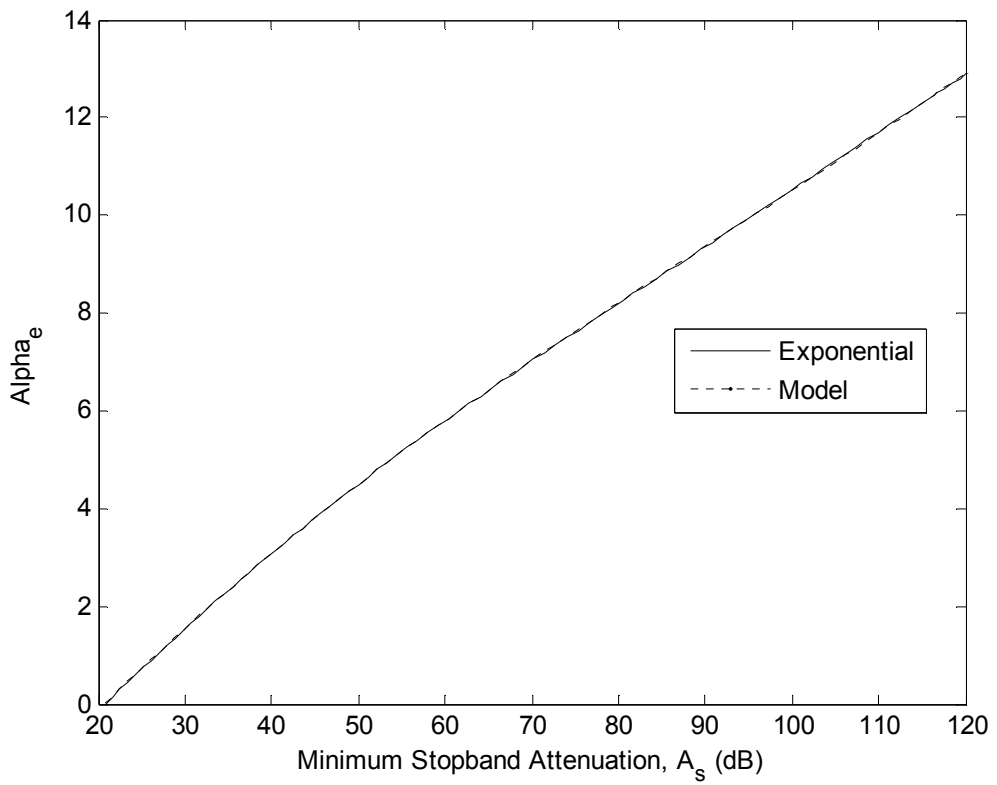


Figure 5.3 Approximated model for α_e of the Exponential window with $N = 127$

The approximation model for the adjustable shape parameter given by Eq. (5.1) is plotted in Fig. 5.3. It is seen that the proposed model provides a good approximation for $N = 127$. Also, the approximation error for $N = 127$ is plotted in Figure 5.4. The largest deviation in alpha is lower than 0.03 which results in a very small error in stopband attenuation.

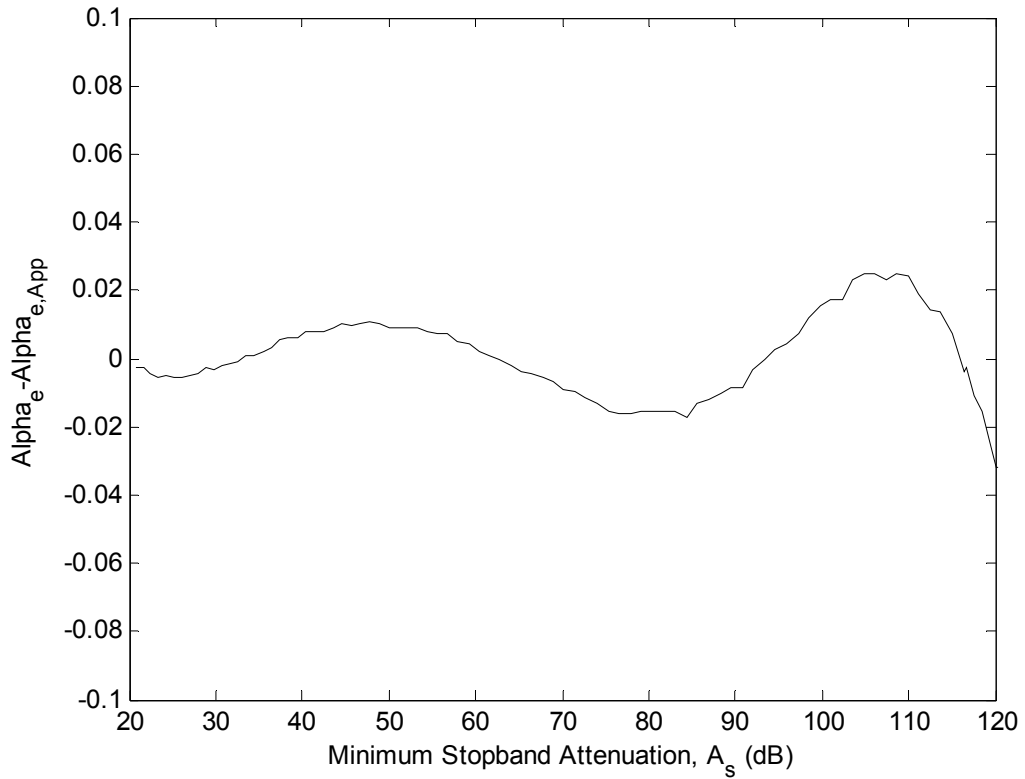


Figure 5.4 Error curve of approximated α_e versus A_s for $N = 127$

The second filter design equation is the relation between the filter length and the ripple ratio. To predict the filter length (N) for a given quantities A_s and Δw , the normalized transition width $D_f = 2 \Delta w(N-1)/w_s$ is used [14]. The relation between D_f and A_s for the Exponential window is found empirically and plotted in Figure 5.5. By using the curve fitting method, an approximate design relationship between the normalized transition width (D_f) and the minimum stopband attenuation (A_s) can be established as [41]

$$D_{f, Appr} = \begin{cases} 0 & A_s < 20.8 \\ 9.738 \times 10^{-5} A_s^2 + 67.94 \times 10^{-3} A_s - 0.4784 & 20.8 \leq A_s < 50 \\ 72.91 \times 10^{-3} A_s - 0.4769 & 50 \leq A_s \leq 120 \end{cases} \quad (5.2)$$

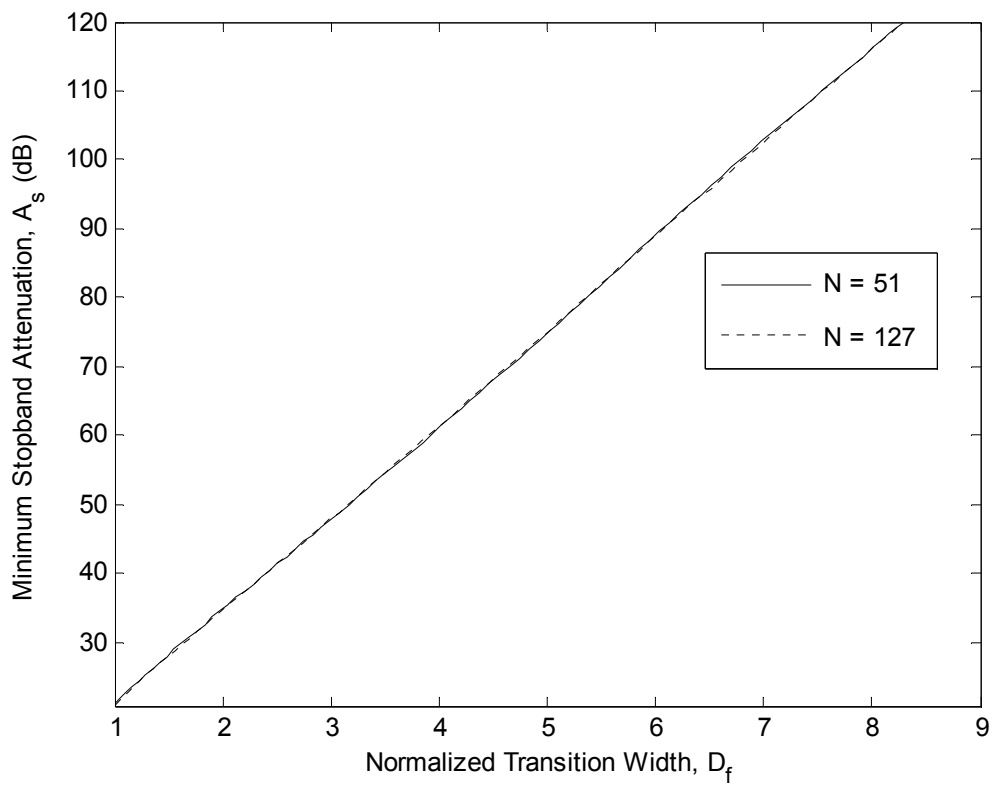


Figure 5.5 Relation between D_f and A_s for the Exponential window with $N = 51$ and 127

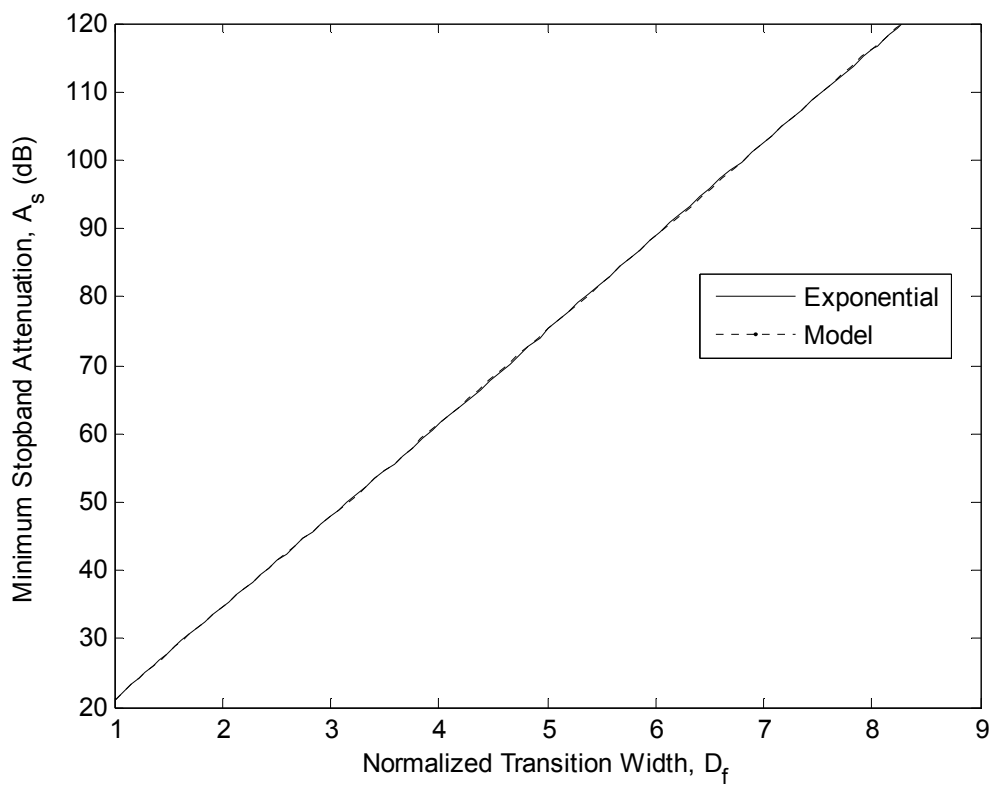


Figure 5.6 Approximated model for D_f of the Exponential window with $N = 127$

The approximation model for the normalized transition width given by Eq. (5.2) is plotted in Figure 5.6. It is seen that the proposed model provides a good approximation for $N = 127$. The relative error of approximated normalized transition width in percent versus the minimum stopband attenuation for $N = 127$ is plotted in Figure 5.7. The percentage error in the model changes between 0.65 and -0.30. This error range satisfies the error criterion in [2] which states that the predicted error in the normalized width must be smaller than 1 %.

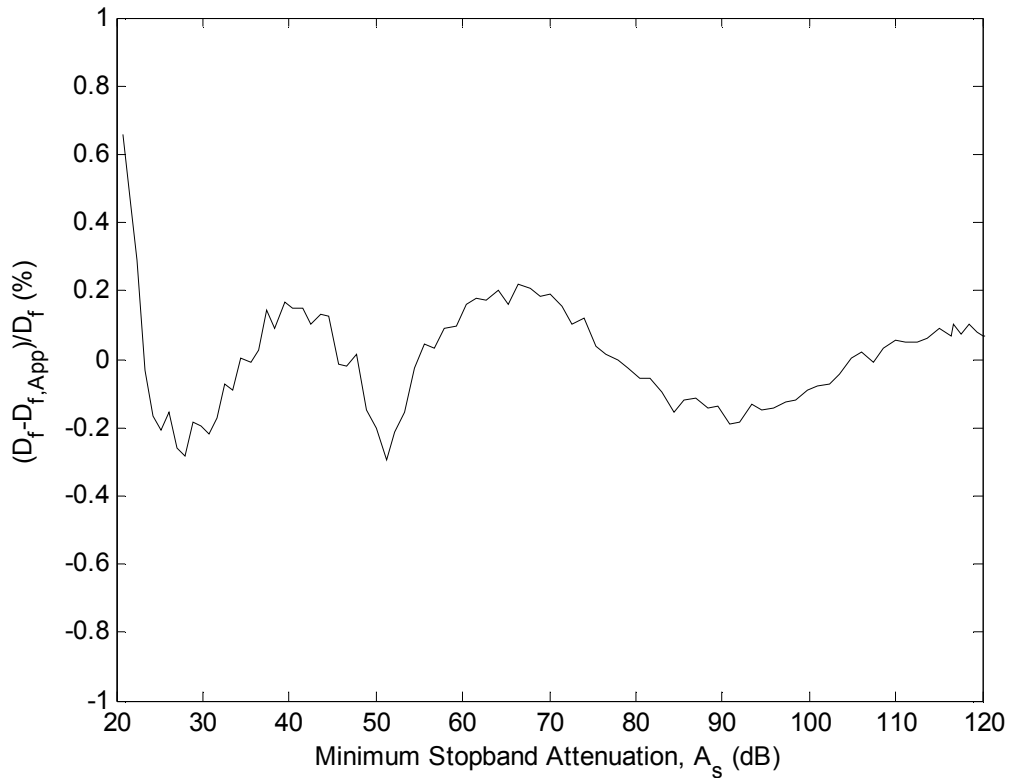


Figure 5.7 Relative error of approximated D_f for the Exponential window in percent versus A_s with $N = 127$

By using Eq. (5.2), the minimum odd integer filter length required for satisfying a given minimum stopband attenuation (A_s) and transition width (Δw) can be determined from [14]

$$N \geq \frac{D_{f,Appr} w_s}{\Delta w} + 1 \quad (5.3)$$

As a result, using the filter design equations given by Eq. (5.1) through (5.3), an Exponential window can be designed to satisfy the prescribed filter characteristic given in terms of A_s and Δw .

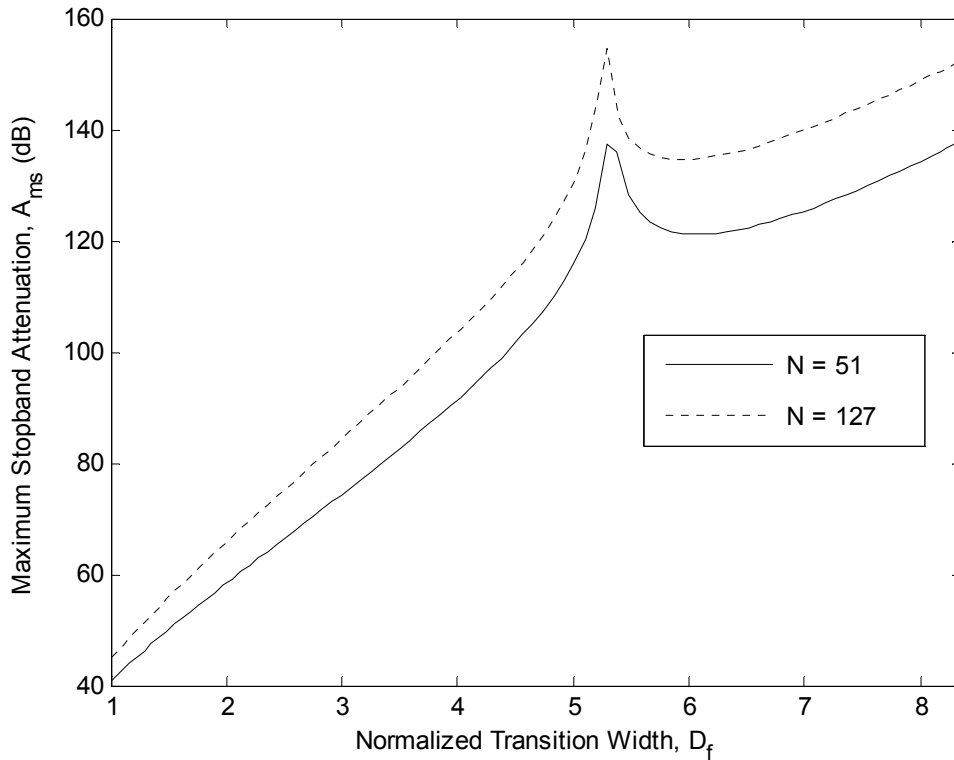


Figure 5.8 Relation between D_f and A_{ms} for the Exponential window with $N = 51$ and 127

Figure 5.8 shows the effect of the filter length on the relation between the maximum stopband attenuation and the normalized transition width for the filters designed by the Exponential window for $N = 51$ and 127 .

5.2.2 Filter spectrum comparisons with Kaiser window

Figure 5.9 shows the comparison of the filters designed by the Exponential and Kaiser windows in terms of the minimum stopband attenuation versus the normalized transition width for $N = 127$. It is observed that the filters designed by the Kaiser window perform better minimum stopband attenuation for the same filter length and transition width.

For the sake of another comparison with the Kaiser window, the far end stopband attenuation, which also gives the maximum stopband attenuation (A_{ms}) for the filters designed by the Exponential window, is taken as a figure of merit. The attenuation of the far end in stopband is important for some applications [40]. The comparison result is shown in Figure 5.10. It is seen that as the transition width becomes wider, the filters designed by the Exponential window performs better far end suppression than the filters designed by the Kaiser window.

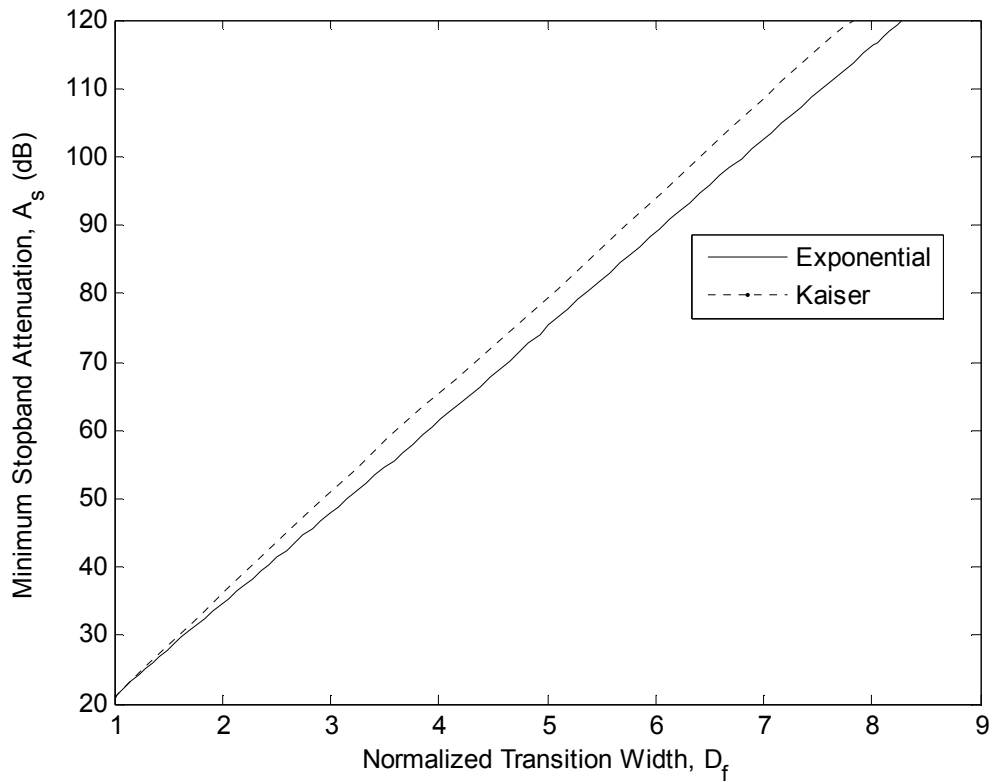


Figure 5.9 Minimum stopband attenuation comparison of the filters designed by the Exponential and Kaiser windows for $N = 127$

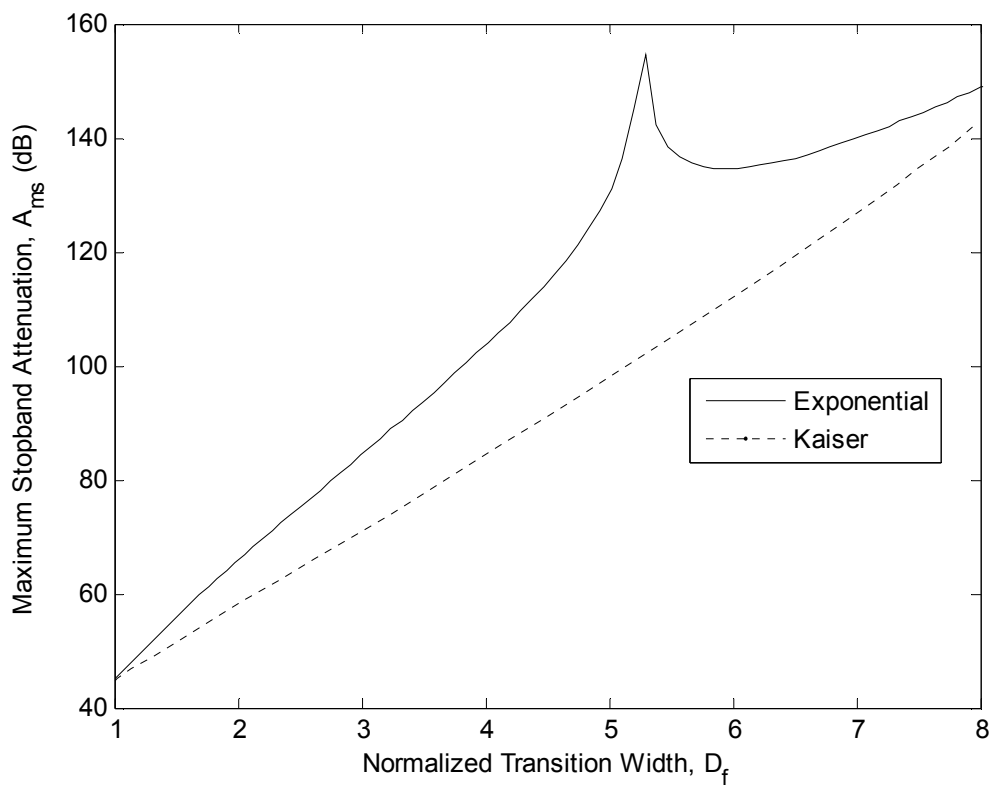


Figure 5.10 Maximum stopband attenuation comparison of the filters designed by the Exponential and Kaiser windows for $N = 127$

5.3 Nonrecursive Filters Design Using the Cosh Window

In Section 4.4 the Cosh window is introduced, and the simulation results demonstrate that it provides worse ripple ratio but better sidelobe roll-off ratio compared to the Kaiser window. As for the comparison with the Exponential window, the Cosh window provides better ripple ratio for narrow mainlobe width but worse sidelobe roll-off ratio. Therefore, it is expected for the filters designed by the Cosh window to provide better minimum stopband attenuation than the filters designed by the Exponential window for narrow transition widths.

Figure 5.11 shows the effect of the adjustable shape parameter, α_c , on the filters designed by the Cosh window. From Figure 5.11 and Table 5.2 which summarizes the figure, it is seen that an increase in the adjustable shape parameter α_c results in a wider transition width and a larger minimum stopband attenuation as in the case for α_e of the Exponential window.

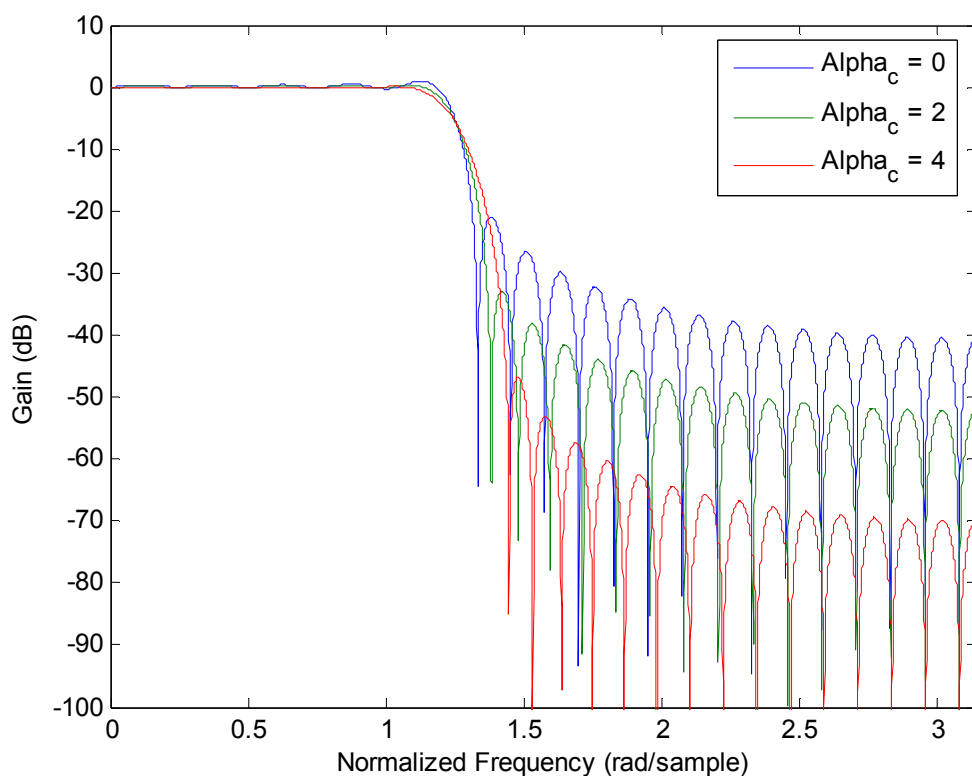


Figure 5.11 Lowpass filters designed by the Cosh window for $\alpha_c = 0, 2,$ and 4 with $N = 51$

Table 5.2 Data for the lowpass filters designed by the Cosh window for various α_c with $N = 51$

Window	N	α_c	Δw	A_s	A_{ms}
Cosh-1	51	0	0.1235	20.98	40.53
Cosh-2	51	2	0.2262	32.96	52.21
Cosh-3	51	4	0.3643	46.81	69.96

5.3.1 Filter design equations

The relation between the adjustable shape parameter α_c and the minimum stopband attenuation for $N = 127$ is empirically obtained, and the numerical result is shown in Figure 5.12. Therefore, using the curve fitting method in MATLAB a design equation for the parameter α_c in terms of the minimum stopband attenuation can be obtained as [36]

$$\alpha_{c, Appr} = \begin{cases} 0 & A_s < 20.8 \\ 0.2445(A_s - 20.78)^{0.4} + 0.1169(A_s - 20.78) & 20.8 \leq A_s < 50 \\ -8.722 \times 10^{-5} A_s^2 + 0.1335 A_s - 1.929 & 50 \leq A_s \leq 120 \end{cases} \quad (5.4)$$

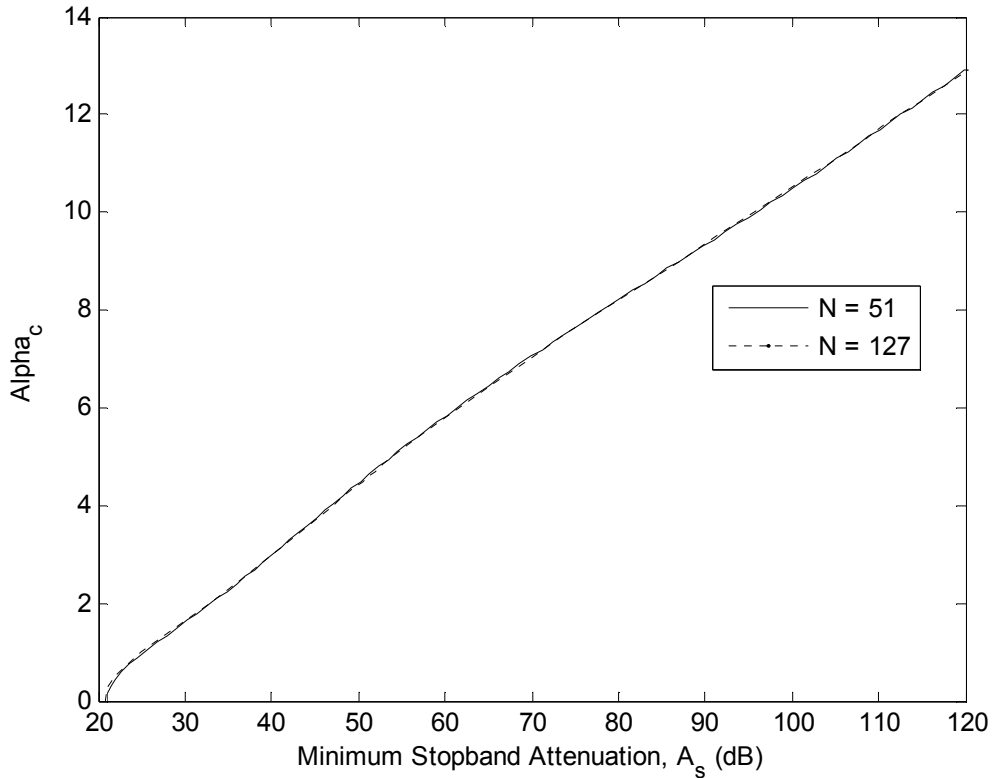


Figure 5.12 Relation between α_c and A_s for the Cosh window with $N = 51$ and 127

The approximation model for the adjustable shape parameter given by Eq. (5.4) is plotted in Fig. 5.13. It is seen that the proposed model provides a good approximation for $N = 127$. Also, the approximation error for $N = 127$ is plotted in Figure 5.14. The largest deviation in α is lower than 0.1 which results in a very small error in stopband attenuation.

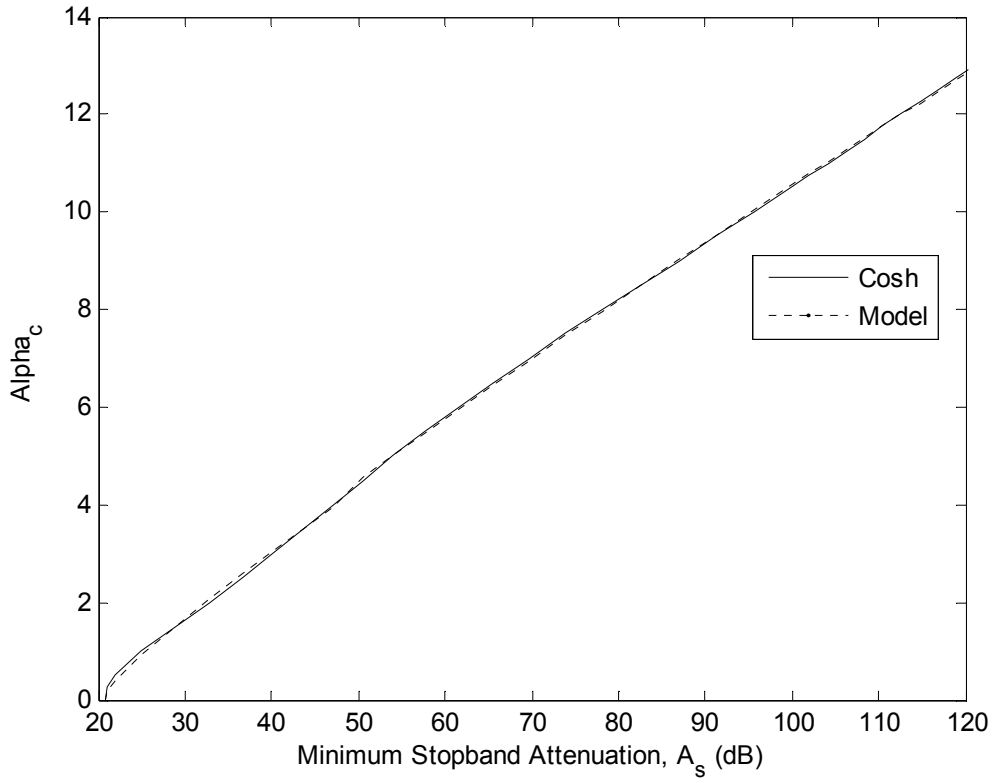


Figure 5.13 Approximated model for α_c of the Cosh window with $N = 127$

To provide the second filter design equation, the relation between D_f and A_s for the Cosh window is found empirically and plotted in Figure 5.15. By using the curve fitting method, an approximate design relationship for the Cosh window between the normalized transition width (D_f) and the minimum stopband attenuation (A_s) can be established as [36]

$$D_{f,Appr} = \begin{cases} 0 & A_s < 20.8 \\ 3.03 \times 10^{-4} A_s^2 + 0.05246 A_s - 0.2397 & 20.8 \leq A_s < 50 \\ -7.771 \times 10^{-6} A_s^2 + 0.07432 A_s - 0.5402 & 50 \leq A_s \leq 120 \end{cases} \quad (5.5)$$

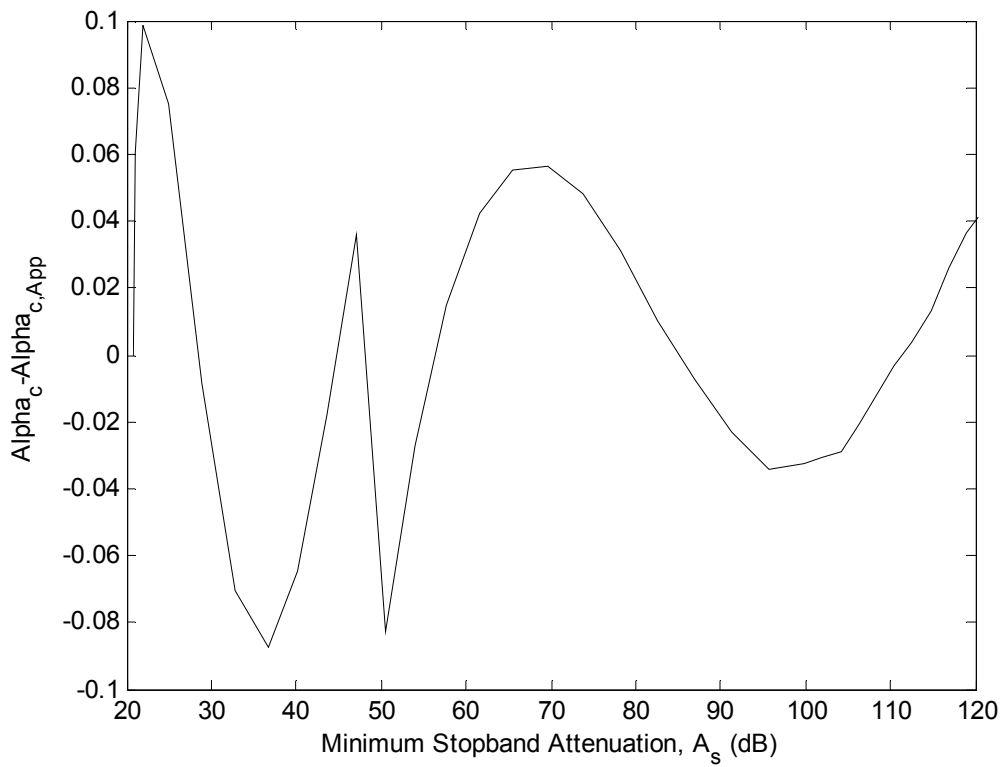


Figure 5.14 Error curve of approximated α_c versus A_s for $N = 127$

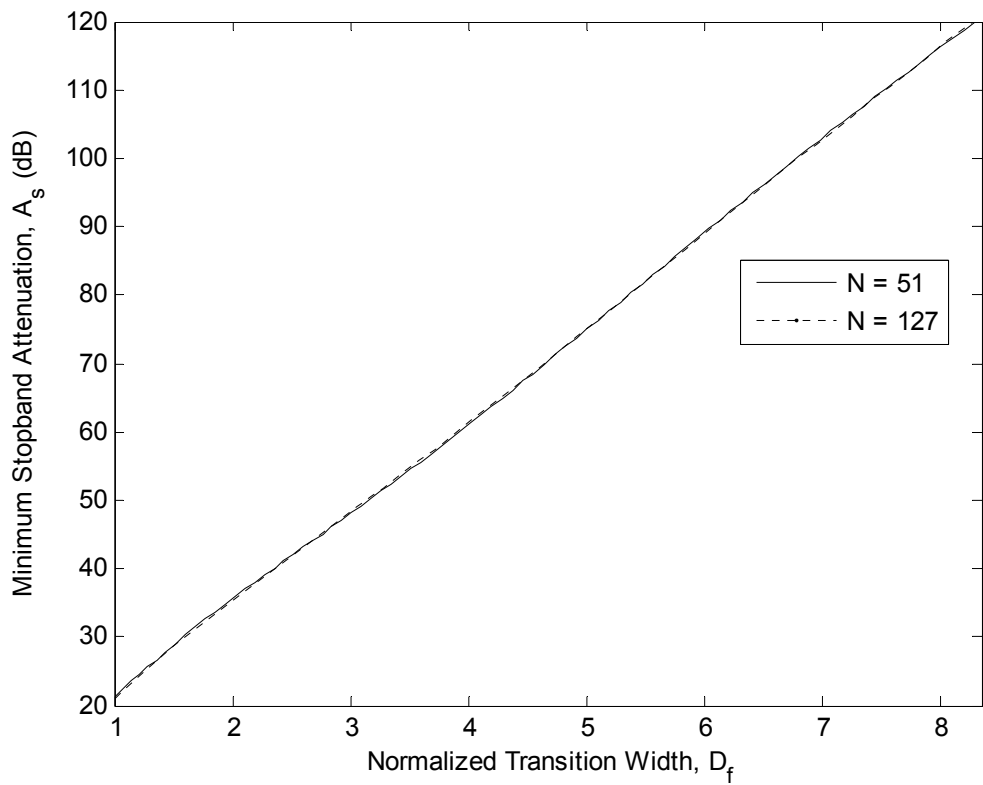


Figure 5.15 Relation between D_f and A_s for the Cosh window with $N = 51$ and 127

The approximation model for the normalized transition width of the Cosh window given by Eq. (5.5) is plotted with the actual normalized transition width in Figure 5.16. It is seen that the proposed model provides a good approximation for $N = 127$. The relative error of approximated normalized transition width in percent versus the minimum stopband attenuation for $N = 127$ is plotted in Figure 5.17. The percentage error in the model changes between 0.48 and -0.58. This error range satisfies the error criterion in [32] which states that the predicted error in the normalized width must be smaller than 1 %. As a result, using the filter design equations given by Eq. (5.3) through (5.5), a Cosh window can be designed to satisfy the prescribed filter characteristic given in terms of A_s and Δw .

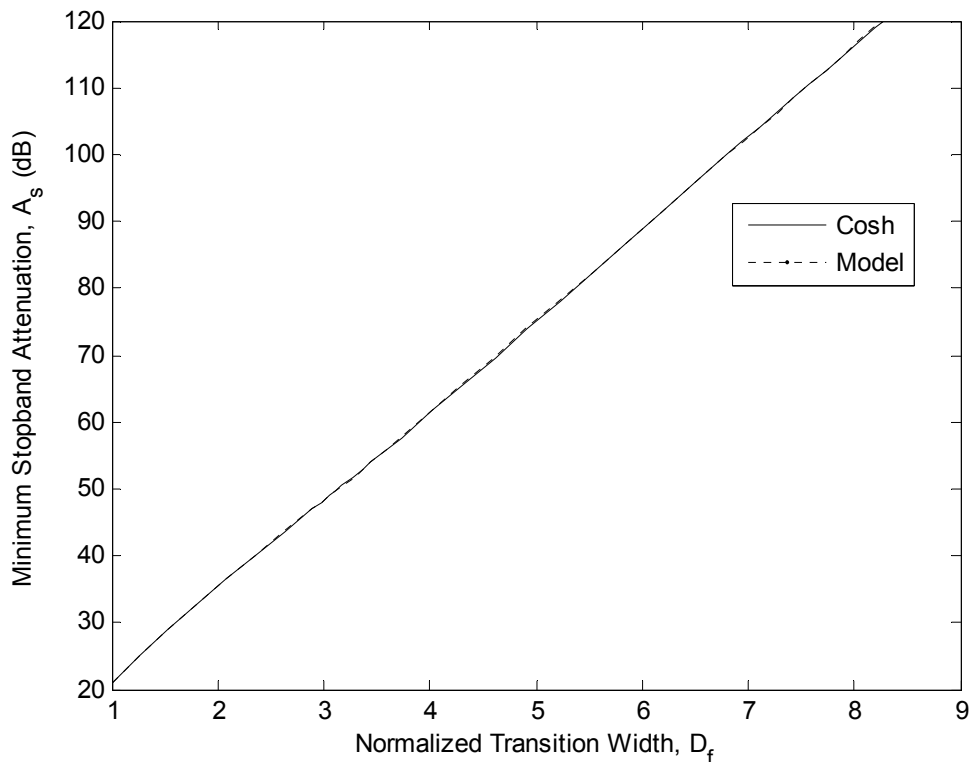


Figure 5.16 Approximated model for D_f of the Cosh window with $N = 127$

Figure 5.18 shows the effect of the filter length on the relation between the maximum stopband attenuation and the normalized transition width for the filters designed by the Cosh window for $N = 51$ and 127 .

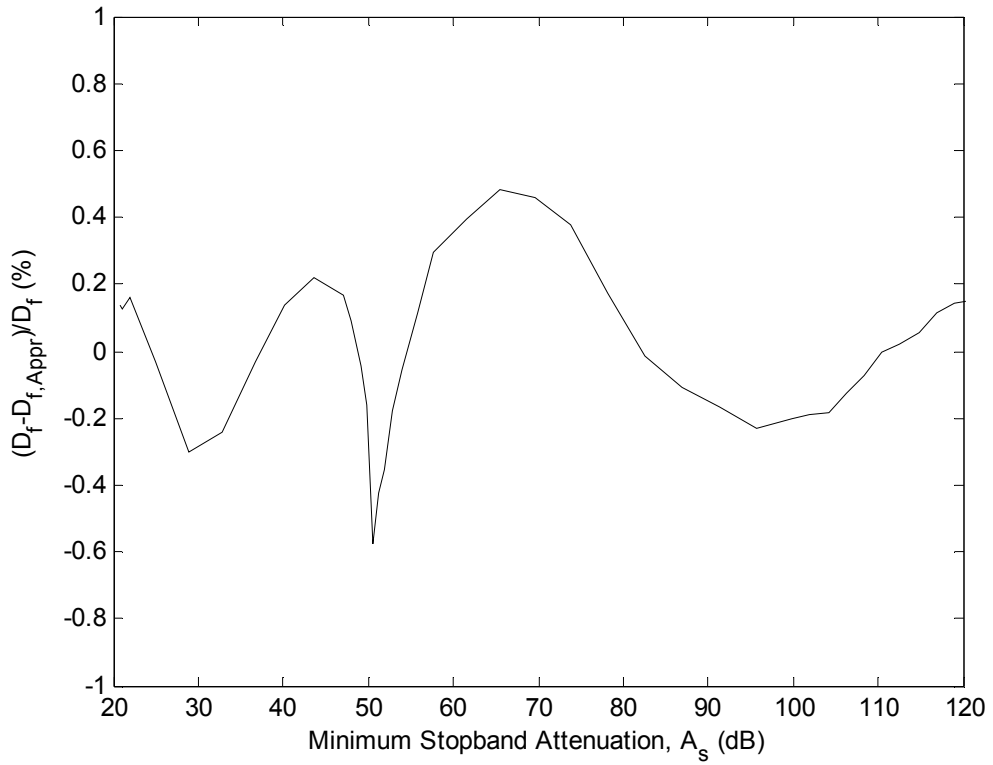


Figure 5.17 Relative error of approximated D_f for the Cosh window in percent versus A_s with $N = 127$

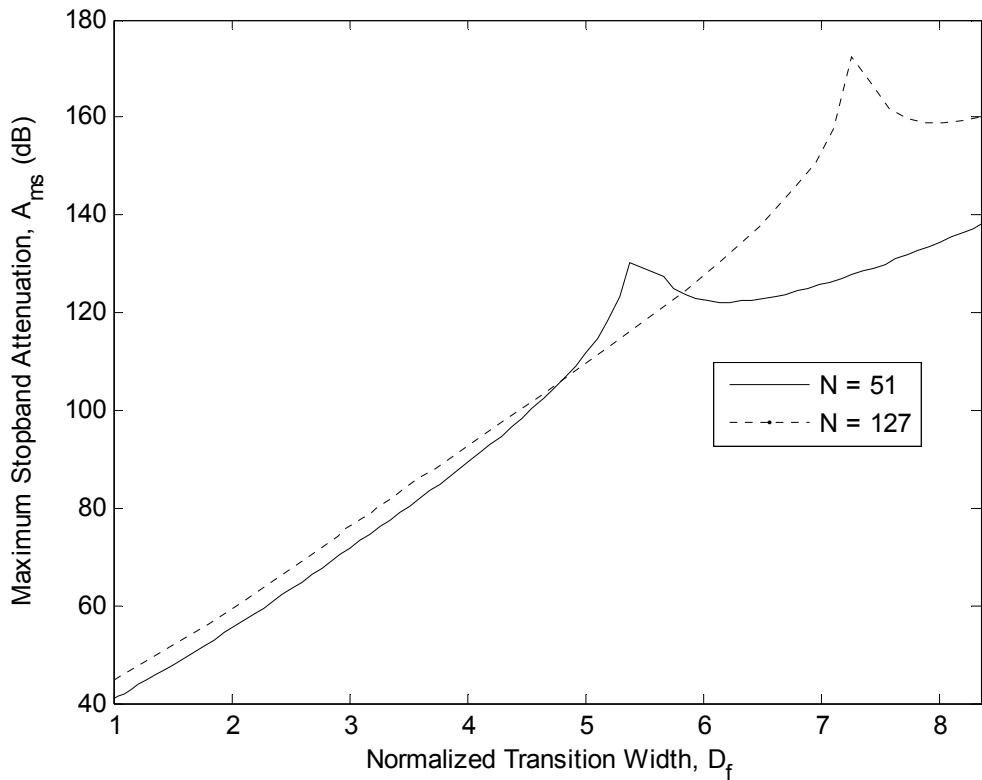


Figure 5.18 Relation between D_f and A_{ms} for the Cosh window with $N = 51$ and 127

5.3.2 Filter spectrum comparisons with Exponential and Kaiser windows

Figure 5.19 shows the comparison of the filters designed by the Cosh, Exponential and Kaiser windows in terms of the minimum stopband attenuation versus the normalized transition width for $N = 127$. It is observed that the filters designed by the Kaiser window perform better minimum stopband attenuation for the same filter length and transition width. Also, it is seen that the filters designed by the Cosh window provide a little better minimum stopband attenuation than the filters designed by the Exponential window for narrower transition width as expected.

As for the maximum stopband attenuation comparison of the filters designed by Cosh, Exponential and Kaiser windows for $N = 127$ is shown in Figure 5.20. It is seen that as the transition width becomes wider, the filters designed by the Cosh window performs better far end suppression than the filters designed by the Kaiser window, but perform worse results compared to the filters designed by the Exponential window until one ripple in the stopband is lost where the peak values occur.

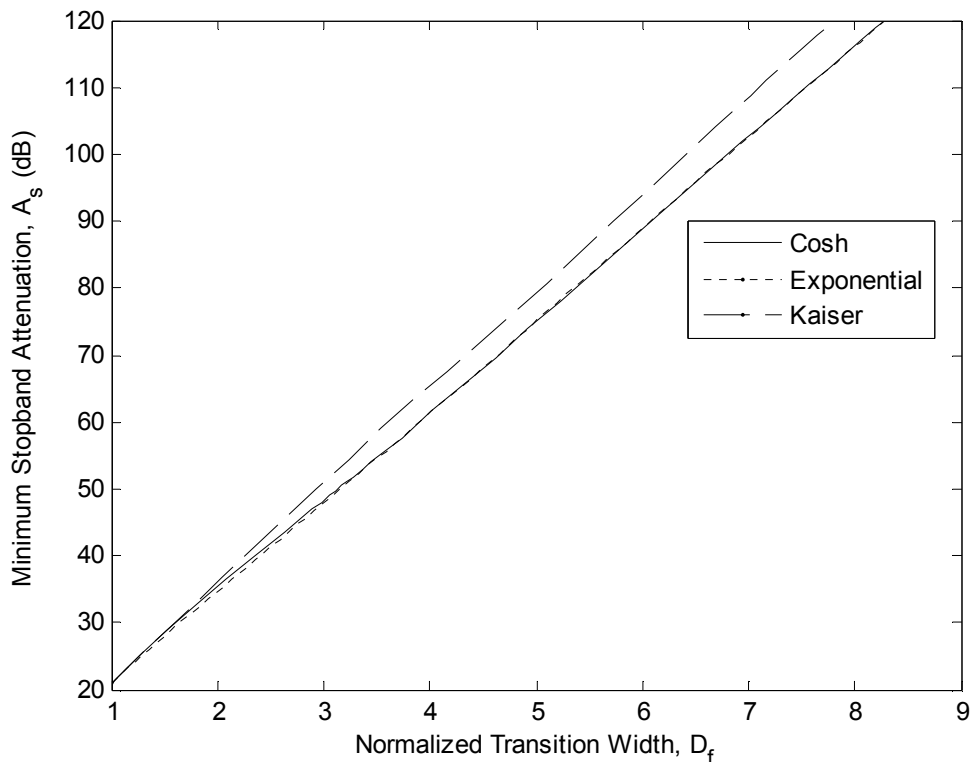


Figure 5.19 Minimum stopband attenuation comparison of the filters designed by the Cosh, Exponential and Kaiser windows for $N = 127$

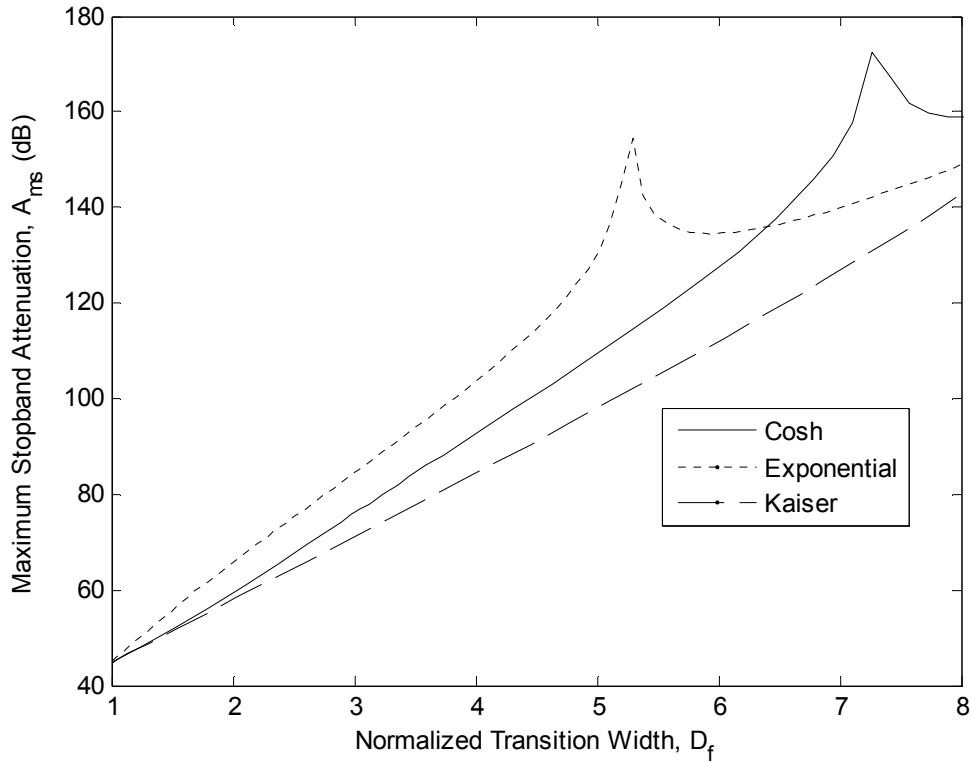


Figure 5.20 Maximum stopband attenuation comparison of the filters designed by the Cosh, Exponential and Kaiser windows for $N = 127$

5.4 Nonrecursive Filters Design Using the Modified Cosh Window

In Section 4.4, a third parameter is introduced for the Cosh window, and the simulation results demonstrate that the spectral characteristic of the modified Cosh window in terms of the ripple ratio is significantly improved compared to the Cosh and Kaiser windows. Therefore, it is expected for the modified Cosh window to provide better minimum stopband attenuation than the Cosh and Kaiser windows.

Figure 5.21 shows the effect of the adjustable shape parameter, ρ_{mc} , on the filter spectrum. From Figure 5.21 and Table 5.3 it is seen that an increase in the parameter ρ_{mc} results in a wider transition width and a larger minimum stopband attenuation.

Table 5.3 Data for the lowpass filters designed by the modified Cosh window for various ρ_{mc} with $\alpha_{mc} = 2$ and $N = 51$

Window	N	ρ_{mc}	Δw	A_s	A_{ms}
Modified Cosh-1	51	1	0.2262	32.96	52.21
Modified Cosh-2	51	2	0.3619	49.60	63.70
Modified Cosh-3	51	3	0.5298	70.60	76.26

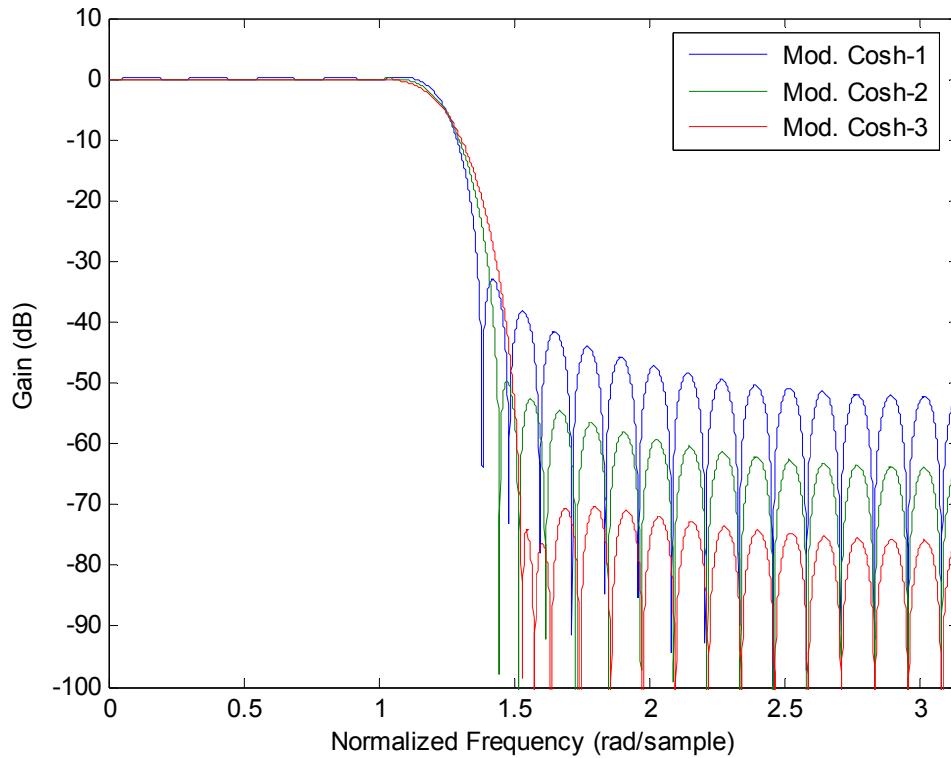


Figure 5.21 Lowpass filters designed by the modified Cosh window for various ρ_{mc} with $\alpha_{mc} = 2$ and $N = 51$

5.4.1 Optimum filter design by the modified Cosh window

Figure 5.22 shows the comparison of the lowpass filters designed by the two-parameter Cosh and modified Cosh windows in terms of the minimum stopband attenuation for a wide range of the normalized transition width for $N = 127$. The plots in Figure 5.22 are obtained as follows: The first plot in blue line is drawn for the Cosh window – which is also a special case of the modified Cosh window for $\rho_{mc} = 1$, and it is found by changing its adjustable parameter α_c from 0 to 13 for $N = 127$. The second plot in green line is drawn for the modified Cosh window for $\rho_{mc} = 1.5$, and it is found by changing its adjustable parameter α_{mc} from 0 through 9. The data for obtaining other plots can be found in Table 5.4.

Table 5.4 Data for the effect of adjustable parameters on the lowpass filters designed by the modified Cosh window with $N = 127$

Window	N	w_{ct}	ρ_{mc}	α_{mc}
Mod. Cosh-1	127	0.4π	1	from 0 to 13
Mod. Cosh-2	127	0.4π	1.5	from 0 to 9
Mod. Cosh-3	127	0.4π	2	from 0 to 6.5
Mod. Cosh-4	127	0.4π	3	from 0 to 4.5

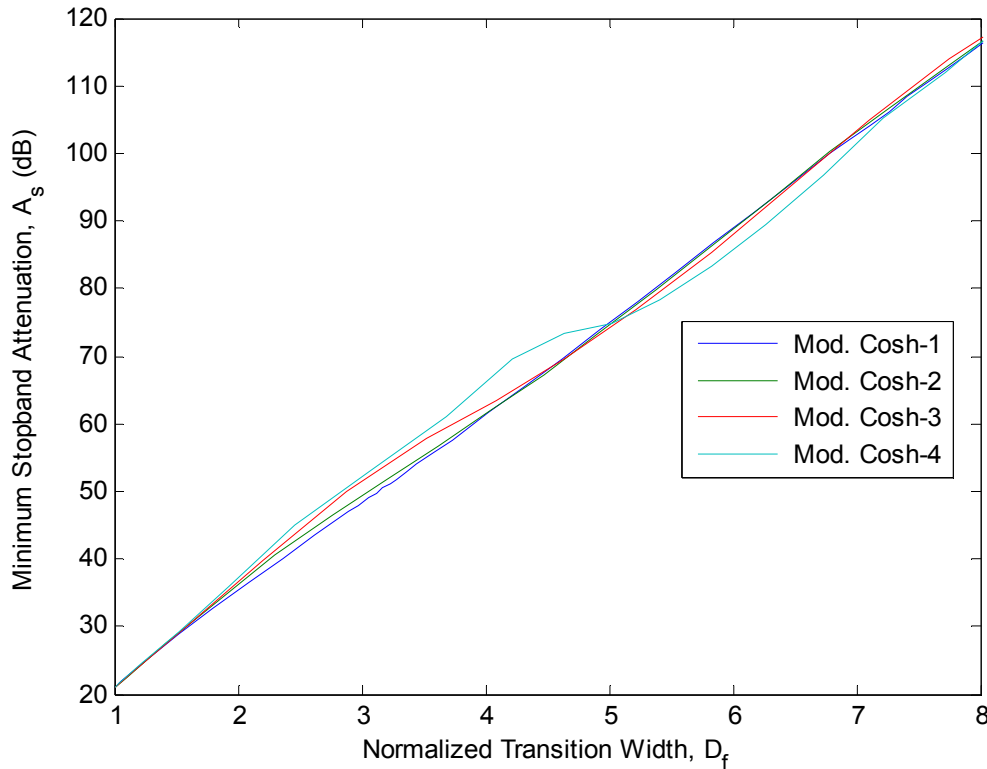


Figure 5.22 Effect of the adjustable parameters on the lowpass filters designed by the modified Cosh window for $N = 127$

Due to its flexibility property, it can be observed from Figure 5.22 that the modified Cosh window has many possibilities for the minimum stopband attenuation for a fixed filter length and transition width while the Cosh window drawn with blue line provides only one possibility. From the figure, it is seen that the modified Cosh window for $\rho_{mc} = 1.5$ in green line provides better minimum stopband attenuation than the others for the range $D_f < 4.98$, but also worst minimum stopband attenuation for the range $D_f > 5.16$. The modified Cosh window for $\rho_{mc} = 2$ in red line provides the second best minimum stopband attenuation for the range $D_f < 4.47$, the second worst one for the range $5.16 < D_f < 6.61$, and the best one for $D_f > 6.78$.

Since many filters using the modified Cosh windows with the combinations of α_{mc} and ρ_{mc} can be designed to satisfy a given transition width for a fixed filter length, it is important to be able to find the optimum filters which yield the largest minimum stopband attenuation. It is observed from many simulation examples that the optimum minimum stopband attenuation for a fixed N value occurs when two ripples including the first one in the stopband have equal amplitude. Figure 5.23 shows the minimum stopband characteristic of the optimum filters designed by the modified Cosh window for $N = 127$. And, Figure 5.24 gives the optimum

combinations of α_{mc} and ρ_{mc} to provide the minimum stopband characteristic for $N = 127$.

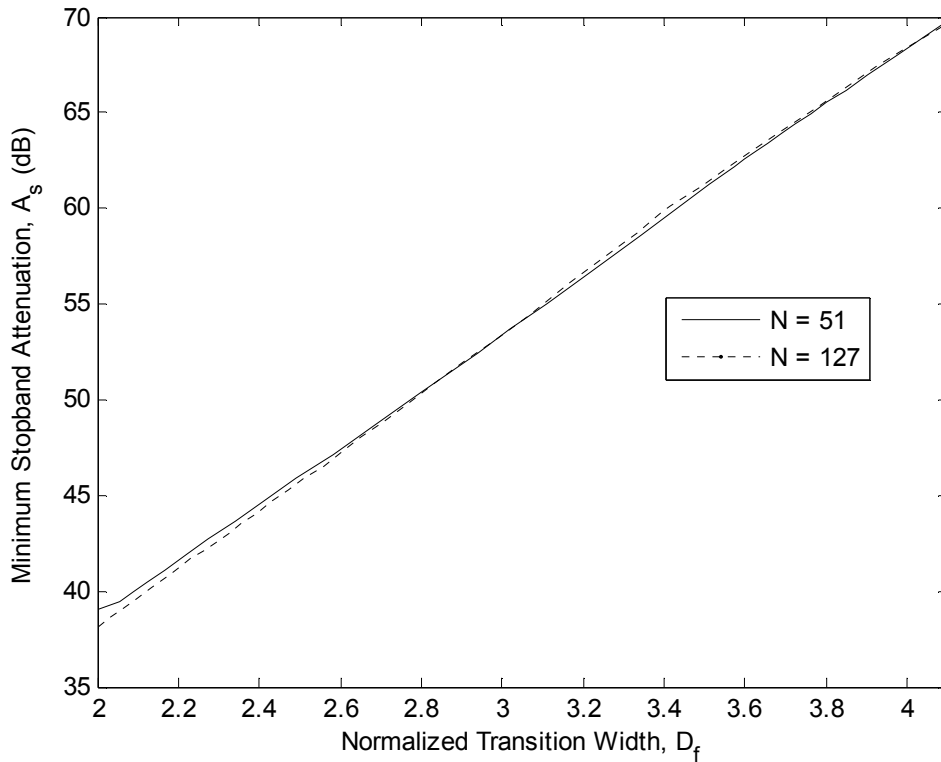


Figure 5.23 Minimum stopband attenuation characteristic of the optimum filters designed by the modified Cosh window for $N = 51$ and 127

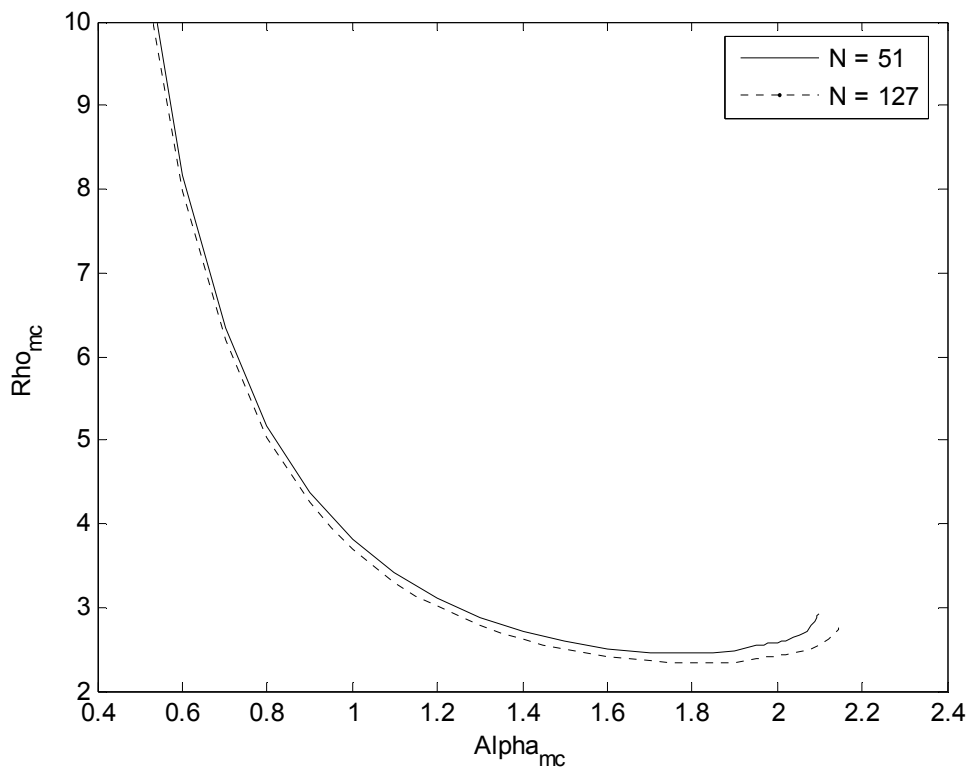


Figure 5.24 Relation between α_{mc} and ρ_{mc} of the modified Cosh window for the optimum filters with $N = 51$ and 127

5.4.2 Filter spectrum comparisons with Cosh, Exponential and Kaiser windows

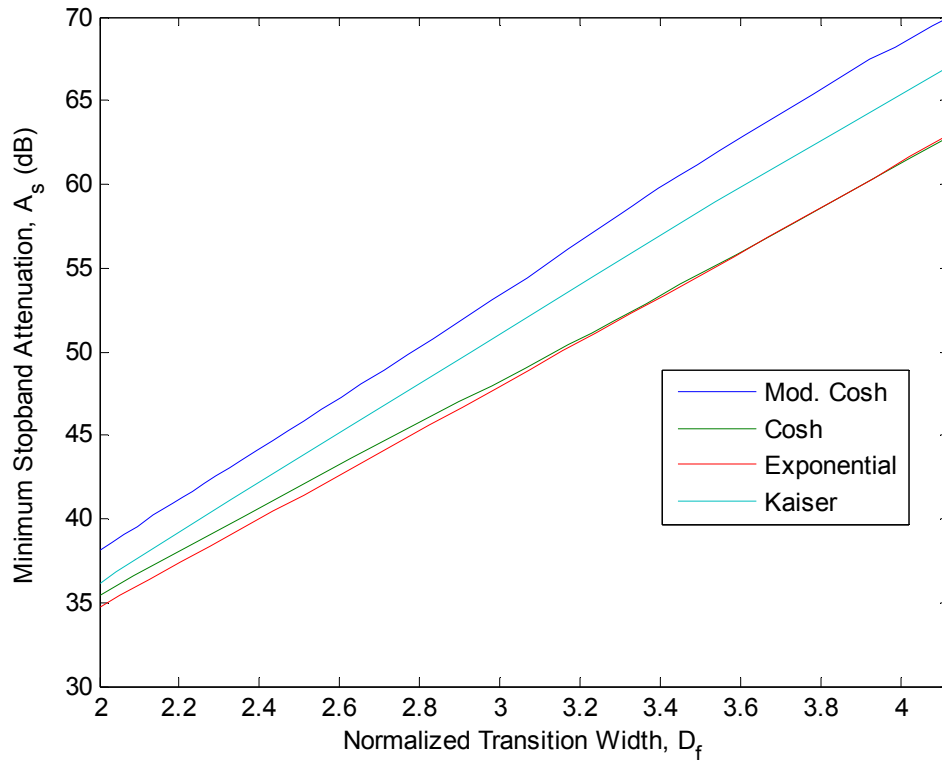


Figure 5.25 Minimum stopband attenuation comparison of the filters designed by the optimum modified Cosh, two-parameter Cosh, Exponential and Kaiser windows for $N = 127$

Figure 5.25 shows the comparison of the filters designed by the optimum modified Cosh, two-parameter Cosh, Exponential and Kaiser windows in terms of the minimum stopband attenuation for $N = 127$. It is seen that the additional parameter ρ_{mc} brings a superior minimum stopband attenuation improvement to the Cosh window. While the filters designed by the Cosh and Exponential windows performed worse results than the filters designed by the Kaiser window, the filters designed by the modified Cosh window can achieve better results in terms of the minimum stopband attenuation.

5.5 Nonrecursive Filters Design Using the Modified Kaiser Window

In Section 4.5, a third parameter is introduced for the Kaiser window, and the simulation results demonstrate that the spectral characteristic of the modified Kaiser window in terms of the ripple ratio is significantly improved compared to the Kaiser window. Therefore, like the modified Cosh window in Section 5.4 it is expected for

the modified Kaiser window to provide better minimum stopband attenuation than the Kaiser window.

Figure 5.26 shows the effect of the adjustable shape parameter, ρ_{mk} , on the filter spectrum. From Figure 5.26 and Table 5.5 it is seen that an increase in the parameter ρ_{mk} results in a wider transition width and a larger minimum stopband attenuation.

Table 5.5 Data for the lowpass filters designed by the modified Kaiser window for various ρ_{mk} with $\alpha_{mk} = 2$ and $N = 51$

Window	N	ρ_m	Δw	A_s	A_{ms}
Mod. Kaiser-1	51	1	0.1911	29.26	47.80
Mod. Kaiser-2	51	2	0.2784	40.97	55.06
Mod. Kaiser-3	51	3	0.3960	52.01	62.34

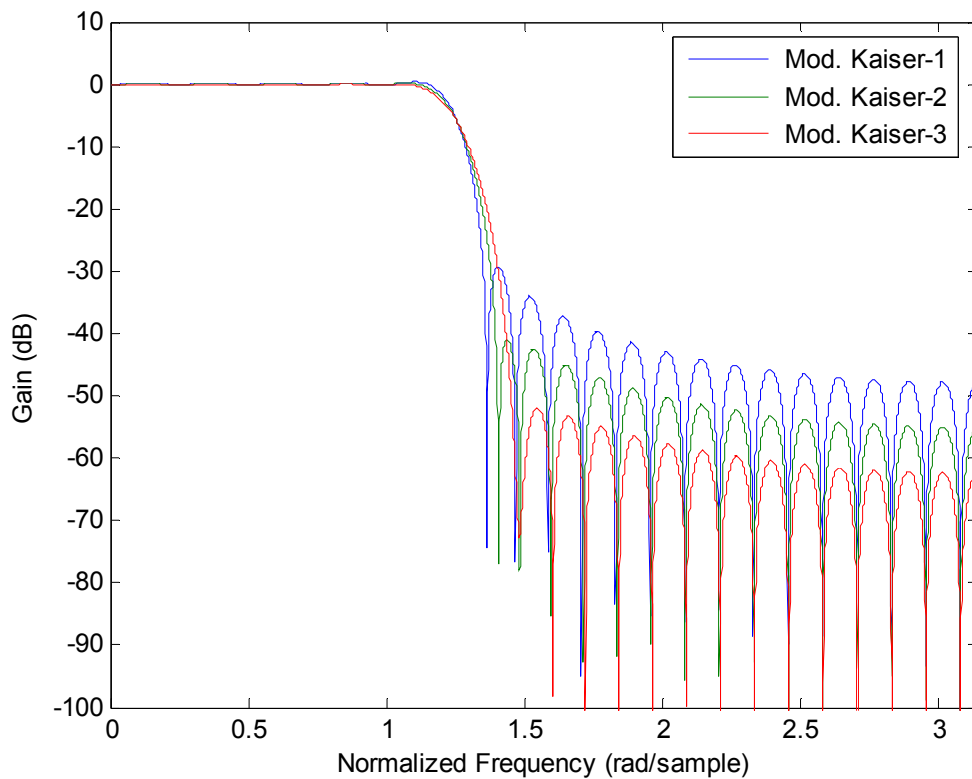


Figure 5.26 Lowpass filters designed by the modified Kaiser window for various ρ_{mk} with $\alpha_{mk} = 2$ and $N = 51$

5.5.1 Optimum filter design by the modified Kaiser window

Figure 5.27 shows the comparison of the lowpass filters designed by the two-parameter Kaiser and modified Kaiser windows in terms of the minimum stopband attenuation for a wide range of the normalized transition width for $N = 127$. The plots in Figure 5.27 are obtained as follows: The first plot in blue line is drawn for the Kaiser window – which is also a special case of the modified Kaiser window for $\rho_{mk} = 1$, and it is found by changing its adjustable parameter α_k from 0 to 12.6 for $N = 127$. The second plot in green line is drawn for the modified Kaiser window for $\rho_{mk} = 1.5$, and it is found by changing its adjustable parameter α_{mk} from 0 through 8.5. The data for obtaining other plots can be found in Table 5.6.

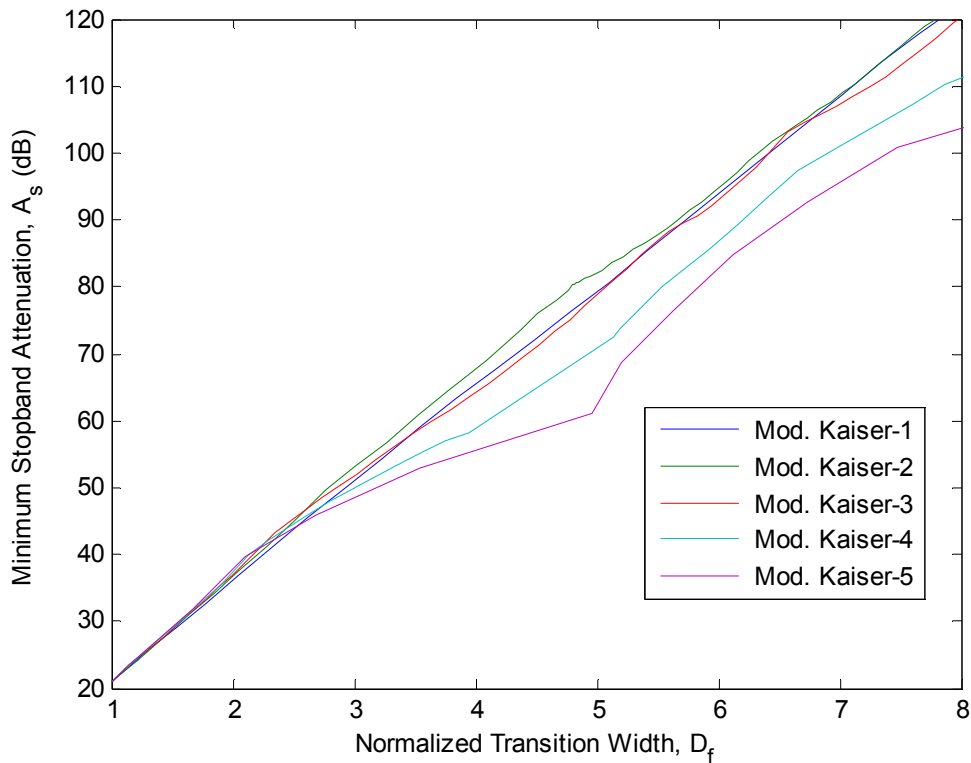


Figure 5.27 Effect of the adjustable parameters on the lowpass filters designed by the modified Kaiser window for $N = 127$

Table 5.6 Data for the effect of the adjustable parameters on the lowpass filters designed by the modified Kaiser window with $N = 127$

Window	N	w_{ct}	ρ_{mk}	α_{mk}
Mod. Kaiser-1	127	0.4π	1	from 0 to 12.6
Mod. Kaiser-2	127	0.4π	1.5	from 0 to 8.5
Mod. Kaiser-3	127	0.4π	2	from 0 to 6.5
Mod. Kaiser-4	127	0.4π	3	from 0 to 4.7
Mod. Kaiser-5	127	0.4π	4	from 0 to 4.0

Like the modified Cosh window, it can be observed from Figure 5.27 that the modified Kaiser window has many possibilities for the minimum stopband attenuation for a fixed filter length and transition width while the Kaiser window drawn with blue line provides only one possibility. Therefore, it is important to be able to find the optimum filters which yield the highest minimum stopband attenuation. It is observed from many simulation examples that the optimum minimum stopband attenuation for a fixed N value occurs when two ripples including the first one in the stopband have equal amplitude. Figure 5.28 shows the minimum stopband characteristic of the optimum filters designed by the modified Kaiser window for $N = 127$. And, Figure 5.29 gives the optimum combinations of α_{mk} and ρ_{mk} to provide the minimum stopband characteristic for $N = 127$.

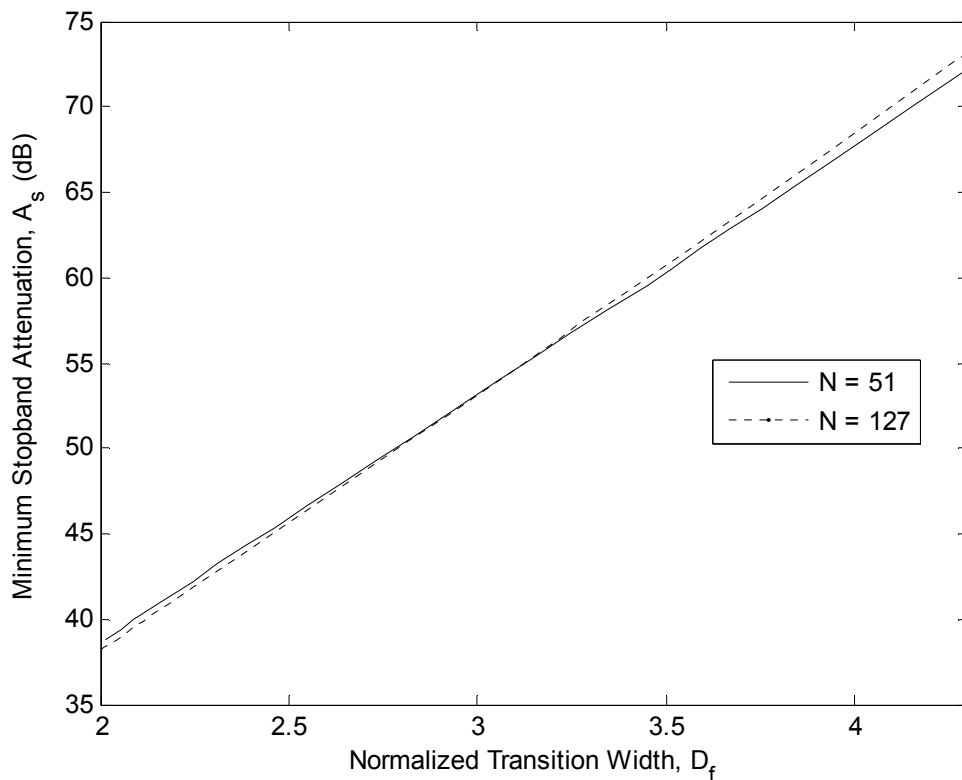


Figure 5.28 Minimum stopband attenuation characteristic of the optimum filters designed by the modified Kaiser window for $N = 51$ and 127

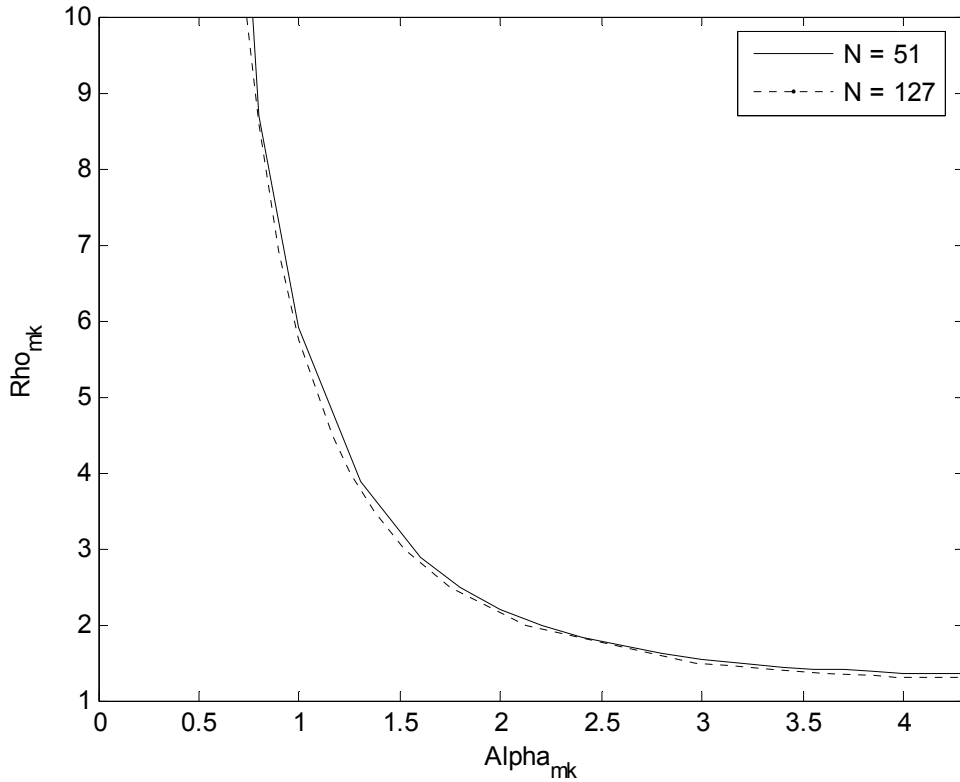


Figure 5.29 Relation between α_{mk} and ρ_{mk} of the modified Kaiser window for the optimum filters with $N = 51$ and 127

5.5.2 Filter spectrum comparisons with modified Cosh, Cosh, Exponential and Kaiser windows

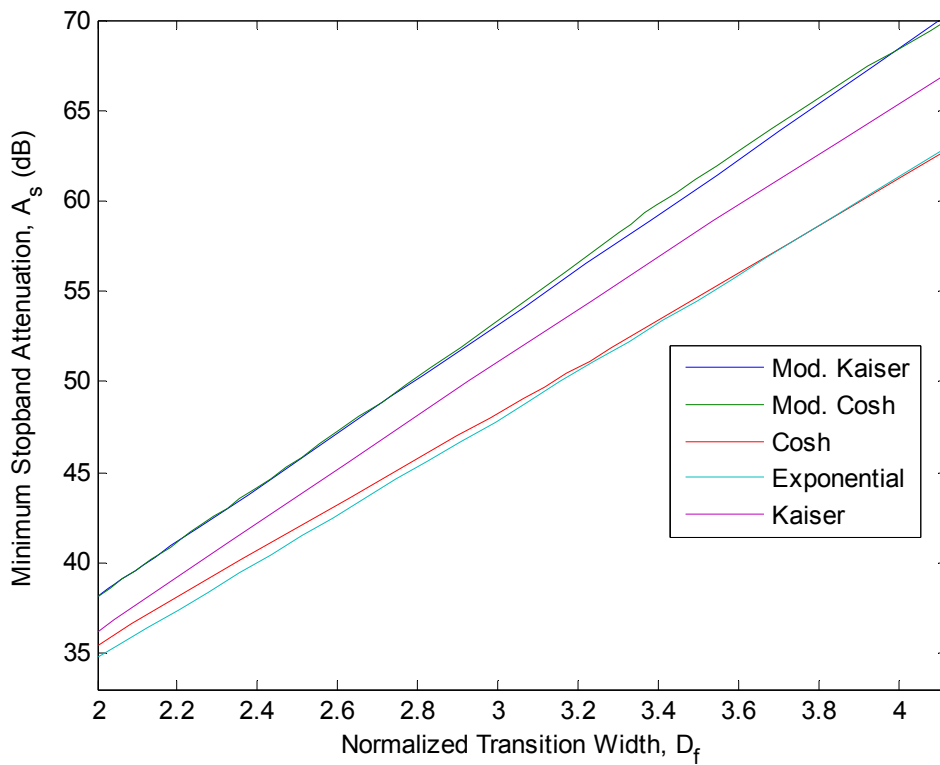


Figure 5.30 Minimum stopband attenuation comparison of the filters designed by the four proposed windows and Kaiser window for $N = 127$

Figure 5.30 shows the comparison of the filters designed by the optimum modified Kaiser, optimum modified Cosh, two-parameter Cosh, Exponential and Kaiser windows in terms of the minimum stopband attenuation for $N = 127$. It is seen that the additional parameter ρ_{mk} brings a superior minimum stopband attenuation improvement to the Kaiser window. While the filters designed by the modified Cosh windows perform a little better results than the filters designed by the modified Kaiser window for $D_f < 4$, the modified Kaiser window achieves better results in terms of the minimum stopband attenuation for $D_f > 4$.

5.5.3 Filter length comparison with modified Cosh, Cosh, Exponential and Kaiser windows

The performance of the four proposed windows with the Kaiser window is compared in terms of the required filter length to achieve a fixed transition width $\Delta\omega = 0.2$ rad/sample. Figure 5.31 shows the simulation results, and can be commented as follows:

For fixed filter length, three-parameter proposed windows provide better minimum stopband characteristics than the Kaiser, Cosh and Exponential windows. The modified Cosh window provides the best results until the length $N = 141$, but then the modified Kaiser window achieves better performance. The similar observation can be seen from Figure 5.30 in which the modified Cosh window has the best performance until $A_s = 68$ dB.

As for the filter length comparison, three-parameter proposed windows provide lower length to achieve fixed minimum stopband attenuation. For example, the filter lengths required to achieve minimum stopband attenuation around 72 dB for $\Delta\omega = 0.2$ rad/sample are $N = 135$ for the modified Cosh and modified Kaiser windows, $N = 141$ for the Kaiser window, and $N = 151$ for the Cosh and Exponential windows. But, for higher minimum stopband attenuations, the modified Cosh window requires more filter length compared to the modified Kaiser window. For example, the filter lengths required to achieve minimum stopband attenuation around 76.50 dB for $\Delta\omega = 0.2$ rad/sample are $N = 145$ for the modified Kaiser window and $N = 151$ for the modified Cosh window.

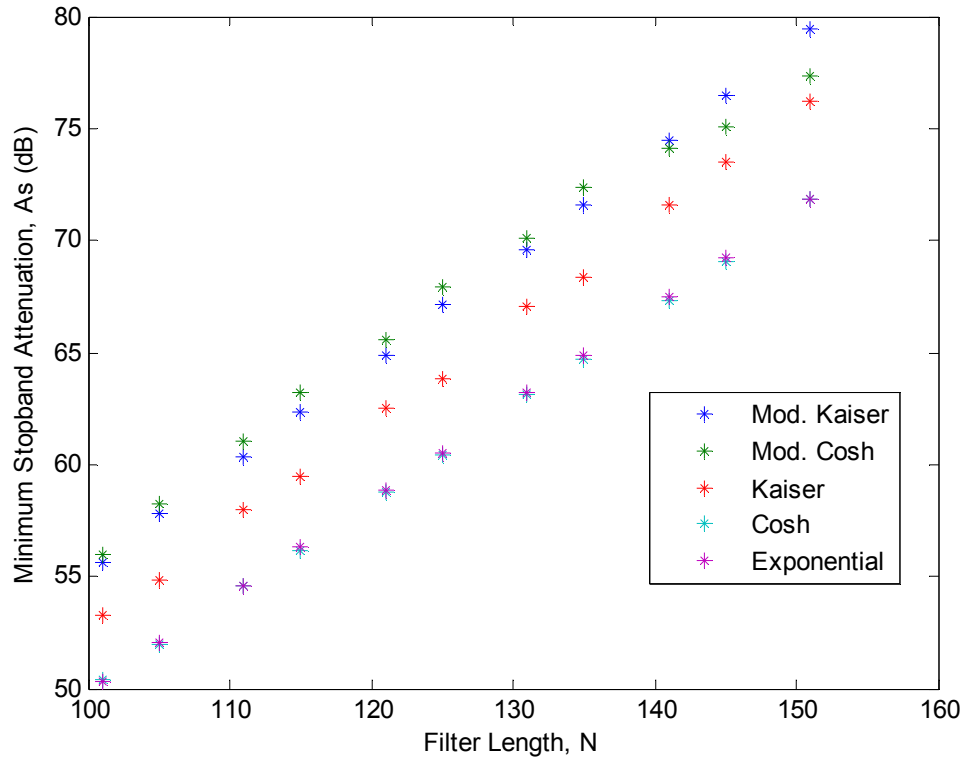


Figure 5.31 Minimum stopband attenuation comparison of the filters designed by the four proposed windows and Kaiser window with various filter length N and $\Delta w = 0.2$ rad/sample

5.6 Comparison Examples for the Filters Designed by the Proposed and Well-Known Windows

In the previous sections of this chapter, the filters designed by the proposed windows are compared with the filters designed by the well-known Kaiser window. In this section, the comparisons are extended to other well-known windows such as the Ultraspherical, Saramaki and Dolph-Chebyshev windows in order to demonstrate that the proposed windows can achieve better results than the windows in literature.

5.6.1 Comparison example for minimum stopband attenuation quality

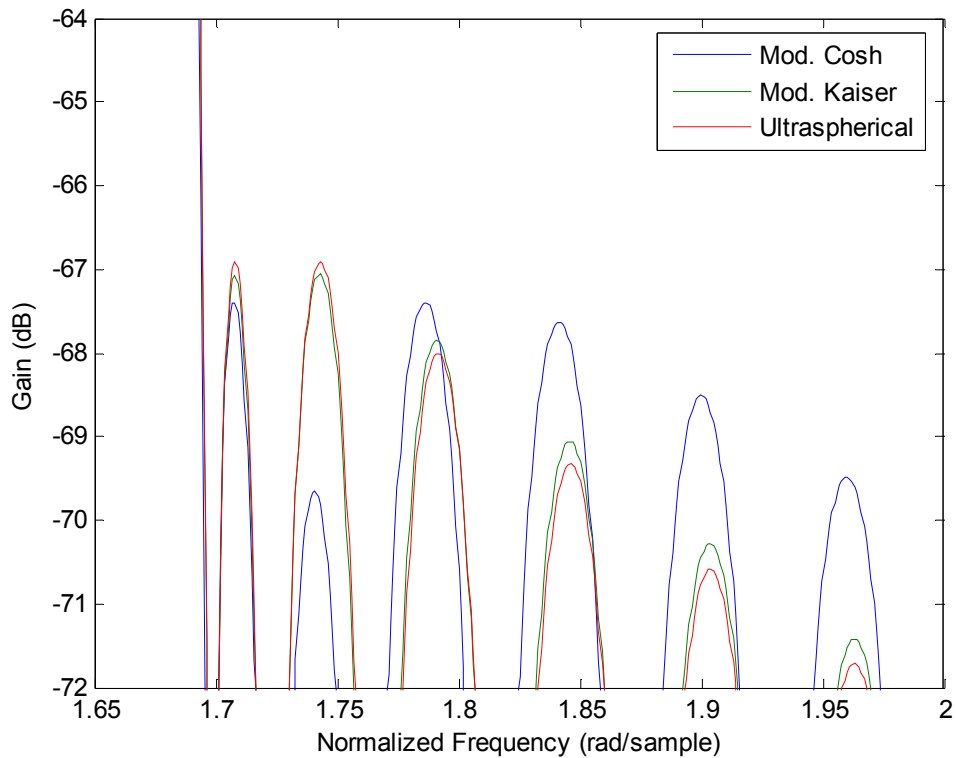
The quality of nonrecursive digital filters for a fixed filter length can be measured in two ways. By fixing the transition width, the resultant minimum stopband attenuations are compared. Or, the transition widths are compared for fixed minimum stopband attenuations. The filter which has the largest minimum stopband attenuation for the first case or the narrowest transition width for the second case can

be said to be the best one. Generally, in literature the first case has been chosen to measure the quality of a filter.

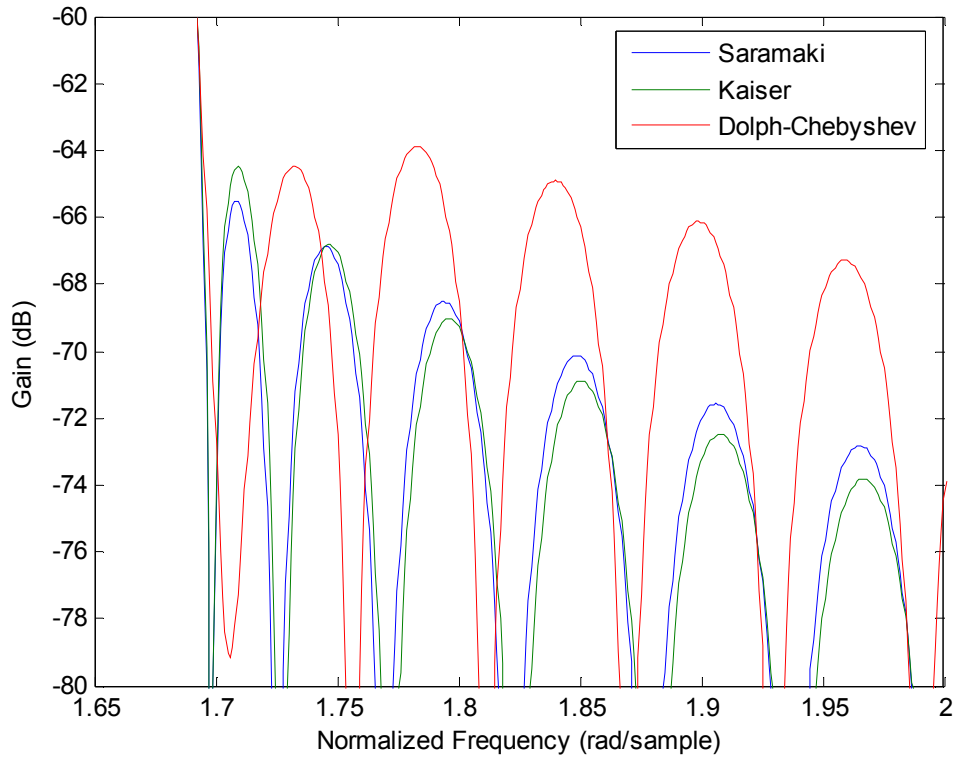
The quality example is chosen from Bergen and Antoniou's paper [14]. They also used the first case for the quality comparison. The nonrecursive digital filters are designed to satisfy the given prescribed filter specifications of a transition width $\Delta w = 0.248$ rad/sample and a filter length $N = 101$. The simulation results are given in Figure 5.32 and Table 5.7. [42, 43]

Table 5.7 Data for the minimum stopband attenuation comparison of the filters designed by the proposed and well-known windows with $w_{ct} = 0.5\pi$ rad/sample and $N = 101$

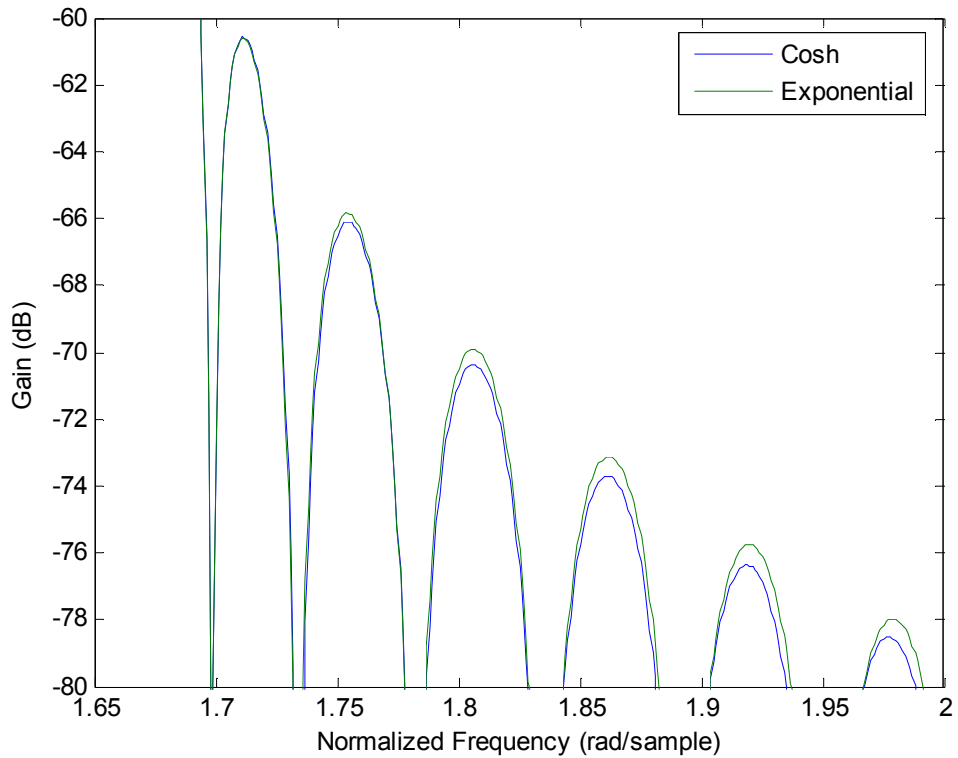
Window Type	N	α	ρ	Δw	A_s
Modified Cosh	101	2.112	2.653	0.2479	67.54
Modified Kaiser	101	4.774	1.300	0.2480	67.06
Ultraspherical	101	-	-	0.2480	66.92
Saramaki	101	-	-	0.2479	65.51
Kaiser	101	6.160	-	0.2480	64.50
Dolph-Chebyshev	101	-	-	0.2484	63.87
Exponential	101	5.880	-	0.2482	60.61
Cosh	101	5.880	-	0.2484	60.59



(a)



(b)



(c)

Figure 5.32 Amplitude responses of the filters designed by (a) modified Cosh, modified Kaiser, and Ultraspherical windows, (b) Saramaki, Kaiser and Dolph-Chebyshev windows, (c) Cosh and Exponential windows for $w_{ct} = 0.5\pi$ rad/sample, $\Delta w = 0.248$ rad/sample and $N = 101$

From Table 5.7, it can be seen that the best filter is achieved by the modified Cosh window although it has narrower transition width. As seen from Figure 5.32, this optimum filter is obtained by making two ripples (first and third ones) in equal amplitude by proper selection of α_{mc} and ρ_{mc} . The second best filter is obtained by the modified Kaiser window by making two ripples (first and second ones) in equal amplitude by proper selection of α_{mk} and ρ_{mk} . The filters designed by two proposed modified windows perform higher quality than the filter designed by the Ultraspherical window - obtained by making two ripples (first and second ones) in equal amplitude by proper selection of μ and x_μ for this example. The filter designed by the Saramaki window is better than the one designed by the Kaiser window as expected from [7]. The filters designed by the Exponential and Cosh windows performed the worst results. From the table, it is seen that the filter designed by Exponential window has a little better than the filter by the Cosh window since it has a little bit narrower transition width.

Interesting result is obtained for the filter designed by the Dolph-Chebyshev window. It is shown in Figure 3.6 that Dolph-Chebyshev window spectrum has sidelobes in equal amplitude. But, it is shown in Figure 5.32b that the filter designed by it has not equal ripples. This is due to the fact that there is a nonlinear relation between the window spectrum and filter spectrum. The other interesting result about the Dolph-Chebyshev window is that the filter designed by it is not the best one although it gives the smallest ripple ratio for a specified mainlobe width. This is due to that Dolph-Chebyshev has more energy under the sidelobes compared to other windows. This large unwanted sidelobe energy makes it perform worse results in filter design compared to the other windows such as Kaiser, Saramaki and Ultraspherical.

The above simulation results for the Ultraspherical, Saramaki and Dolph-Chebyshev windows are obtained by the following parameters.

Ultraspherical window: $\mu = 0.862$ and $x_\mu = 1.00194$.

Saramaki window: $\mu = 1$ and $x_\mu = 1.0019$.

Dolph-Chebyshev window: $R = 52.5$ dB in magnitude.

Additional information for the windows used in the filter design above is given in Table 5.8. In this table, w_R and w_N are the half mainlobe width and null-to-null half mainlobe width, respectively. In literature, it is observed that w_R or w_N are chosen as the reference point.

Table 5.8 Data for the spectrums of the windows used in the filter comparison example

Window Type	N	w_R	w_N	R	STR-1 (%) ($\times 10^{-3}$)	STR-2 (%) ($\times 10^{-3}$)
Modified Cosh	101	0.1330	0.1375	-47.32	3.737	3.684
Modified Kaiser	101	0.1327	0.1370	-46.07	4.446	3.219
Ultraspherical	101	0.1328	0.1375	-45.99	3.263	3.188
Saramaki	101	0.1332	0.1380	-45.43	3.019	2.931
Kaiser	101	0.1335	0.1385	-45.03	2.918	2.864
Dolph-Chebyshev	101	0.1344	0.1380	-52.42	19.290	19.275
Cosh	101	0.1352	0.1410	-43.17	3.270	3.102
Exponential	101	0.1350	0.1410	-43.08	3.490	3.317

As said in the previous page, the interesting results are obtained for the filter designed by the Dolph-Chebyshev window. Although it provides the best ripple ratio as shown in the table, it can not perform the best minimum stopband attenuation for the filter design example. This is due to that the Dolph-Chebyshev window has more energy under the sidelobes compared to other windows. This more energy is obviously seen in Table 5.8 from the sidelobe energy (E_S)-to-total energy (E_T) ratio (STR-1) parameter for w_R - which can be calculated from the following equation

$$STR = \frac{E_S}{E_T} \times 100\% = \frac{\int_{-\pi/T}^{\pi/T} |W(e^{jwT})|^2 dw}{\int_0^{\pi/T} |W(e^{jwT})|^2 dw} \times 100\% \quad (5.6)$$

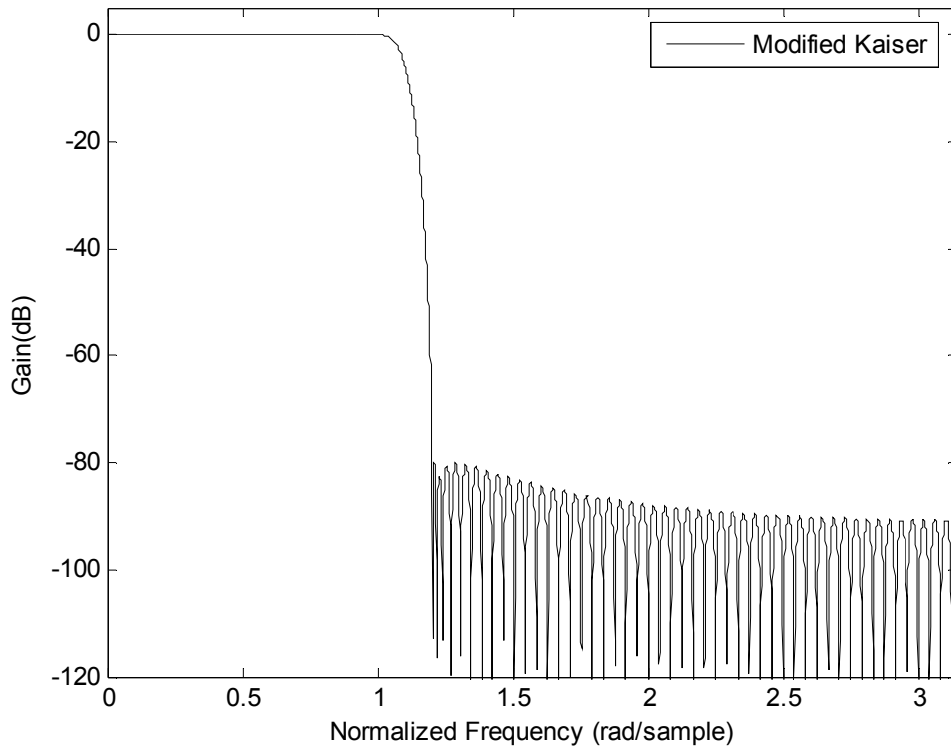
Note that the results in the table are obtained for $T = 1$. The parameter STR-2 can be calculated from Eq. (5.6) by substituting w_n instead of w_R . The Kaiser window has the lower sidelobe energy than the Saramaki window in Table 5.8 because its mainlobe width is wider. Kaiser window for $N = 101$ and $\alpha_k = 6.13$ provides $R = -44.82$ dB and 2.969×10^{-3} % in terms of STR-2 for $w_n = 0.138$ rad/sample which confirms that the Saramaki window (2.931×10^{-3} %) minimizes the sidelobe energy better than the Kaiser window as resulted in [7].

5.6.2 Comparison example for filter order

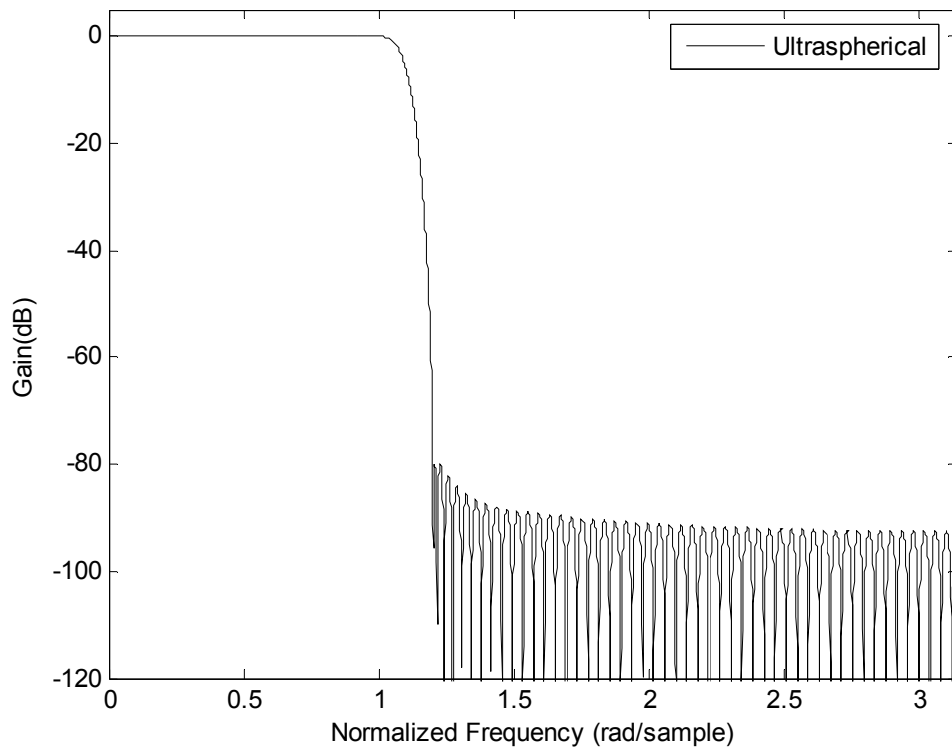
The filter order comparison example is also chosen from Bergen and Antoniou's paper [14]. The nonrecursive digital filters are designed to satisfy the given prescribed filter specifications of a passband frequency $\omega_p = 1$ rad/sample, a stopband frequency $\omega_{st} = 1.2$ rad/sample, and a minimum stopband attenuation $A_s = 80$ dB. The simulation results are given in Table 5.9 with the some simulation plots in Figure 5.33 [43].

Table 5.9 Data for the filter order comparison of the filters designed by proposed and well-known windows for $\omega_p = 1$ rad/sample, $\omega_{st} = 1.2$ rad/sample, and $A_s = 80$ dB

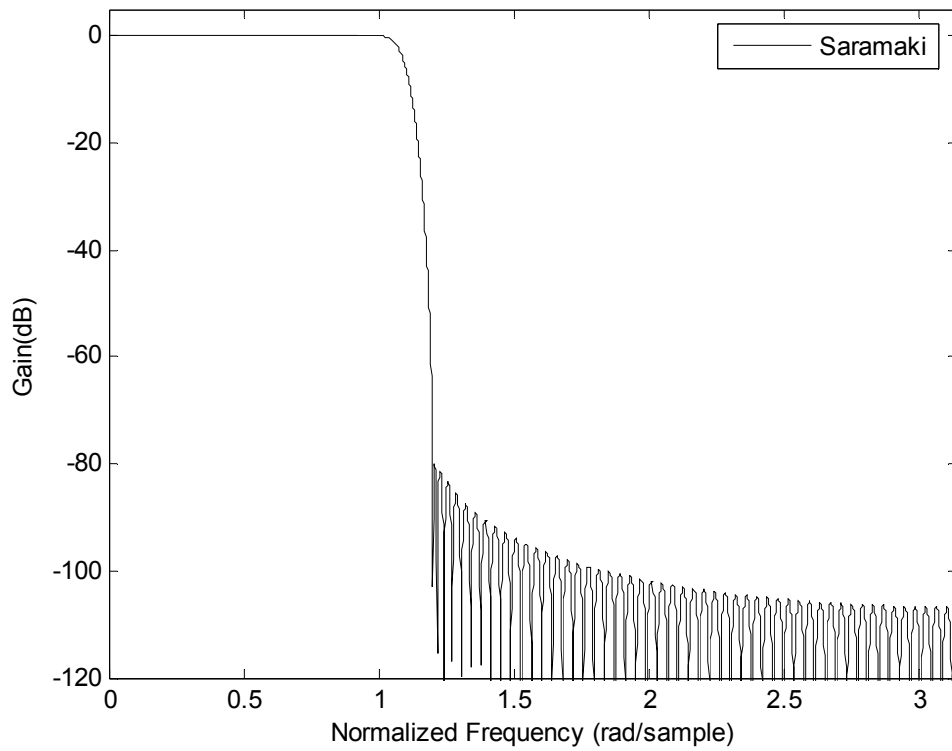
Window Type	N	α	ρ	A_s	Δw
Modified Kaiser	151	5.0307	1.497	80.00	0.2001
Ultraspherical	153	-	-	80.00	0.1996
Saramaki	159	-	-	80.00	0.1988
Kaiser	159	7.9210	-	80.00	0.2006
Dolph-Chebyshev	165	-	-	80.00	0.1918
Exponential	169	8.2010	-	80.00	0.2003
Cosh	169	8.2230	-	80.00	0.2007
Modified Cosh	169	7.8317	1.050	80.00	0.2007



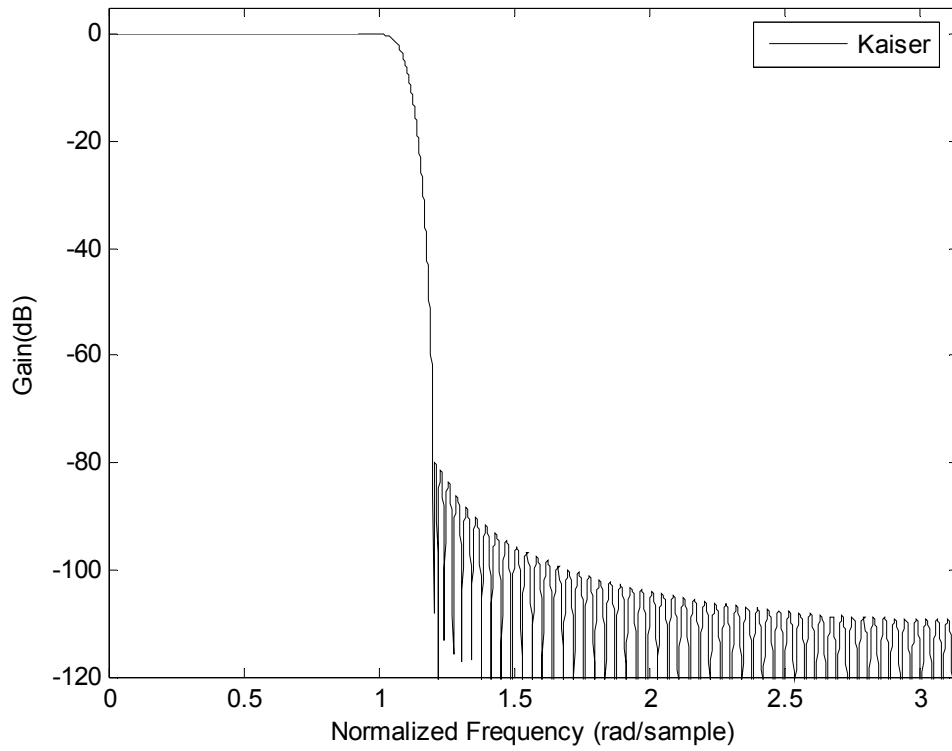
(a)



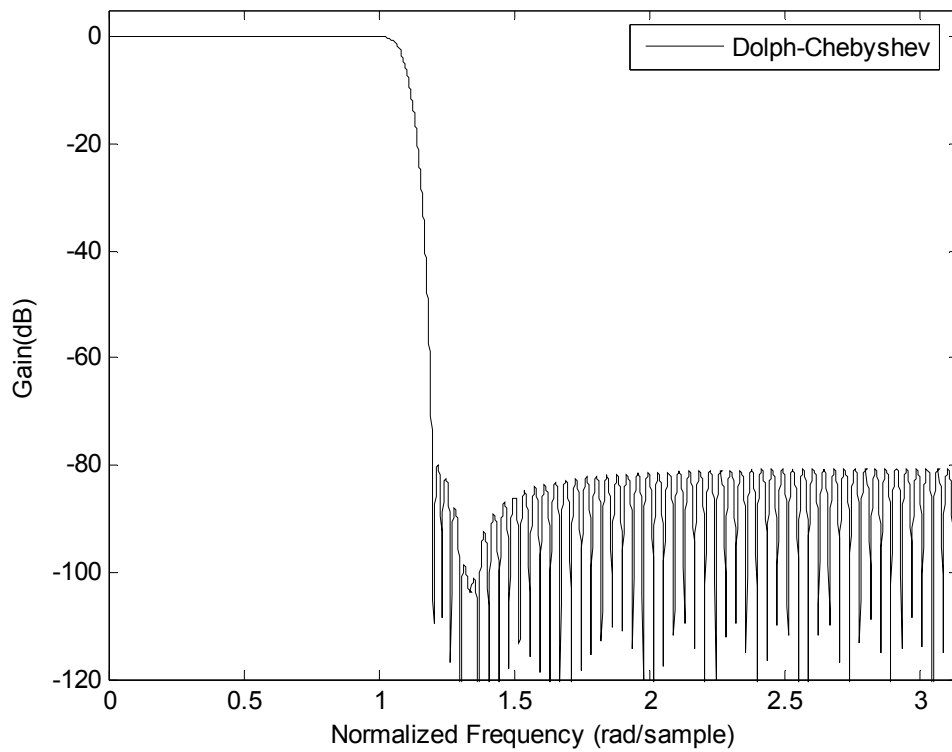
(b)



(c)



(d)



(e)

Figure 5.33 Comparison of the filters designed by (a) modified Kaiser window, (b) Ultraspherical window, (c) Saramaki window, (d) Kaiser window, (e) Dolph-Chebyshev window for $w_p = 1$ rad/sample, $w_{st} = 1.2$ rad/sample and $A_s = 80$ dB

The desired filter orders (N-1) are given in Table 5.9. It is seen that the lowest order filter is obtained by using the modified Kaiser window. The Saramaki and Kaiser windows produce the same order, but the Saramaki window is better in terms of the transition width. The Dolph-Chebyshev window provides worse order than the Kaiser window because it has large sidelobe energy as explained in the example given in Section 5.6.1. The filters designed by the Exponential and Cosh windows performed the same results but the filter designed by the Exponential window has a little better transition width. Interesting result is obtained for the filter designed by the modified Cosh window. While it performed the best result in the first example, now it provides the worst order result. This is due to that the cosh function includes the terms of e^x and e^{-x} , and when analyzing for this example it is observed that only the term of e^x is dominant for the given filter specification. Therefore, the modified Cosh and two-parameter Cosh windows performed the same result with the Exponential window. And also, due to this reason, two equal ripples in the stopband couldn't be obtained for the modified Cosh window. This causes the modified Cosh window not to be able to perform the same good performance in the first example.

The above simulation results for the Ultraspherical, Saramaki and Dolph-Chebyshev windows are obtained by the following parameters.

Ultraspherical window: $\mu = 0.684$ and $x_\mu = 1.00128$.

Saramaki window: $\mu = 1$ and $x_\mu = 1.00123$.

Dolph-Chebyshev window: $R = 66.69$ dB in magnitude.

CHAPTER-6

CONCLUSIONS AND FUTURE WORKS

This thesis study presents four proposed window functions - namely Exponential, Cosh, modified Cosh and modified Kaiser - with their applications in the design of nonrecursive digital filters. In this chapter, a brief summary for the results of thesis work is presented. In addition, some future directions are mentioned in the base of the results found.

6.1 Conclusions to Spectrum Analysis of the Proposed Windows

It is known from the literature that smaller mainlobe width of a window's spectrum causes smaller transition width between the passband and stopband regions in a filter; and smaller ripple ratio causes smaller ripples in the passband and stopband regions. Therefore, the window spectral characteristic parameters give important information for the resultant filter design characteristic.

Before applying the proposed windows directly to the nonrecursive digital filter design, their spectral characteristics are analyzed and their spectrum design equations which are also useful for some applications such as the spectrum estimation are established.

The first proposed window is the two-parameter Exponential window. This window is derived by replacing the modified Bessel function of first kind of order zero in the Kaiser window with the exponential function. But, the Exponential window has advantage that it has no power series expansion in its time domain representation. After analyzing the effect of the window adjustable parameters, the spectrum design equations - which define the window independent parameters in terms of the spectral parameters such as the ripple ratio and mainlobe width, for the Exponential window are established. The simulation results show that compared to

the Kaiser window for the same window length and mainlobe width, the Exponential window provides very good sidelobe roll-off ratio characteristic-which may be useful for some applications. In terms of the ripple ratio, the Kaiser window performs better results. As for comparison with the three-parameter Ultraspherical window, the Exponential window performs better in ripple ratio characteristic for narrower mainlobe width and larger sidelobe roll-off ratio with fixing the window length, mainlobe width and sidelobe roll-off ratio. For wider mainlobe width and smaller sidelobe roll-off ratio, the Ultraspherical window provides better ripple ratio.

The second proposed window is the two-parameter Cosh window. Like the Exponential window, this window based on the cosine hyperbolic function is also derived using the Kaiser approach, and has no power series expansion in its time domain representation. From the simulation results, it is demonstrated that having no power series expansion in the Cosh window results in computationally cost efficiency of calculating the window coefficients compared to the Kaiser window. Then, the spectrum design equations for the Cosh window are found. The simulation results show that the Cosh window provides a little bit better ripple ratio for smaller mainlobe width, but then almost the same results for the rest of the mainlobe width compared to the Exponential window. Its sidelobe roll-off ratio characteristic is better than the Kaiser window, but its ripple ratio characteristic is worse. To improve its spectral characteristic in terms of the ripple ratio, the combination with the Hamming window is suggested. The results show that the Cosh window with the combination of Hamming window provides better ripple ratio than the Kaiser window and its combination with the Hamming window. The comparisons with the Ultraspherical window demonstrate that the Cosh window provides significantly better results in terms of ripple ratio for wider mainlobe width and larger sidelobe roll-off ratio, but a little bit worse ripple ratio results for narrower mainlobe width and smaller sidelobe roll-off ratio.

Third window function is the modified Cosh window, which is derived by proposing an additional parameter to the two-parameter Cosh window. The simulation results show that an increase in the additional parameter results in a wider mainlobe width and a smaller ripple ratio. Since the modified Cosh window can provide many ripple ratio for a fix length, its optimum values are found for $N = 51$

and 101. Comparison examples for $N = 51$ and 101 demonstrate that the three-parameter modified Cosh window provides superior ripple ratio characteristic compared to the Kaiser and Cosh windows.

The last proposed window is the modified Kaiser window, which is derived by proposing the same additional parameter in the modified Cosh window to the two-parameter Kaiser window. The simulation results show that the three-parameter modified Kaiser window also provides superior ripple ratio characteristic compared to the Kaiser and Cosh windows. Moreover, the advantage of the modified Kaiser window is that it provides better ripple ratio characteristics than the modified Cosh window for wider mainlobe width. The comparison of the modified Kaiser window with the Ultraspherical window shows that the proposed window performs better ripple ratio for the same window length, mainlobe width and sidelobe roll-off ratio.

6.2 Conclusions to Nonrecursive Filters Design Using Proposed Windows

The first task in the design of nonrecursive filters using the Exponential window is to find the filter design equations. The error analyses show that the proposed models perform good approximations with the actual values. The comparison results with the filters designed by the Kaiser window show that the filters designed by the Exponential window performs superior maximum stopband attenuations- which may be useful for some applications, but also worse minimum stopband attenuations.

The filter design equations for the Cosh window are established, and the corresponding error analyses for the proposed models are carried out. The simulation results show that the Cosh window provides better results compared to the Exponential window in terms of the minimum stopband attenuation for narrower transition widths. For wider transition widths, they perform almost the same results. Comparison results with the Kaiser window show that the Cosh window provides better maximum stopband attenuations, but also worse minimum stopband attenuation.

The filter design by the modified Cosh window is started with analyzing the effect of the third parameter on the amplitude response of the filter. Simulation

example shows that an increase in the adjustable parameter ρ_{mc} results in a wider transition width and a larger minimum stopband attenuation. Since the modified Cosh window has many possibilities to provide the minimum stopband attenuation for a fixed filter length and transition width, the optimum solutions for $N = 51$ and 127 are found from the observation that the minimum stopband attenuation occurs when two ripples including the first one in the stopband have equal amplitude. The comparison simulations show that the modified Cosh window performs better minimum attenuation than the Kaiser, Cosh and Exponential windows.

The filter design by the modified Kaiser window is also started with analyzing the effect of the third parameter on the amplitude response of the filter. It is observed that an increase in the adjustable parameter ρ_{mk} results in a wider transition width and a larger minimum stopband attenuation like in the modified Cosh window. Since the modified Kaiser window has also many possibilities to provide the minimum stopband attenuation for a fixed filter length and transition width, the optimum solutions for $N = 51$ and 127 are found from the same observation in the case for the modified Cosh window. The comparison simulations show that the modified Kaiser window performs better minimum stopband attenuation and requires lower order than the Kaiser, Cosh and Exponential windows. As for the comparison with the modified Cosh window, the simulations results show that the modified Kaiser window performs better minimum stopband attenuation and requires lower order for wider transition widths.

Since the ultimate aim of the thesis is to provide better results in the filter design compared to the other windows, the proposed windows are compared with the well-known and best windows in the literature. Two comparison examples are chosen from [14].

In the first example, the filters designed by eight windows are analyzed for the quality comparison. Four windows are the proposed ones, and the other four ones are the Ultraspherical, Saramaki, Kaiser and Dolph-Chebyshev windows. Since the filter length and the transition width are fixed for all ones, the quality comparison is carried out in terms of the minimum stopband attenuation. The results show that the

filters designed by the modified Cosh and modified Kaiser windows perform better stopband attenuation than the filters designed by other six windows.

In the second example, the filters designed by eight windows are analyzed for the filter order comparison to satisfy a given stopband attenuation and transition width. The results show that the lowest filter order is obtained by the modified Kaiser window. But, the modified Cosh window performs worst result although it has three parameters. This is due to fact that it performs worse results for wider transition width and larger stopband attenuation.

It is shown in [14] that the best window which produces the optimum filter is the Ultraspherical window. But, in this thesis it is demonstrated with two examples that the proposed windows can achieve better results than the Ultraspherical window for filter design applications.

6.3 Recommendations for Future Work

The study is open to further developments. Future work can be the following:

- In Sections 4.2 and 4.3, two windows using the Kaiser approach are proposed since the exponential and cosine hyperbolic functions have the same amplitude characteristic with the modified Bessel function of first kind of order zero in the Kaiser window. From Figure 4.15, new functions that will have the same amplitude characteristic with smaller amplitude compared to the modified Bessel function of first kind of order zero can be obtained and then they can be used to provide new windows using the Kaiser approach. The resultant two-parameter windows are expected to perform better ripple ratio and minimum stopband attenuation characteristics than the Kaiser window. Also, proposing the parameter ρ like in the modified Cosh and modified Kaiser windows as a third independent parameter to those obtained two-parameter windows, the resultant three-parameter windows are expected to perform better results than the Ultraspherical window.

- It is shown that the Cosh window with the combination of Hamming window can provide better ripple ratio than the Kaiser window. This is due to that the first ripple of the Hamming window is smaller than the ripple ratio. Other suitable windows that have the same characteristic with the Hamming can be combined with the Cosh window, and the resultant combinational window may perform better results. Also, the same combinations can be obtained for filter design. It is shown in Chapter-5 that the first ripple in the filter designed by the Dolph-Chebyshev window is smaller than the maximum ripple. A combination of proposed windows with the Dolph-Chebyshev window is expected to perform better minimum stopband attenuation results.

- Nonrecursive filter design using the Fourier series method is suffered from the Gibbs' phenomena. Another suitable series can be found which does not produce such undesirable oscillations.

REFERENCES

- [1] El-Ali, T.S. (2004). *Discrete systems and digital signal processing with MATLAB*. CRC Press.
- [2] Antoniou, A. (2005). *Digital signal processing: Signal, systems, and filters*. McGraw-Hill, New York, NY, USA.
- [3] Dolph, C.L. (1946). A current distribution for broadside arrays which optimizes the relationship between beamwidth and side-lobe level” *Proc. IRE*, June, **34**, 335-348.
- [4] Kaiser, J.F. (1974). Nonrecursive digital filter design using I_0 -sinh window function. *Proc. IEEE Int. Symp. Circuits and Systems (ISCAS'74)*, San Francisco, Calif, USA, April, 20-23.
- [5] Abed, A.-E. and Cain, G. (1984). The host windowing technique for FIR digital filter design. *IEEE Transactions on Acoustics, Speech, and Signal Processing*. **32/4**, 683-694.
- [6] Ha, Y.H. and Pearce, J.A. (1989). A New Window and Comparison to Standard Windows. *IEEE Transactions on Acoustics, Speech, and Signal Processing*. **37/2**, 298-301.
- [7] Saramaki, T. (1989). A class of window functions with nearly minimum sidelobe energy for designing FIR filters. *Proc. IEEE Int. Symp. Circuits and systems (ISCAS'89)*, Portland, Ore, USA, May, **1**, 359-362.
- [8] Adams, J.W. (1991). A new optimal window. *IEEE Transactions on Signal Processing*. **39/8**, 1753-1769.
- [9] Saramaki, T. (1991). Adjustable windows for the design of FIR filters-A tutorial. *6th Mediterranean Electrotechnical Conference*. May. Ljubljana, Slovenia, 28–33.
- [10] Yang, S. and Ke, Y. (1992). On the three-coefficient window family. *IEEE Transactions on Signal Processing*. **40/12**, 3085-3088.
- [11] Gautam, J.K., Kumar, A. and Saxena R. (1996). On the modified Bartlett-Hanning window (family). *IEEE Transactions on Signal Processing*. **44/8**, 2098-2102.
- [12] Fuchs, J.J. (2002). New windows for tunable length FIR Filter Design. *Proc. IEEE ICASSP'02*. May, Orlando, USA, **2**, 1521-1524.

- [13] Sharma, S.N., Saxena R., Alok, J. (2002). FIR digital filter design with Parzen and $\text{Cos}^6(\pi t)$ combinational window family. *6th Int. conf. on Signal Processing*. Aug, **1**, 92-95.
- [14] Bergen, S.W.A. and Antoniou, A. (2005). Design of Nonrecursive Digital Filters Using the Ultraspherical Window Function *EURASIP Journal on Applied Signal Processing*, **12**, 1910-1922.
- [15] Saramaki, T. (1993). Finite impulse response filter design. in *Handbook for Digital Signal Processing*, S.K. Mitra and J.F.Kaiser,Eds. Wiley&Sons, New York, NY, USA.
- [16] Gibbs, J.W. Fourier series. (1899). *Nature*, **59**, pp. 200 and 606.
- [17] Fejer, L. (1900). Sur les fonctions bornees et integrables,. *Comptes Rendus Hebdomadaires, Seances de l'Academie de Sciences*, Paris, **131**, 984-987.
- [18] Lanczos, C. (1956). *Applied Analysis*. Van Nostrand, Princeton, NJ.
- [19] Bergen, S.W.A. (2005). Design of the Ultraspherical window function and its applications. PhD Dissertation. University of Victoria. Department of Electrical and Computer Engineering. Victoria. Canada.
- [20] Kaiser, J.F. (1966). Digital filters. *Chapter-7 in book System analysis by digital computer*, Kuo and Kaiser, John Wiley, 228-243.
- [21] Harris, F.J. (1978). On the use of windows for harmonic analysis with the discrete Fourier transform. *Proc. IEEE*. **66**, 51-83.
- [22] Deczky, A.G. (2001). Unispherical windows. *IEEE Int. Symp. on Circuits and Systems*. Sydney, Australia, May, **2**, 85-88.
- [23] Schwarzweller A.R. and Wintermantel M. (2002). On designing FIR filters using windows based on Gegenbauer Polynomials. *IEEE International Symposium on Circuits and Systems (ISCAS 2002)*. **1**, 413-416
- [24] Bergen, S.W.A. and Antoniou, A. (2002). Generation of Ultraspherical window functions” in *XI European Signal Processing Conference*, Toulouse, France, September, **2**, 607-610
- [25] <http://www.dsptutor.freeuk.com/dfilt1.htm#analog>
- [26] <http://www.dsptutor.freeuk.com/dfilt2.htm>
- [27] Schlichtharle, D. (2000). *Digital filters: Basics and design*. Springer-Verlag, Berlin Heidelberg, Germany
- [28] Proakis J.G. and Manolakis, D.G. (2007). *Digital signal processing: Principles, Algorithms and Applications*. (4th Edition). Prentice-Hall. USA

- [29] Roychowdhury, A. (2002). *FIR filter design techniques*. Seminar Report. Electronic Systems Group. EE Dept. IIT Bombay. India.
- [30] McClellan, J., Parks, T. and Rabiner, L. (1973). A computer program for designing optimum FIR linear phase digital filters. *IEEE Transactions on Audio and Electroacoustics*. **21**, 506-526.
- [31] Kaiser, J.F. and Schafer, R.W. (1980). On the use of the Io-sinh window for spectrum analysis. *IEEE Trans. Acoustics, Speech, and Signal Processing*, **28/1**, 105-107.
- [32] Bergen, S.W.A. and Antoniou, A. (2004). Design of Ultraspherical window functions with prescribed spectral characteristics. *EURASIP Journal on Applied Signal Processing*, **13**, 2053-2065.
- [33] Avci, K. and Nacaroğlu, A. (2008). A new window based on exponential window. *IEEE Ph.D. Research in Microelectronics and Electronics (PRIME 2008)*. June. Istanbul, Turkey, 69-72.
- [34] Jain, A., Saxena, R., Saxena S.C. (2005). A simple alias-free QMF system with near-perfect reconstruction. *J Indian Ins Sci*, **12**, 1-10.
- [35] Avci, K. and Nacaroğlu, A. (2008). Cosine hyperbolic window family with its application to FIR filter design. *Proc. of Third International Conference on Information and Communication Technologies (ICTTA'08)*. April. Damascus, Syria, 289-290. (Extended Abstract)
- [36] Avci, K. and Nacaroğlu, A. (2008). Cosh window family and its application to FIR filter design. Accepted for the publication in *International Journal of Electronics and Communications-AEU*
- [37] Avci, K. and Nacaroğlu, A. (2008). Modification of Cosh window family. *Proc. of Third International Conference on Information and Communication Technologies (ICTTA'08)*. April. Damascus, Syria, 291-292. (Extended Abstract)
- [38] Avci, K. and Nacaroğlu, A. (2008). An efficient study on the modification of Kaiser window. *Proc. of 7th International Conference COMMUNICATIONS 2008*. June. Bucharest, Romania, 63-66.
- [39] Avci, K. and Nacaroğlu, A. (2008). An efficient study on the modification of Kaiser window. Accepted for the publication in Romanian *MTA Review*.
- [40] Sharma, S.N., Saxena R., Saxena, S.C. (2004). Design of FIR filter using variable window families: A comparative study. *J. Indian Inst. Sci.*, Sept.-Oct., **84**, 155-161.
- [41] Avci, K. and Nacaroğlu, A. (2008). Nonrecursive digital filter design by the Exponential window obtained using the Kaiser Approach. Accepted for the publication for *the conference proceedings in Symposium of 30th year in Cukurova*

University Engineering and Architecture Faculty. October. Adana, Turkey. (in Turkish).

[42] Avci, K. and Nacaroglu, A. (2008). Nonrecursive digital filter design using a three-parameter window based on cosine hyperbolic function. *Proc. of 10th International Conference Digital Signal Processing and its Applications (DSPA'08)*. March. Moscow, Russia, 121-124.

[43] Avci, K. and Nacaroglu, A. (2008). High quality low order Nonrecursive digital filter design using modified Kaiser window. *Proc. of 6th Symposium on Communication Systems, Networks and Digital Signal processing (CSNDSP'08)*. July. Graz, Austria, 239-242.

APPENDIX-A

MATLAB PROGRAMS

In this section, some MATLAB programs used in this thesis are given. The program in the first section (A.1) calculates and plots the window spectrums and filter amplitude responses for the Modified Kaiser, Modified Cosh, Kaiser, Cosh and Exponential windows. To execute a desired command, the prompt % before that command should be removed. The programs in the second section (A.2) calculate the Ultraspherical coefficients and its adjustable parameters for prescribed specifications.

A.1 MATLAB Program for the Proposed Windows

```
clc; clear all; close all; format short
ws=2*pi; % Normalized sampling frequency
T=(2*pi/ws); % Sampling period
wc=0.4*pi; % Cut-off frequency

% Length of the windows or filters
Na=input('odd Na = '); N1a=(Na+1)/2;
Nb=input('odd Nb = '); N1b=(Nb+1)/2;
Nc=input('odd Nc = '); N1c=(Nc+1)/2;
Nd=input('odd Nd = '); N1d=(Nd+1)/2;
Ne=input('odd Ne = '); N1e=(Ne+1)/2;
Nf=input('odd Nf = '); N1f=(Nf+1)/2;
Ng=input('odd Ng = '); N1g=(Ng+1)/2;

% Second adjustable parameter for the windows
alpha1=input('Alpha1 = '); alpha2=input('Alpha2 = '); alpha3=input('Alpha3 = ');
alpha4=input('Alpha4 = '); alpha5=input('Alpha5 = '); alpha6=input('Alpha6 = ');
alpha7=input('Alpha7 = ');

% Third adjustable parameter for the windows
a1=input('rho1 = '); a2=input('rho2 = '); a3=input('rho3 = '); a4=input('rho4 = ');
a5=input('rho5 = '); a6=input('rho6 = '); a7=input('rho7 = ');

m1=0;
%%%%%%%%%%%%%%%%%%%%%%%%%%%%%%%%%%%%%%%%%%%%%%%%%%%%%%%%%%%%%%%%%%%%%%%%
% 1 X (Length+1)/2 window coefficients
%%%%%%%%%%%%%%%%%%%%%%%%%%%%%%%%%%%%%%%%%%%%%%%%%%%%%%%%%%%%%%%%%%%%%%%%
for n=0:(Na-1)/2;
```



```

beta1 = alpha1*sqrt(1-(2*n/(Na-1))^2) ;
% w1(n+1)=(cosh(beta1)/cosh(alpha1))^a1;
w1(n+1)=(BESSELI(m1,beta1)/BESSELI(m1,alpha1))^a1;
% w1(n+1)=(exp(beta1)/exp(alpha1))^a1;
end
for n=0:(Nb-1)/2;
beta2 = alpha2*sqrt(1-(2*n/(Nb-1))^2) ;
w2(n+1)=(BESSELI(m1,beta2)/BESSELI(m1,alpha2))^a2;
% w2(n+1)=(cosh(beta2)/cosh(alpha2))^a2;
% w2(n+1)=(exp(beta2)/exp(alpha2))^a2;
end
for n=0:(Nc-1)/2;
beta3 = alpha3*sqrt(1-(2*n/(Nc-1))^2) ;
w3(n+1)=(BESSELI(m1,beta3)/BESSELI(m1,alpha3))^a3;
% w3(n+1)=(cosh(beta3)/cosh(alpha3))^a3;
% w3(n+1)=(exp(beta3)/exp(alpha3))^a3;
end
for n=0:(Nd-1)/2;
beta4 = alpha4*sqrt(1-(2*n/(Nd-1))^2);
w4(n+1)=(BESSELI(m1,beta4)/BESSELI(m1,alpha4))^a4;
% w4(n+1)=(cosh(beta4)/cosh(alpha4))^a4;
% w4(n+1)=(exp(beta4)/exp(alpha4))^a4;
end
for n=0:(Ne-1)/2;
beta5 = alpha5*sqrt(1-(2*n/(Ne-1))^2) ;
w5(n+1)=(BESSELI(m1,beta5)/BESSELI(m1,alpha5))^a5;
% w5(n+1)=(cosh(beta5)/cosh(alpha5))^a5;
% w5(n+1)=(exp(beta5)/exp(alpha5))^a5;
end
for n=0:(Nf-1)/2;
beta6 = alpha6*sqrt(1-(2*n/(Nf-1))^2) ;
w6(n+1)=(BESSELI(m1,beta6)/BESSELI(m1,alpha6))^a6;
% w6(n+1)=(cosh(beta6)/cosh(alpha6))^a6;
% w6(n+1)=(exp(beta6)/exp(alpha6))^a6;
end
for n=0:(Ng-1)/2;
beta7 = alpha7*sqrt(1-(2*n/(Ng-1))^2) ;
w7(n+1)=(BESSELI(m1,beta7)/BESSELI(m1,alpha7))^a7;
% w7(n+1)=(cosh(beta7)/cosh(alpha7))^a7;
% w7(n+1)=(exp(beta7)/exp(alpha7))^a7;
end

% the first elements of the ideal impulse responses
h1(1)=(2*wc/ws); h2(1)=h1(1); h3(1)=h1(1); h4(1)=h1(1); h5(1)=h1(1);
h6(1)=h1(1); h7(1)=h1(1);

% the second to (Length+1)/2'th elements of the ideal impulse responses
for n=1:N1a-1; h1(n+1)= (1/(n*pi))*sin(wc*n*T); end
for n=1:N1b-1; h2(n+1)= (1/(n*pi))*sin(wc*n*T); end
for n=1:N1c-1; h3(n+1)= (1/(n*pi))*sin(wc*n*T); end

```

```

for n=1:N1d-1; h4(n+1)= (1/(n*pi))*sin(wc*n*T); end
for n=1:N1e-1; h5(n+1)= (1/(n*pi))*sin(wc*n*T); end
for n=1:N1f-1; h6(n+1)= (1/(n*pi))*sin(wc*n*T); end
for n=1:N1g-1; h7(n+1)= (1/(n*pi))*sin(wc*n*T); end

% 1 x (Length+1)/2 windowed impulse responses
b1=w1.*h1; b2=w2.*h2; b3=w3.*h3; b4=w4.*h4; b5=w5.*h5; b6=w6.*h6;
b7=w7.*h7;
%% 1 x (Length+1)/2 window coefficients
% b1=w1; b2=w2; b3=w3; b4=w4; b5=w5; b6=w6; b7=w7;

%%%%%%%%%%%%%%%%%%%%%%%%%%%%%%%%%%%%%%%%%%%%%%%%%%%%%%%%%%%%%%%%%%%%%%%%
% 1 X Length symmetric window or filter coefficients
%%%%%%%%%%%%%%%%%%%%%%%%%%%%%%%%%%%%%%%%%%%%%%%%%%%%%%%%%%%%%%%%%%%%%%%%
for p1=1:N1a-1; d1(p1)=b1(N1a+1-p1); end; f1=[d1 b1]; e1=f1;
for p2=1:N1b-1; d2(p2)=b2(N1b+1-p2); end; f2=[d2 b2]; e2=f2;
for p3=1:N1c-1; d3(p3)=b3(N1c+1-p3); end; f3=[d3 b3]; e3=f3;
for p4=1:N1d-1; d4(p4)=b4(N1d+1-p4); end; f4=[d4 b4]; e4=f4;
for p5=1:N1e-1; d5(p5)=b5(N1e+1-p5); end; f5=[d5 b5]; e5=f5;
for p6=1:N1f-1; d6(p6)=b6(N1f+1-p6); end; f6=[d6 b6]; e6=f6;
for p7=1:N1g-1; d7(p7)=b7(N1g+1-p7); end; f7=[d7 b7]; e7=f7;

z1=0; z2=0; z3=0; z4=0; z5=0; z6=0; z7=0;
%%%%%%%%%%%%%%%%%%%%%%%%%%%%%%%%%%%%%%%%%%%%%%%%%%%%%%%%%%%%%%%%%%%%%%%%
% Fourier transform of the window or filter coefficients
%%%%%%%%%%%%%%%%%%%%%%%%%%%%%%%%%%%%%%%%%%%%%%%%%%%%%%%%%%%%%%%%%%%%%%%%
for w=0:0.001:ws/2;
for n=1:Na; HAa=(exp(-j*w*T*(n-1))); HFa(n)=HAa;
for n=1:Nb; HAB=(exp(-j*w*T*(n-1))); HFb(n)=HAB;
for n=1:Nc; HAC=(exp(-j*w*T*(n-1))); HFc(n)=HAC;
for n=1:Nd; HAd=(exp(-j*w*T*(n-1))); HFd(n)=HAd;
for n=1:Ne; HAE=(exp(-j*w*T*(n-1))); HFe(n)=HAE;
for n=1:Nf; HAF=(exp(-j*w*T*(n-1))); HFf(n)=HAF;
for n=1:Ng; HAG=(exp(-j*w*T*(n-1))); HFg(n)=HAG;
end
%%%%%%%%%%%%%%%%%%%%%%%%%%%%%%%%%%%%%%%%%%%%%%%%%%%%%%%%%%%%%%%%%%%%%%%%
c1=e1*HFa'; MA1=abs(c1); z1=z1+1; M1(z1)=MA1;
c2=e2*HFb'; MA2=abs(c2); z2=z2+1; M2(z2)=MA2;
c3=e3*HFc'; MA3=abs(c3); z3=z3+1; M3(z3)=MA3;
c4=e4*HFd'; MA4=abs(c4); z4=z4+1; M4(z4)=MA4;
c5=e5*HFe'; MA5=abs(c5); z5=z5+1; M5(z5)=MA5;
c6=e6*HFf'; MA6=abs(c6); z6=z6+1; M6(z6)=MA6;
c7=e7*HFg'; MA7=abs(c7); z7=z7+1; M7(z7)=MA7;
end
plot(0:0.001:ws/2,20*log10(M1/M1(1)),0:0.001:ws/2,20*log10(M2/M2(1)),0:0.001:
ws/2,20*log10(M3/M3(1)),0:0.001:ws/2,20*log10(M4/M4(1)),0:0.001:ws/2,20*log1
0(M5/M5(1)),0:0.001:ws/2,20*log10(M6/M6(1)),0:0.001:ws/2,20*log10(M7/M7(1))
)
legend('Kaiser-1','Kaiser-2','Kaiser-3','Kaiser-4','Kaiser-5','Kaiser-6','Kaiser-7');
xlabel('Normalized Frequency (rad/sample)'); ylabel('Gain (dB)')

```

A.2 MATLAB Programs for the Ultraspherical Window

To find the Ultraspherical coefficients, *ultra.m* file should be executed. The adjustable parameters μ and x_μ for given sidelobe roll-off ratio (S) and mainlobe width (w_R) for fixed window length can be found by using seven m-files as follows:

- Put N and S for *myubound.m*. Then, find μ by executing *myu.m*
- Put N, w_r and μ for *xmyuforab.m*. Then, execute it to find *a* and *b*
- Put N, μ , *a* and *b* for *xmyuforxa.m*. Then, execute it to find x_a
- Put N, μ , w_r and x_a for *xmyu.m*. Then, execute it to find x_μ
- The subroutines *largestZero.m* and *smallestZero.m* are used by the programs *myubound.m* and *xmyuforab.m*

A.2.1 *ultra.m*

```
function w = ultra(N, mu, par, partype)
error(nargchk(4,4,nargin));
% Check window length N
N = ceil(N);
if N < 1, error('The window length N must be >= 1.');
```

end

```
if N == 1, w=1; return; end % Trivial window
% Check parameter MU
if mu <= -1.5 | mu == -1, error('MU must be > -1.5 and ~= -1.');
```

end

```
% Check parameter BETA/XMU
partypelength = length(partype);
if partypelength == 4,
    if partype == 'beta',
        if par < 1, error('BETA must be >= 1.');
```

end

```
        xmu = largestZero(N-1,mu)/cos(pi*par/N); % calculate xmu from beta
    else
        error('PARTYPE must be "beta" or "xmu".');
```

end

```
elseif partypelength == 3,
    if partype == 'xmu',
        if par < 1, error('XMU must be >= 1.');
```

end

```
        xmu = par; % par supplied is xmu
    else
        error('PARTYPE must be "beta" or "xmu".');
```

end

```
else
    error('PARTYPE must be "beta" or "xmu".');
```

end

```
%%%%%%%%%%%%%%%%%%%%%%%%%%%%%%%%%%%%%%%%%%%%%%%%%%%%%%%%%%%%%%%%%%%%%%%%
% Calculate window coefficients
```

```

%%%%%%%%%%%%%%%%%%%%%%%%%%%%%%%%%%%%%%%%%
% Calculate constants.
isodd=mod(N,2); if isodd, A=(N-1)/2; else A=N/2-1; end
p=N-1; Cval=1-xmu^-2;
if mu==0, B=xmu^p; else B=mu*xmu^p; end % Limiting value for Chebyshev
polynomial.
% Working vector initializations.
v0(1,A+1)=0; v1(1,A+1)=0; v2(1,A+1)=0; C(1,A+1)=0;
ww(1,A+1)=0; w(1:N)=0;
% Generate fixed v0(n+1) and C(n+1)^n for n=0,1,...,A.
a0=mu+p-1; b0=p-1; v0(1)=1; C(1)=1;
for g=0:b0-1, v0(1)=(a0-g)/(b0-g)*v0(1); end % v0(1)=binomial(a0,b0).
for n=1:A, nl=n+1; v0(nl)=(b0-n+1)/(a0-n+1)*v0(nl-1); C(nl)=Cval*C(nl-1); end
% Calculate 'half' the window coefficients ww(n+1) for n=0,1,...,A.
for n=0:A, nl=n+1;
% Generate v1(g+1) for g=n,n-1,...,0 and v2(g+1) for g=0,1,...,n.
v1(nl)=1; v2(1)=1; alpha2=p-n;
for g=1:n, gl=g+1; m=n-g; ml=m+1;
v1(ml)=(mu+m)/(n-m)*v1(ml+1); v2(gl)=(alpha2-g+1)/g*v2(gl-1);
end
sum1=sum((v1(1:nl).*v2(1:nl)).*C(1:nl)); % Perform summation.
ww(nl)=B/alpha2*v0(nl)*sum1; % Window coefficients.
end
% Obtain symmetrical normalized window coefficients.
ww=ww/ww(end);
if isodd, w=[ww ww(end-1:-1:1)]';
else w=[ww fliplr(ww)]'; end
return

```

A.2.2 myubound.m

```

function f=myubound(mu)
N= input(' Odd window length N = ');
S= input(' Sidelobe roll-off ratio S = ');
s=10^(S/20);
xl = largestZero(N-2,mu+1);
xs = smallestZero(N-2,mu+1);
alpha=mu;
n=N-1;
    C1(1)=2*alpha.*xl; C1(2)=-alpha+2*alpha*(1+alpha).*(xl.^2);
    for ii=3:n,
        C1(ii)=2*(ii+alpha-1)/(ii).*xl.*C1(ii-1)-(ii+2*alpha-2)/(ii).*C1(ii-2);
    end
    C2(1)=2*alpha.*xs; C2(2)=-alpha+2*alpha*(1+alpha).*(xs.^2);
    for ii=3:n,
        C2(ii)=2*(ii+alpha-1)/(ii).*xs.*C2(ii-1)-(ii+2*alpha-2)/(ii).*C2(ii-2);
    end
f=(s-abs(C1(n)/C2(n)))^2;

```

A.2.3 myu.m

```
format long
clc;
clear all;
mu = fminbnd(@myubound,0,10)
```

A.2.4 xmuforab.m

```
format long
N= input(' Odd window length N = ');
wr= input(' Mainlobe width wr = ');
xl2 = largestZero(N-2,mu+1);
xs2 = smallestZero(N-2,mu+1);
alpha= input(' myu = ');
n=N-1;
C11(1)=2*alpha.*xl2; C11(2)=-alpha+2*alpha*(1+alpha).*(xl2.^2);
for ii=3:n,
C11(ii)=2*(ii+alpha-1)/(ii).*xl2.*C11(ii-1)-(ii+2*alpha-2)/(ii).*C11(ii-2);
end
a=abs(C11(n))
C22(1)=2*alpha.*xs2; C22(2)=-alpha+2*alpha*(1+alpha).*(xs2.^2);
for ii=3:n,
C22(ii)=2*(ii+alpha-1)/(ii).*xs2.*C22(ii-1)-(ii+2*alpha-2)/(ii).*C22(ii-2);
end
b=abs(C22(n))
```

A.2.5 xmuforxa.m

```
% Check bounds for parameters.
if (floor(n)~=n) | (n<=1), error('N should be a positive integer > 1'); xstar=NAN;
return; end
if alpha<=-1.5, error('ALPHA should be >= -1.5'); xstar=NAN; return;
elseif alpha== -1 error('ALPHA cannot be -1'); xstar=NAN; return; end

% Check for special instances of the ultraspherical polynomial where
% analytical expressions for the zeros exist.
if alpha==0, xstar=cos(pi/(2*n)); return; % Chebyshev polynomial of the first kind,
Tn(x).
elseif alpha==1, xstar=cos(pi/(n+1)); return; % Chebyshev polynomial of the second
kind, Un(x).
elseif alpha== -0.5, xstar=1; return; end % Always 1.

% Step 1
N= input(' Odd window length N = ');
a= input(' a = ');
b= input(' b = ');
alpha= input(' myu = ');
epsilon=10^-6; ktol=20; C3(1,n)=0; y(1,ktol+1)=0;
% y1(1)=1;; % Upper bound
y1(1)=sqrt(n*n+2*(n-1)*alpha-1)/(n+alpha);
```

```

% Step 2
for k=1:ktol
x=y1(k);      C3(1)=2*alpha.*x; C3(2)=-alpha+2*alpha*(1+alpha).*(x.^2);
for ii=3:n,
C3(ii)=2*(ii+alpha-1)/(ii).*x.*C3(ii-1)-(ii+2*alpha-2)/(ii).*C3(ii-2);
end
den=(1/(1-x^2))*((2*alpha+n-1)*C3(n-1)-(n*x)*C3(n)); % derivative.
y1(k+1)=y1(k)-(C3(n)-((sign(alpha)*max(a,b))))/den; % Newton-Raphson iteration.
% Step 3
if abs(y1(k+1)-y1(k))<epsilon, xstar=y1(k+1); break; end
end
if k==ktol, error('Algorithm did not converge within ten iterations - stopping.');
```

A.2.6 xmyu.m

```

format long
N= input(' Odd window length N = ');
mu= input(' myu = ');
wr= input(' Mainlobe width wr = ');
xa=xmyuforxa(N-1,mu);
xmu=xa/cos(wr/(2))
```

A.2.7 largestZero.m

```

function xstar = largestZero(n,alpha)
% Check bounds for parameters.
if (floor(n)~=n) | (n<=1), error('N should be a positive integer > 1'); xstar=NAN;
return; end
if alpha<=-1.5, error('ALPHA should be >= -1.5'); xstar=NAN; return;
elseif alpha== -1 error('ALPHA cannot be -1'); xstar=NAN; return; end

% Check for special instances of the ultraspherical polynomial where
% analytical expressions for the zeros exist.
if alpha==0, xstar=cos(pi/(2*n)); return; % Chebyshev polynomial of the first kind,
Tn(x).
elseif alpha==1, xstar=cos(pi/(n+1)); return; % Chebyshev polynomial of the second
kind, Un(x).
elseif alpha== -0.5, xstar=1; return; end % Always 1.
```

```

% Step 1
epsilon=10^-6; ktol=20; C(1,n)=0; y(1,ktol+1)=0;
y(1)=sqrt(n*n+2*n*alpha-2*alpha-1)/(n+alpha); % Upper bound
```

```

% Step 2
for k=1:ktol
x=y(k);      C(1)=2*alpha.*x; C(2)=-alpha+2*alpha*(1+alpha).*(x.^2);
for ii=3:n,
C(ii)=2*(ii+alpha-1)/(ii).*x.*C(ii-1)-(ii+2*alpha-2)/(ii).*C(ii-2);
end
```

```

den=1/(1-x^2)*((2*alpha+n-1)*C(n-1)-(n*x)*C(n)); % derivative.
y(k+1)=y(k)-C(n)/den; % Newton-Raphson iteration.

% Step 3
    if abs(y(k+1)-y(k))<epsilon, xstar=y(k+1); break; end
end
if k==ktol, error('Algorithm did not converge within ten iterations - stopping.');
```

A.2.8 smallestZero.m

```

function xstar = smallestZero(n,alpha)
l=round((n-2)/2);
% Check bounds for parameters.
if (floor(n)~=n) | (n<=1), error('N should be a positive integer > 1'); xstar=NAN;
return; end
if alpha<=-1.5, error('ALPHA should be >= -1.5'); xstar=NAN; return;
elseif alpha==-1 error('ALPHA cannot be -1'); xstar=NAN; return; end

% Check for special instances of the ultraspherical polynomial where
% analytical expressions for the zeros exist.
if alpha==0, xstar=cos(pi(l-1/2)/(n)); return; % Chebyshev polynomial of the first
kind, Tn(x).
elseif alpha==1, xstar=cos(l.*pi/(n+1)); return; % Chebyshev polynomial of the
second kind, Un(x).
elseif alpha==-0.5, xstar=1; return; end % Always 1.

% Step 1
epsilon=10^-6; ktol=20; C(1,n)=0; y(1,ktol+1)=0;
y(1)=(sqrt(n*n+2*n*alpha-2*alpha-1)/(n+alpha))*cos((l-1)*pi/(n-1)); % Upper
bound

% Step 2
for k=1:ktol
    x=y(k); C(1)=2*alpha.*x; C(2)=-alpha+2*alpha*(1+alpha).*(x.^2);
    for ii=3:n,
        C(ii)=2*(ii+alpha-1)/(ii).*x.*C(ii-1)-(ii+2*alpha-2)/(ii).*C(ii-2);
    end
    den=1/(1-x^2)*((2*alpha+n-1)*C(n-1)-(n*x)*C(n)); % derivative.
    y(k+1)=y(k)-C(n)/den; % Newton-Raphson iteration.

% Step 3
    if abs(y(k+1)-y(k))<epsilon, xstar=y(k+1); break; end
end
if k==ktol, error('Algorithm did not converge within ten iterations - stopping.');
```

CURRICULUM VITAE

PERSONAL INFORMATION

Surname, Name: Avci, Kemal
Nationality: Turkish (TC)
Date and Place of Birth: 9 February 1980 , Adiyaman
Marital Status: Single
Phone: +90 5353791129
Fax: +90 3423601103
email: avci@gantep.edu.tr

EDUCATION

Degree	Institution	Year of Graduation
MS	University of Gaziantep	2004
BS	University of Gaziantep	2002
High School	Adiyaman Atatürk Lisesi	1997

WORK EXPERIENCE

Year	Place	Enrollment
2003- Present	University of Gaziantep	Research Assistant

FOREIGN LANGUAGES

Turkish (Native), English (Good), German (Elementary), Dutch (Elementary)

PUBLICATIONS

INTERNATIONAL JOURNALS

Avci K., Nacaroglu A. "Cosh Window Family and its Application to FIR Filter Design". Accepted for the publication in International Journal of Electronics and Communications-AEU

Avci K., Nacaroglu A. "An Efficient Study on the Modification of Kaiser Window". Accepted for the publication in MTA Review

INTERNATIONAL CONFERENCES

Avci K., Nacaroğlu A. (2008) “High Quality Low Order Nonrecursive Digital Filter Design Using Modified Kaiser Window”. *Proc. of 6th Symposium on Communication Systems, Networks and Digital Signal Processing (CSNDSP’08)*. July. Graz, Austria, 239-242.

Avci K., Nacaroğlu A. (2008) “A New Window Based on Exponential Function”. *Proc. of IEEE Ph.D. Research in Microelectronics and Electronics (PRIME 2008)*. June. İstanbul, Turkey, 69-72.

Avci K., Nacaroğlu A. (2008) “An Efficient Study on the Modification of Kaiser Window”. *Proc. of 7th International Conference COMMUNICATIONS 2008*. June. Bucharest, Romania, 63-66.

Avci K., Nacaroğlu A. (2008) “Modification of Cosh Window Family”. *Proc. of Third International Conference on Information and Communication Technologies (ICTTA’08)*. April. Damascus, Syria, 291-292. (Extended Abstract)

Avci K., Nacaroğlu A. (2008) “Cosine Hyperbolic Window Family with Its Application to FIR Filter Design”. *Proc. of Third International Conference on Information and Communication Technologies (ICTTA’08)*. April. Damascus, Syria, 289-290. (Extended Abstract)

Avci K., Nacaroğlu A. (2008) “Nonrecursive Digital Filter Design using a Three-parameter Window based on Cosine Hyperbolic Function”. *Proc. of 10th International Conference Digital Signal Processing and its Applications (DSPA’2008)*. March. Moscow, Russia, 121-124.

Avci K., Nacaroğlu A. (2004) “Computation of Noise in Switched Capacitor Networks Due to the Random Fluctuation of the Switching Instants”. *Proc. of 1st International Conference on Informatics (ICI-2004)*. September. Cesme, Turkey

NATIONAL CONFERENCES

Avci K., Nacaroğlu A. (2008) “Nonrecursive Digital Filter Design by the Exponential Window obtained using the Kaiser Approach”. Accepted for the publication for the conference proceedings in Symposium of 30th year in Çukurova University Engineering and Architecture Faculty. October. Adana, Turkey. (in Turkish)

HOBBIES

Football. Taekvando. Swimming. Guitar. Voyages.